ANALYSIS OF SEISMIC BEHAVIOR OF UNDERGROUND STRUCTURES:
A CASE STUDY ON BOLU TUNNELS

A THESIS SUBMITTED TO
THE GRADUATE SCHOOL OF NATURAL AND APPLIED SCIENCES
OF
MIDDLE EAST TECHNICAL UNIVERSITY

BY

NİYAZİ ERTUĞRUL

IN PARTIAL FULFILLMENT OF THE REQUIREMENTS
FOR
THE DEGREE OF MASTER OF SCIENCE
IN
CIVIL ENGINEERING

DECEMBER 2010

Approval of the thesis:

"ANALYSIS OF SEISMIC BEHAVIOR OF UNDERGROUND STRUCTURES: A CASE STUDY ON BOLU TUNNELS"

submitted by **NİYAZİ ERTUĞRUL** in partial fulfillment of the requirements for the degree of **Master of Science in Civil Engineering Department, Middle East Technical University** by,

Prof. Dr. Canan Özgen
Dean, Graduate School of **Natural and Applied Sciences**

Prof. Dr. Güney Özcebe
Head of Department, **Civil Engineering**

Prof. Dr. B. Sadık Bakır
Supervisor, **Civil Engineering Dept., METU**

Examining Committee Members:

Prof. Dr. Celal Karpuz
Mining Engineering Dept., METU

Prof. Dr. B. Sadık Bakır
Civil Engineering Dept., METU

Asst. Prof. Dr. Nejan Huvaj Sarıhan
Civil Engineering Dept., METU

Inst. Dr. N. Kartal Toker
Civil Engineering Dept., METU

Dr. Ebu Bekir Aygar
SIAL

Date: December 16, 2010

I hereby declare that all information in this document has been obtained and presented in accordance with academic rules and ethical conduct. I also declare that, as required by these rules and conduct, I have fully cited and referenced all material and results that are not original to this work.

Name, Last name: Niyazi ERTUĞRUL

Signature:

ABSTRACT

ANALYSIS OF SEISMIC BEHAVIOR OF UNDERGROUND STRUCTURES:
A CASE STUDY ON BOLU TUNNELS

Ertuğrul, Niyazi

M.Sc., Department of Civil Engineering

Supervisor: Prof. Dr. B. Sadık Bakır

December 2010, 127 pages

In today's world, buried structures are used for a variety of purposes in many areas such as transportation, underground depot areas, metro stations and water transportation. The serviceability of these structures is crucial in many cases following an earthquake; that is, the earthquake should not impose such damage leading to the loss of serviceability of the structure. The seismic design methodology utilized for these structures differs in many ways from the above ground structures. The most commonly utilized approach in dynamic analysis of underground structures is to neglect the inertial forces of the substructures since these forces are relatively insignificant contrary to the case of surface structures. In seismic design of these underground structures, different approaches are utilized like free-field deformation approach and soil-structure interaction approach.

Within the confines of this thesis, seismic response of highway tunnels is considered through a case study on Bolu Tunnels, which are well documented and subjected to Düzce earthquake. In the analyses, the seismic response of a section of the Bolu tunnels is examined with 2-D finite element models and results are compared with the recorded data to evaluate the capability of the available analysis methods. In general, the results of analyses did not show any distinct difference from the recorded data regarding the seismic performance of the analyzed section and that the liner capacities were sufficient, which is consistent with the post earthquake condition of the Bolu Tunnels.

Keywords: Seismic Analysis, Bolu Tunnels, Finite Element Analysis, Soil-Structure Interaction

ÖZ

YERALTI YAPILARININ SİSMİK DAVRANIŞININ ANALİZİ: BOLU TÜNELLERİ ÜZERİNE BİR ÇALIŞMA

Ertuğrul, Niyazi

Yüksek Lisans, İnşaat Mühendisliği Bölümü

Tez Yöneticisi: Prof. Dr. B. Sadık Bakır

Aralık 2010, 127 sayfa

Günümüz dünyasında, gömülü yapılar ulaşım, yeraltı depo alanları, metro istasyonları ve su taşıma gibi pek çok alanda farklı amaçlar için kullanılmaktadır. Bir çok durumda bu yapıların depremden sonra kullanılabilir olması önemlidir, yani deprem bu yapılara kullanılabilirliğini kaybedecek kadar büyük bir zarar vermemelidir. Bu yapıların deprem tasarımında kullanılan yöntemler yerin üzerinde olan yapılarda kullanılan yöntemlerden farklıdır. Yeraltı yapılarının dinamik analizlerinde en yaygın yaklaşım yapının atalet kuvvetlerini, yüzey yapılarında sismik davranışa hakim olmasının aksine, ihmal etmektir. Yeraltı yapılarının sismik tasarımda serbest saha deformasyon yaklaşımı, zemin-yapı etkileşimi gibi farklı yaklaşımlar vardır.

Bu çalışma kapsamında, karayolu tünellerinin sismik davranışı Düzce depremine maruz kalmış ve iyi belgelenmiş Bolu Tünelleri üzerinde bir çalışma ile değerlendirilmiştir. Analizlerde, Bolu Tünellerinin bir kesitinin sismik davranışı 2-D sonlu eleman modelleri ile incelenmiş ve sonuçlar ile kaydedilen veriler mevcut analiz yöntemlerinin yeterliliğini değerlendirmek için karşılaştırılmıştır. Genel olarak, analiz kesitinin deprem performansı dikkate alındığında analiz sonuçlarının

kayıtlı verilerden belirgin bir fark içermediği ve kaplama kapasitelerinin yeterli olduğu görülmüştür. Bu da Bolu Tünellerinin deprem sonrası durumuyla tutarlılık içermektedir.

Anahtar Kelimeler: Sismik Analiz, Bolu Tüneli, Sonlu Elemanlar, Zemin-Yapı Etkileşimi

ACKNOWLEDGMENTS

I would like to thank to all the people who have helped and inspired me during my M.Sc. study.

I particularly would like to thank to my supervisor, Prof. Dr. B. Sadık Bakır for his guidance during my study. His perpetual energy and enthusiasm in research have motivated me. In addition, he was always accessible and willing to help me with my study.

My deepest gratitude goes to my family for their unflagging love and support throughout my life. This thesis would be impossible without them.

TABLE OF CONTENTS

LIST OF TABLES

LIST OF FIGURES

CHAPTER 1

INTRODUCTION

1.1 General

Underground structures are becoming increasingly popular because of the fast growth of the population and decreasing of the ground space, particularly in urban areas all over the world including high seismic risk zones. Accordingly, in many cases the design of such structures must incorporate not only the static loading but the earthquake loading as well. Underground structures have distinct features that make their seismic behavior radically different from surface structures in general, most notably due to (i) their complete enclosure in soil or rock, and (ii) their significant length (i.e. tunnels) (Hashash, 2001).

In underground structures, the response is mainly dominated by the surrounding soil medium rather than the inertial properties because of the very large inertia of the ground with respect to that of the structure.

Main differences of the seismic response of underground structures from those of the surface structures are the following:

- The seismic effect is controlled by the deformation imposed on the structure by the ground, not by the forces or stresses.
- The inertia of the surrounding soil is much larger relative to the inertia of the structure for most underground facilities.

Therefore, the free-field deformation of the ground and its interaction with the structure are the main interests in the seismic design of underground structures.

1.2 Aim of the Thesis

The main focus of this study is to evaluate the seismic performance of highway tunnels having non-circular shaped cross-sections constructed at relatively greater depths. The Bolu Tunnels, which were under construction during the two major earthquakes that occurred in the year 1999, had a variety of structural damages, constituting an excellent opportunity for a case study. There exists recorded data regarding the seismic behavior of the tunnels during the two earthquakes. Accordingly, the essential aim of the thesis is to examine the seismic response of the tunnels through numerical models and to compare the results to the recorded data to test the predictive capability of the available analyses methods. This is done by performing dynamic finite element analyses for a selected section using the finite element computer program PLAXIS 8.2 (2D).

1.3 Scope of the Thesis

Following the introduction, available analytical formulations on the seismic design of underground circular structures will be summarized in Chapter 2. Different approaches available in literature used for the seismic assessment of these types of structures will be discussed.

Chapter 3 is devoted to provide general information about the history of the Bolu Tunnels project, the investigation program implemented following the earthquakes, and the geology of the area.

Chapter 4 consists of the main body of the study. The generation of the model in PLAXIS is explained in detail and the analysis of the so called section C2 that forms a large fraction of the Bolu Tunnels is evaluated. Also, the generation of the earthquake record that is used in the dynamic analyses is presented in this chapter.

Chapter 5 contains the comparison of the results obtained from the analyses with the field recorded data and evaluations.

Chapter 6 presents conclusions reached and recommendations for future studies.

CHAPTER 2

LITERATURE REVIEW

2.1 Engineering Approach to the Seismic Analysis and Design of Tunnels

Earthquake effects on underground structures can be grouped into two categories: i) ground shaking, and ii) ground failure such as liquefaction, fault displacement, and slope instability. The focus of this study is ground shaking, which means the deformation of the ground developed by the seismic waves propagating through the Earth's crust. The major factors influencing the damage due to ground shaking include i) the shape, dimensions and depth of the structure, ii) the properties of the surrounding soil or rock, iii) the properties of the structure, and iv) the severity of the ground shaking (Dowding and Rozen, 1978; St. John and Zahrah, 1987).

According to Hashash et al. (2001) the evaluation of underground structure seismic response requires an understanding of the anticipated ground shaking as well as an evaluation of the response of the ground and the structure to such shaking. Evaluation of the seismic response and subsequent design of buried structures can be summarized in three major steps:

1) Definition of the seismic environment and development of the seismic parameters for analysis.

2) Evaluation of the ground response to shaking, which includes ground failure and ground deformations.

3) Assessment of the structural behavior due to seismic shaking including; (i) development of seismic design loading criteria, (ii) underground structure response to ground deformations, and (iii) special seismic design issues.

For most underground structures, the inertia of the surrounding soil is large relative to the inertia of the structure. Measurements made by Okamoto et al. (1973) of the

4

seismic response of an immersed tube tunnel during several earthquakes show that the response of a tunnel is dominated by the surrounding ground response and not the inertial properties of the tunnel structure itself. Therefore, the main point of underground seismic design is on the free-field deformation of the ground and its interaction with the structure. The emphasis on displacement is totally in contrast to the seismic design of surface structures, in which the focus is on inertial effects of the structure itself. This difference requires development of the alternative design methods in which the seismically induced deformations of the ground is the controlling factor.

Historically, there exist simplified approaches for evaluating the response of a buried structure:

i.   Dynamic earth pressure approach (Mononobe - Okabe)
ii.   Free field deformation approach

The dynamic earth pressure method have been suggested for the underground box structures and used widely for not only underground structures but also for the surface structures such as the retaining walls. This method supplies designer a good estimate for the loading mechanism if the structure is situated at relatively shallow depths and having a rectangular cross section. For a buried rectangular structural frame, the ground and the structure would move together, making it unlikely that a yielding active wedge could form. Therefore, its applicability in the seismic design of underground structures has been the subject of controversy (Wang, 1993).

In the free field deformation approach, the ground is subjected to seismic wave propagation without existence of the structure. Hence, this approach ignores the existence of the structure and the cavity. The estimated deformations occurring at the ground is applied to the structure and the response of the structure is calculated. Newmark (1968) and (Kuesel, 1969) suggest a simplified approach which is based on the theory of wave propagation in homogeneous, isotropic, elastic media. The ground strains are calculated by assuming a harmonic wave of any wave type propagating at an angle (angle of incidence) with respect to the axis of a planned

structure. They represent free-field ground deformations along a tunnel axis due to a harmonic wave propagating at a given angle of incidence (Figure 2.1). Because of the uncertainty involved in the angle of incidence for the predominant seismic waves, a conservative path is followed by using of the most critical angle of incidence yielding the maximum strain.

Figure 2.1 Simple harmonic wave and tunnel (Wang, 1993).

Where;

L= wavelength

D= displacement amplitude

Φ = angle of incidence

St. John and Zahrah (1987) improved Newmark's approach to extend solutions for free-field axial and curvature strains due to compression, shear and Rayleigh waves. Solutions for all three wave types are shown in Table 2.1, though S-waves are typically associated with peak particle accelerations and velocities (Power et al., 1996). The seismic waves causing longitudinal and bending strains are shown in Figure 2.2. It is often hard to determine which type of wave will govern. Strains produced by Rayleigh waves tend to dominate only in shallow structures and when the seismic source is distant from the sites (Wang, 1993).

Table 2.1 Strains and curvature due to body and surface waves (After St. John and Zahrah, 1987).

Wave type	Longitudinal strain	Normal strain	Shear strain	Curvature
P-wave	$\varepsilon_l = \frac{V_P}{C_P}\cos^2\phi$	$\varepsilon_n = \frac{V_P}{C_P}\sin^2\phi$	$\gamma = \frac{V_P}{C_P}\sin\phi\cos\phi$	$K = \frac{a_P}{C_P^2}\sin\phi\cos^2\phi$
	$\varepsilon_{lm} = \frac{V_P}{C_P}$ for $\phi = 0°$	$\varepsilon_{nm} = \frac{V_P}{C_P}$ for $\phi = 90°$	$\gamma_m = \frac{V_P}{2C_P}$ for $\phi = 45°$	$K_m = 0.385\frac{a_P}{C_P^2}$ for $\phi = 35°16'$
S-wave	$\varepsilon_l = \frac{V_S}{C_S}\sin\phi\cos\phi$	$\varepsilon_n = \frac{V_S}{C_S}\sin\phi\cos\phi$	$\gamma = \frac{V_S}{C_S}\cos^2\phi$	$K = \frac{a_S}{C_S^2}\cos^3\phi$
	$\varepsilon_{lm} = \frac{V_S}{2C_S}$ for $\phi = 45°$	$\varepsilon_{nm} = \frac{V_S}{2C_S}$ for $\phi = 45°$	$\gamma_m = \frac{V_S}{C_S}$ for $\phi = 0°$	$K_m = \frac{a_S}{C_S^2}$ for $\phi = 0°$
Rayleigh wave				
Compressional component	$\varepsilon_l = \frac{V_{RP}}{C_R}\cos^2\phi$	$\varepsilon_n = \frac{V_{RP}}{C_R}\sin^2\phi$	$\gamma = \frac{V_{RP}}{C_R}\sin\phi\cos\phi$	$K = \frac{a_{RP}}{C_R^2}\sin\phi\cos^2\phi$
	$\varepsilon_{lm} = \frac{V_{RP}}{C_R}$ for $\phi = 0°$	$\varepsilon_{nm} = \frac{V_{RP}}{C_R}$ for $\phi = 90°$	$\gamma_m = \frac{V_{RP}}{2C_R}$ for $\phi = 45°$	$K_m = 0.385\frac{a_{RP}}{C_R^2}$ for $\phi = 35°16'$
Shear component		$\varepsilon_n = \frac{V_{RS}}{C_R}\sin\phi$	$\gamma = \frac{V_{RS}}{C_R}\cos\phi$	$K = \frac{a_{RS}}{C_R^2}\cos^2\phi$
		$\varepsilon_{nm} = \frac{V_{RS}}{C_R}$ for $\phi = 90°$	$\gamma_m = \frac{V_{RS}}{C_R}$ for $\phi = 0°$	$K_m = \frac{a_{RS}}{C_R^2}$ for $\phi = 0°$

Where,

r: radius of circular tunnel or half height of a rectangular tunnel

α_p: peak particle acceleration associated with P-wave

α_s: peak particle acceleration associated with S-wave

α_R: peak particle acceleration associated with Rayleigh wave

Φ: angle of incidence of wave with respect to tunnel axis

v_l: Poisson's ratio of tunnel lining material

V_p: peak particle velocity associated with P-wave

C_p: apparent velocity of P-wave propagation

V_s: peak particle velocity associated with S-waves

C_s: apparent velocity of S-wave propagation

V_R: peak particle velocity associated with Rayleigh wave

C_R: apparent velocity of Rayleigh wave propagation
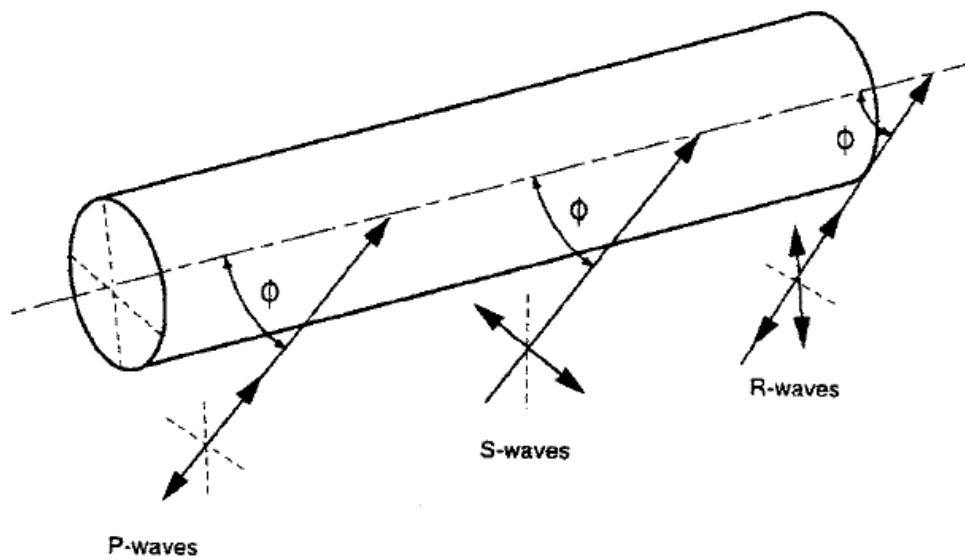
Figure 2.2 Seismic waves causing longitudinal and bending strains (Power et al., 1996).

According to the method proposed by St. John and Zahrah (1987) moments and forces generated in tunnel lining are expressed in the following equations:

$$M = \left(\frac{2\pi}{L}\right)^2 . (\cos^3 \theta). E_l. I_l. D. \sin\left(\frac{2\pi}{L / \cos\theta}\right) \qquad (2.1)$$

$$V = \left(\frac{2\pi}{L}\right)^3 . (\cos^4 \theta). E_l. I_l. D. \cos\left(\frac{2\pi}{L/\cos\theta}\right) \qquad (2.2)$$

$$Q = \left(\frac{2\pi}{L}\right). \cos\theta. \sin\theta. E_l. A_l. D. \cos\left(\frac{2\pi}{L/\cos\theta}\right) \qquad (2.3)$$

Where,

M: flexural moment

V: shear force

Q: thrust force

θ : angle of wave impact

I_l : moment of inertia of tunnel lining

E_l: modulus of elasticity of lining material

D: amplitude of sine wave

L: shear wave length

A_l: section area of lining.

In addition to these simplified approaches, there exist more detailed design applications:

i.   Soil-Structure interaction using numerical methods (finite element or finite difference) with elastic or inelastic material properties utilizing 2-D/3-D models in frequency or time domain,

ii.   Simplified frame analysis model in which the effects of the soil-structure interaction are simulated using an appropriate set of springs and dampers.

The numerical methods have obvious benefits for the solution of difficult situations involving geometric irregularities or nonlinear material behavior over conventional approaches and closed-form formulations. In seismic design and analysis of tunnels, they provide highly precise solutions

An approximate solution can be provided by simplified frame analysis for the design of underground structures. The following is a step-by-step procedure for such an

approach, proposed by Hashash et al. (2001), based in part on the work by Monsees and Merritt, (1988), and Wang (1993):

1.   Structural dimensions and members are designed based on static loading requirements

2.   The free-field shear strains/deformations of the ground based on ground response analyses for a vertically propagating shear wave are estimated.

3.   The relative stiffness i.e. the flexibility ratio between the ground and the structure is determined

4.   The racking coefficient, R based on the flexibility ratio is determined

5.   The actual racking deformation of the structure as $\Delta_{structure}=R\Delta_{free\text{-}field}$ is calculated

6.   The seismically-induced racking deformation in a static structural analysis is imposed

7.   The racking-induced internal demands to other static loading components is added

8.   If the results from 7 show that the structure has adequate capacity, the design is considered satisfactory. Otherwise, the structure is revised and process is repeated

9.   The structure should be redesigned if the strength requirements are not met, and/or the resulting inelastic deformations exceed allowable levels depending on the structure performance objectives

10.   The sizes of the structural elements are to be modified as necessary. Reinforcing steel percentages may need to be adjusted to avoid brittle behavior. Under static or pseudo-static loads, the maximum usable compressive concrete strain is 0.004 for flexural and 0.002 for axial loading.

Wang (1993) evaluated the seismic design approaches for an underground structure as presented in Table 2.2

Table 2.2 Seismic design approaches for an underground structure (after Wang, 1993).

Seismic Racking Design Approaches [after Wang, 1993]			
Approaches	Advantages	Disavantages	Applicability
Dynamic earth pressure methods	- Used with reasonable results in the past - Require minimal parameters and computation error - Serve as additional safety measures against seismic loads	- Lack of rigorous theoretical basis - Resulting in excessive racking deformations for tunnels with significant burial - Use limited to certain types of ground properties	For tunnels with minimal soil cover thickness
Free-field racking deformation method	- Conservative for tunnel structure stiffer than ground - Comparatively easy to formulate - Used with reasonable results in the past	- Non conservative for tunnel structure more flexible than ground - Overly conservative for tunnel structures significantly stiffer than ground - Less precision with highly variable ground conditions	For tunnel structures with equal stiffness to ground
Soil-Structure interaction finite element analysis	- Best representation of soil-structure system - Best accuracy in determining structure response - Capable of solving problems with complicated tunnel geometry and ground conditions	- Requires complex and time consuming computer analysis - Uncertainly of design seismic input parameters may be several times the uncertainty of the analysis	All conditions
Simplified frame analysis model	- Good approximation of soil-structure interaction - Comparatively easy to formulate - Reasonable accuracy in determining structure response	- Less precision with highly variable ground	All conditions except for compacted subsurface ground profiles

2.2 Review of Seismically-Induced Deformations at Tunnel Linings

In this section, a brief summary of deformation modes are presented at tunnel linings under cycling loading conditions. Owen and Scholl (1981) claimed that the behavior of a tunnel can be approximated to that of an elastic beam subject to deformations imposed by the surrounding ground. Three types of deformations represent the response of underground structures to seismic motions: 1) Axial compression and extension (Figure 2.3 a, b), 2) longitudinal bending (Figure 2.3 c, d), and 3) ovaling / racking (Figure 2.3 e, f). Axial deformations in tunnels are created by the components of seismic waves that produce motions parallel to the axis of the tunnel and cause interchanging compression and tension. Bending deformations are caused by the components of seismic waves producing particle motions perpendicular to the

11

longitudinal axis. Design considerations for axial and bending deformations are generally in the direction along the tunnel axis (Wang, 1993).

Ovaling or racking deformations in a tunnel structure develop when shear waves propagate normal or nearly normal to the tunnel axis, resulting in a distortion of the cross-sectional shape of the tunnel lining. Design considerations for this type of deformation are in the transverse direction. The general behavior of the lining may be simulated as a buried structure subject to ground deformations under a two-dimensional plane-strain condition. Ovaling and racking of the tunnel are the most crucial deformation modes for the tunnel sections.
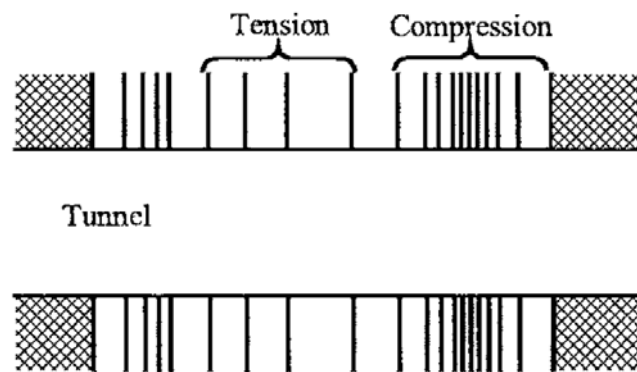
a) Compression-extension created by the components of seismic waves that produce motions parallel to the axis of the tunnel.
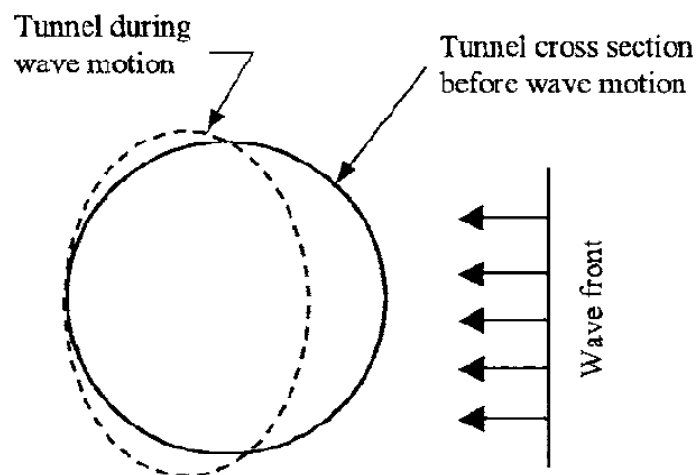
b) Compression of tunnel section.
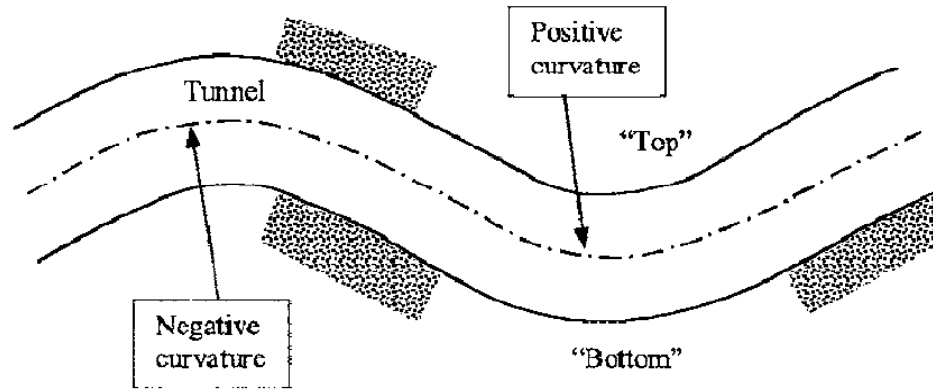
c) Longitudinal bending deformation.
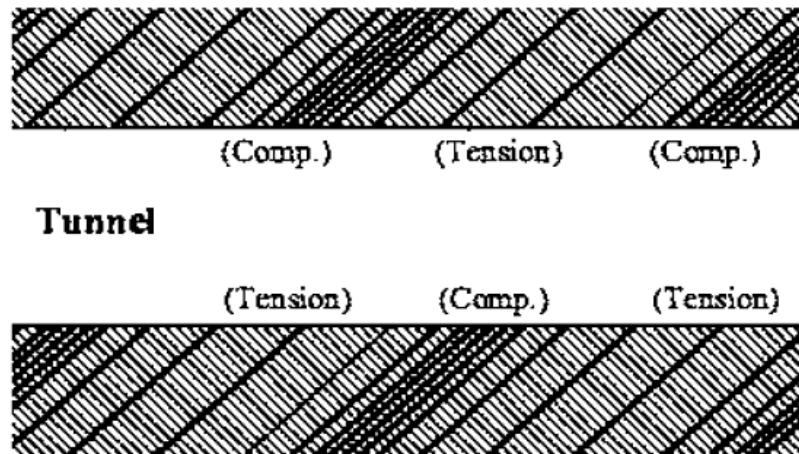
d) Diagonally propagating wave deformations.
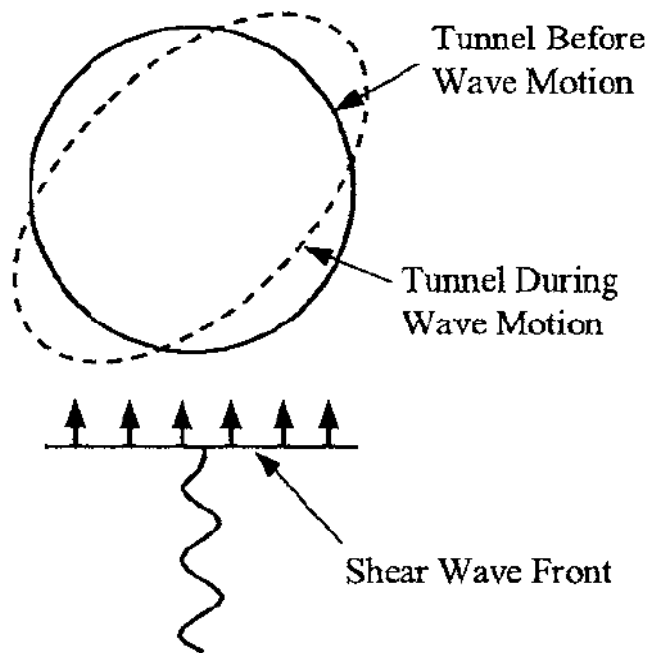
e) Ovaling of tunnel section.
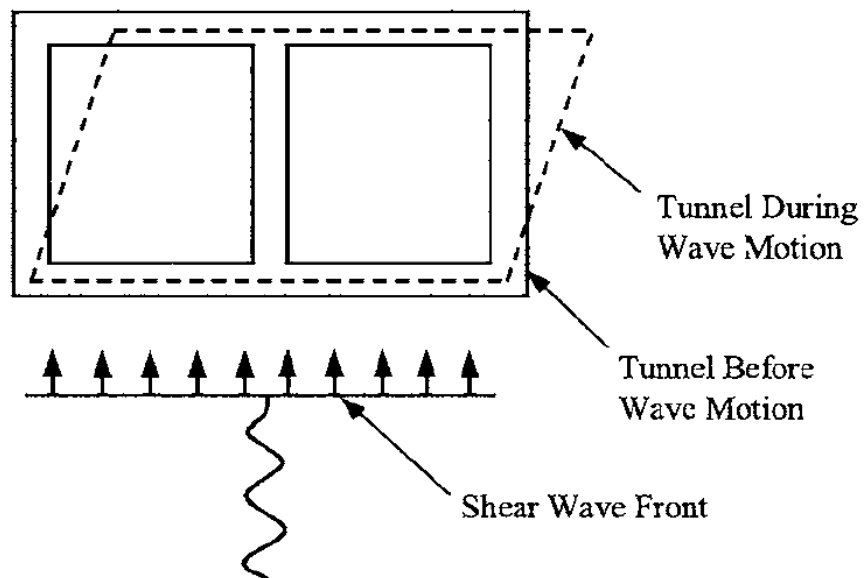
f) Racking of tunnel section.

Figure 2.3 Deformation modes of the tunnels due to seismic waves (After Owen and Scholl, 1981).

Ovaling and racking of the tunnel are the most crucial deformation mode for the tunnel sections.

Next, the approaches used for the design of circular tunnels are discussed in detail.

2.3 Seismic Design Approaches Used for Circular Tunnels

In this section, seismic design approaches including analytical, pseudo-static, and numerical methods are described in detail.

2.3.1 Ovaling deformation of circular tunnels with free-field deformation approach

Like racking deformations, ovaling deformations develop in the transverse direction of the tunnel axis. Vertically propagating shear waves are the predominant form of the earthquake loading that causes these types of deformations (Wang, 1993).

Shear distortions of the ground can be defined in two ways: (1) non-perforated ground, and (2) perforated ground (Figure 2.4). Plane strain conditions are considered. The maximum diametric strain ε_d is a function of the maximum free-field shear strain γ_{max} in the non-perforated ground.

$$\varepsilon_d = \frac{\Delta d}{d} = \mp \frac{\Delta \gamma_{max}}{2} \qquad (2.4)$$

where d is the diameter of the tunnel.

In the perforated ground, the diametric strain is related to the Poisson's ratio of the medium.

$$\varepsilon_d = \frac{\Delta d}{d} = \mp 2 \, \Delta \gamma_{max}(1 - v) \qquad (2.5)$$

In the equations the liner and the affect of soil-structure interaction are ignored. As would be expected, the perforated ground yields much greater distortion than the

15

non-perforated ground. Results obtained from the perforated ground case are acceptable for the soft lining. For the lining stiffness equal to that of the surrounding ground, non-perforated results provide reasonable estimations. A lining with large relative stiffness should experience distortions smaller than those given by Equation 2.5 (Wang, 1993).
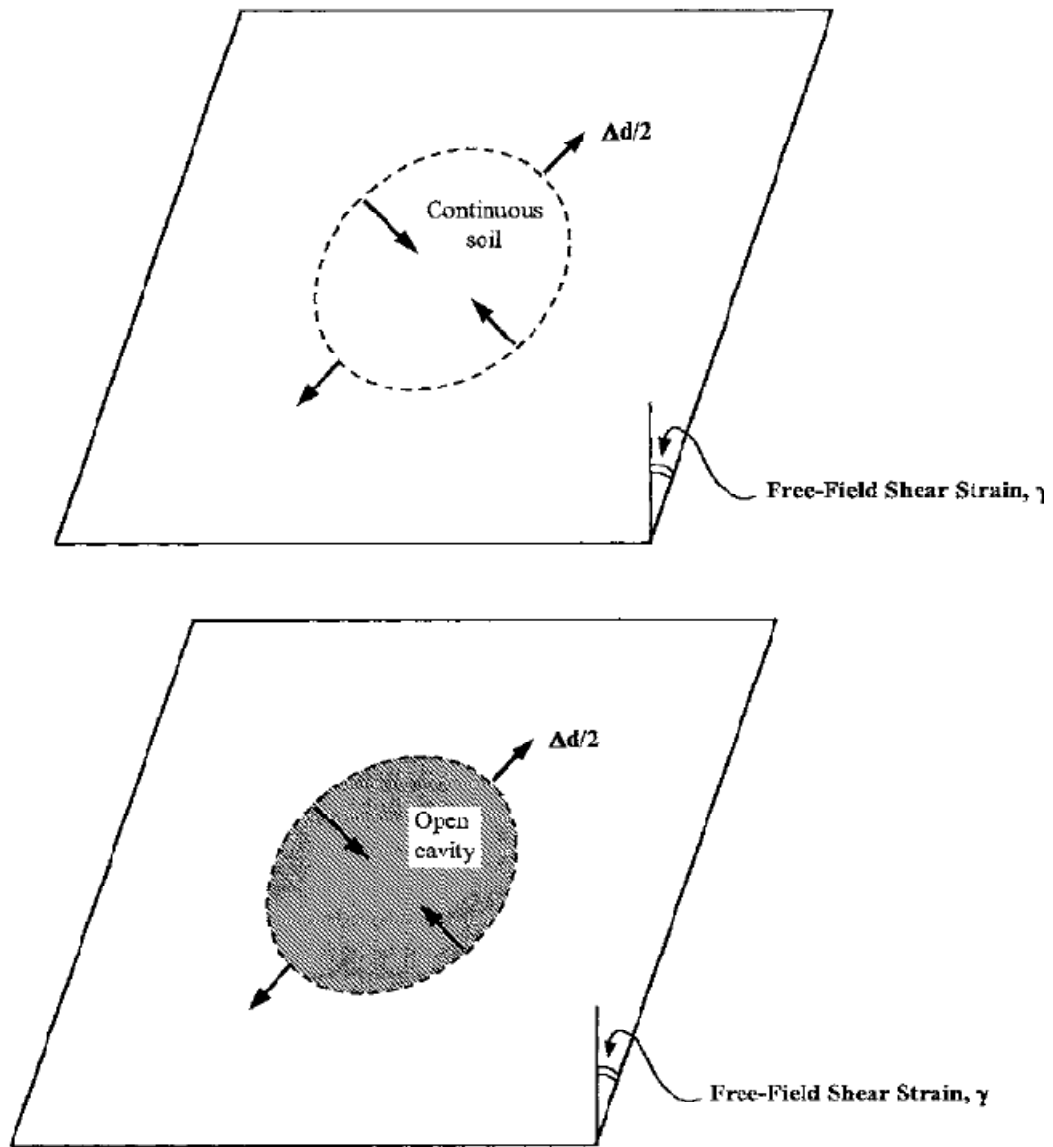
Figure 2.4 Free-field shear distortion of perforated and non-perforated ground, circular shape tunnels. (after Wang, 1993).

2.3.2 Longitudinal deformation of circular tunnels with ground-structure interaction approach

In this approach, the presence of the buried structure is evaluated. It is supposed that the existence of the structure modifies the deformation behavior of the surrounding medium. To model soil-structure interaction, beam-on-elastic foundation theory is used. Dynamic inertial interaction effects are assumed to be ignored in this solution. Under seismic loading, the cross-section of a tunnel will experience axial bending and shear strains due to free field axial, curvature, and shear deformations (Figure 2.5). St. John and Zahrah (1987) suggested that maximum strains are caused by a wave with angle of incidence 45°. The resulting maximum axial strain, ε^a_{max}, is formed by a 45° shear wave (Figure 2.2) is:

$$\varepsilon^a_{\ max} = \frac{\left(\frac{2\pi}{L}\right) A}{2 + \frac{E_l A_c}{K_a}\left(\frac{2\pi}{L}\right)^2} \leq \frac{fL}{4E_l A_c} \tag{2.6}$$

Where

L: wavelength of an ideal sinusoidal shear wave

K_a: longitudinal spring coefficient of ground medium; in force per unit deformation per unit length of tunnel)

A: free-field displacement response amplitude of an ideal sinusoidal shear wave

A_c: cross-sectional area of tunnel lining

E_l: elastic modulus of the tunnel lining

f: ultimate friction force (per unit length) between tunnel and surrounding soil

(a)

Shear force and moment
due to curvature
in the vertical plane

Axial force

H

H V

V

Shear force and moment
due to curvature
in the horizontal plane

(b)

t

b

V M T

$$I_l = \frac{bt^3}{12}$$

$$A_l = bt$$
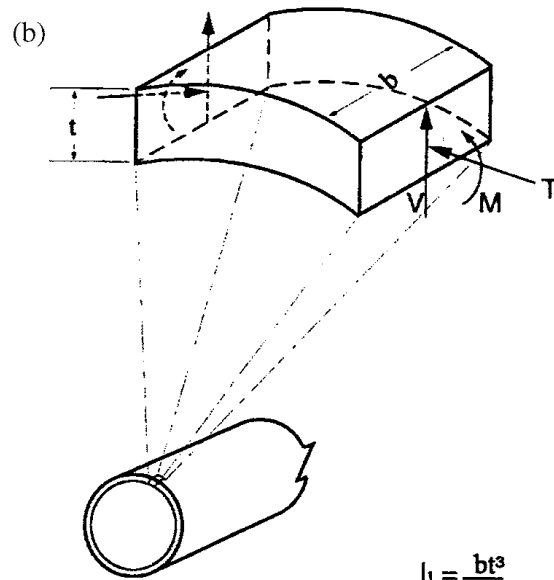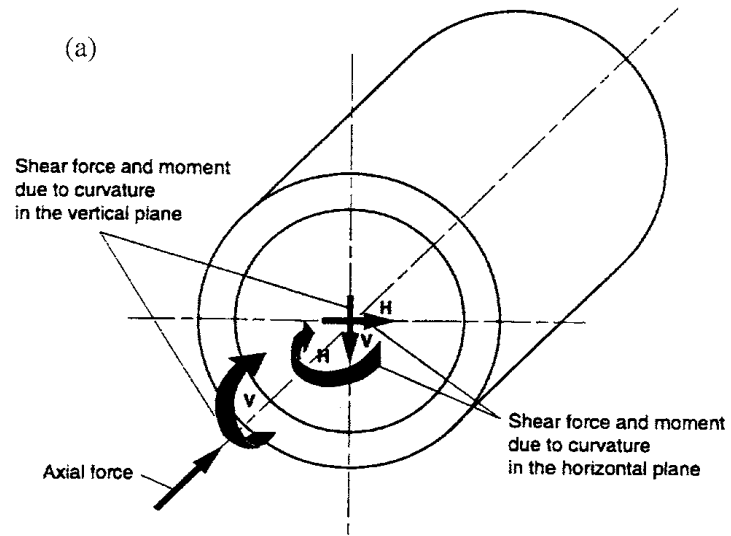
$$b_l = 1 \text{ unit}$$

Figure 2.5 Induced forces and moments caused by seismic waves (Power et al., 1996). (a) Induced forces and moments caused by waves propagating along tunnel axis, (b) induced circumferential forces and moments caused by waves propagating perpendicular to tunnel axis.

18

In Equation 2.6, it is stated that the maximum frictional forces that can occur between the lining and the medium restrict the axial strain in the lining. The maximum frictional shear is dependent on the roughness of the ground-tunnel interface and the normal force applied to the tunnel from the ground (Hongbin Huo, 2005). When the incident angle of shear wave is zero, the maximum bending strain occurs (Figure 2.2):

$$\varepsilon^b{}_{max} = \frac{\left(\frac{2\pi}{L}\right)^2 A}{1 + \frac{E_l I_c}{K_t}\left(\frac{2\pi}{L}\right)^4} r \tag{2.7}$$

Where,

I_c: moment of inertia of the tunnel section

K_t: transverse spring coefficient of the medium (in force per unit deformation per unit length of tunnel (see Equation 2.12).

r: radius of circular tunnel or half height of a rectangular tunnel

The maximum shear force on the tunnel cross-section can be written as a function of this maximum bending strain:

$$V_{max} = \frac{\left(\frac{2\pi}{L}\right)^3 E_l I_c A}{1 + \frac{E_l I_c}{K_l}\left(\frac{2\pi}{L}\right)^4} = \left(\frac{2\pi}{L}\right)\left(\frac{E_l I_c \varepsilon^b{}_{max}}{r}\right) \tag{2.8}$$

The maximum bending moment is:

$$M_{max} = \frac{\left(\frac{2\pi}{L}\right)^2 E_l I_c A}{1 + \frac{E_l I_c}{K_l}\left(\frac{2\pi}{L}\right)^4} \tag{2.9}$$

19

The maximum axial force is:

$$Q_{max} = \frac{\left(\frac{2\pi}{L}\right) E_l I_c A}{2 + \frac{E_l I_c}{K_a}\left(\frac{2\pi}{L}\right)^2}$$

(2.10)

A conservative estimate of the total maximum axial strain is obtained by combining the axial and bending strains because of assuming the liner and the surrounding medium are linear elastic (Power et al., 1996):

$$\varepsilon^{ab} = \varepsilon^a{}_{max} + \varepsilon^b{}_{max}$$

(2.11)

In the equations stated above the response is modeled by using springs with the spring coefficients K_a and K_l for longitudinal and transverse soil section.

K_a and K_l are functions of incident wave length (St. John and Zahrah, 1987):

$$K_l = K_a = \frac{16\pi G(1 - \nu_m)}{(3 - 4\nu_m)} \frac{d}{L}$$

(2.12)

where, G_m and ν_m: shear modulus and Poisson's ratio of the medium, d: diameter of circular tunnel or height of rectangular structure, L: wavelength.

According to Wang (1993), the derivations of these springs differ from those for the conventional beam on elastic foundation problems in that:

-The spring coefficients should be representative of the dynamic modulus of the ground under seismic loads.

-The derivations should consider the fact that loading felt by the surrounding soil is alternately positive and negative due to the assumed sinusoidal seismic wave.

Some researchers suggested approximate values for the wave length of ground motion (e.g., Matsubara et al., 1995):

$$L = T . C_s \qquad (2.13)$$

Where, T is the predominant natural period of the soil deposit, and C_s is the shear wave velocity.

$$T = \frac{4h}{C_s} \quad \text{Idriss and Seed (1968)} \qquad (2.14)$$

Where, h is the thickness of the soil layer.

The ground displacement response amplitude, A, represents the spatial variations of ground motions along a horizontal alignment and should be derived by site-specific subsurface conditions. Generally, the displacement amplitude increases with increasing wave length (SFBART, 1960).

A displacement amplitude, A, can be calculated by assuming a sinusoidal compression wave with a displacement amplitude A and a wavelength, L:

For free-field axial strains:

$$\frac{2\pi A}{L} = \frac{V_s}{C_s} \sin \phi \cos \phi \qquad (2.15)$$

For free-field bending strains:

$$\frac{4\pi^2 A}{L^2} = \frac{a_s}{C_s{}^2} \cos^3 \phi \qquad (2.16)$$

2.3.3 Ovaling deformation of circular tunnels with ground-structure interaction approach

Tunnel liners are grouped as flexible and rigid liners by Peck et al. (1972). If the distribution of the pressure and the moments occurred due to corresponding deflected shape of the liner is negligible, the liner is said to be flexible liner. On the contrast, a liner which carries larger moments with small deflections under loads imposed by the ground called rigid liner.

The definition of the tunnel, rigid or flexible, may change with the strength properties of the ground. For instance, a tunnel that may be flexible in a stiff ground may behave as a rigid liner in very soft ground conditions. To describe the relative stiffness of the ground to the structure, Peck et al. (1972) proposed closed-form solutions in terms of thrusts, bending moments, and displacements under external loading conditions. The response of the tunnel liner is related to the compressibility and the flexibility ratios between ground and the structure. The stiffness of a tunnel relative to the surrounding ground is quantified by the compressibility and flexibility ratios (C and F), which are measures of the extensional stiffness and the flexural stiffness (resistance to ovaling), respectively, of the medium relative to the lining (Merritt et al., 1985). The first type is extensional stiffness, which is a measure of the equal uniform pressure to cause a unit diametric strain of the tunnel without changing the shape of the tunnel. The second type is flexural stiffness, which is a measure of the non-uniform pressure to cause a unit diametric strain resulting in a change in shape or an ovaling of the tunnel.

The compressibility ratio, a measure of the extensional stiffness of the ground to that of the liner, is obtained by considering an infinite, elastic, homogeneous and isotropic ground subjected to a uniform external pressure. The compressibility ratio is expressed as the ratio between the pressure required to cause a unit diametric strain (contraction) of the free-field ground and the pressure required to cause a unit diametric strain (contraction) of the liner. Note that in order to obtain the diametric

22

strain of the free-field ground, a circle with its size identical to the liner is assumed. The compressibility ratio can be expressed as:

$$C = \frac{E_m(1 - v_l^2)r}{E_l t(1 + v_m)(1 - 2v_m)} \qquad (2.17)$$

The flexibility ratio, a measure of the flexural stiffness of the ground to that of the liner, is obtained by considering an infinite, elastic, homogeneous and isotropic ground subjected to a pure shear loading. The flexibility ratio is equal to the ratio between the shear stress required to cause a unit diametric strain (ovaling) of the free-field ground and the shear stress required to cause a unit diametric strain (ovaling) of the liner. Note that in order to obtain the diametric strain of the free-field ground, a circle with size identical to the liner is assumed. The flexibility ratio is:

$$F = \frac{E_m(1 - v_l^2)R^3}{6E_l I(1 + v_m)} \qquad (2.18)$$

It is often suggested that the flexibility ratio is more significant because it is related to the ability of the lining to resist distortion imposed by the ground.

Burns and Richard (1964) have shown that the forces and deformations of ground and structure depend on (1) the compressibility ratio, C; (2) the flexibility ratio, F, and (3) the slippage at the interface between the ground and the liner. The interface between ground and support has often been assumed to be frictional, i.e. the shear stress and normal stress developed at the interface follow the Coulomb friction law. In other words, the maximum shear stress at the interface is equal to the normal stress times the friction coefficient between ground and support. Two extreme cases are considered: full-slip and no-slip.

The full-slip case assumes that the friction coefficient is zero and no shear force develops at the interface. The ground may detach from the tunnel during an earthquake. In the no-slip case, the friction coefficient is such that the ground and structure are tied together. The ground and structure cannot be separated. Actual conditions may be in between these two extreme cases. However, due to the

complexity of the problem, most of the work has focused on either full-slip or no-slip interface conditions.

a)   Full-slip conditions

Peck et al. (1972) provided closed-form solutions for diametric strain ε^d, thrust T, and bending moment M, for the full-slip case under static loading conditions, i.e. tunnels under overburden and lateral earth pressures. The displacements and forces are functions of the compressibility ratio C, flexibility ratio F and the in-situ overburden pressure of the soil $\gamma_t H$.

At the crown and invert of a circular tunnel:

$$\varepsilon_d = \frac{\Delta d}{d} = \frac{1}{2}\frac{\gamma_t Hr}{M_c}\left[(1-v)(1+K_0)b_1 C + \frac{2}{3}\left(\frac{1-v}{1-2v}\right)(1-K_0)b_2 F\right] \tag{2.19}$$

$$T = \frac{1}{2}\gamma_t Hr\left[(1+K_0)b_1 - \frac{1}{3}(1-K_0)b_2\right] \tag{2.20}$$

$$M = \frac{1}{6}\gamma_t Hr^2[(1-K_0)b_2] \tag{2.21}$$

At the springline of a circular tunnel:

$$\varepsilon_d = \frac{\Delta d}{d} = \frac{1}{2}\frac{\gamma_t Hr}{M_c}\left[(1-v)(1+K_0)b_1 C + \frac{2}{3}\left(\frac{1-v}{1-2v}\right)(1-K_0)b_2 F\right] \tag{2.22}$$

$$T = \frac{1}{2}\gamma_t Hr\left[(1+K_0)b_1 - \frac{1}{3}(1-K_0)b_2\right] \tag{2.23}$$

$$M = -\frac{1}{6}\gamma_t Hr^2[(1-K_0)b_2] \tag{2.24}$$

Where

γ_t: total unit weight of the soil

K_0: lateral earth pressure coefficient;

H: burial depth of the tunnel, measured from free surface to the center of tunnel;

M_c: concentrated modulus of soil which is given as follows;

$$M_c = \frac{E(1-v)}{(1+v)(1-2v)} \tag{2.24}$$

E: Young's modulus of the ground

v: Poisson's ratio of the ground

r: radius of the tunnel;

$$b_1 = 1 - \frac{(1-2v)(C-1)}{(1-2v)C+1} \tag{2.25}$$

$$b_2 = 1 + 3\frac{2F+1-2v}{2F+5-6v} - 4\frac{2F-1}{2F+5-6v} \tag{2.26}$$

This solution can be used to obtain deformations and forces due to shear wave; this can be done by using $K_0 = $ -1, which replaces the far field normal stress σ_v and $\sigma h = K_0 \sigma_v$ by a far field shear stress τ (Wang, 1993). After some mathematical manipulations, the diametric strain maximum thrust T_{max} and bending moment M_{max} can be presented in the following forms (see Figure 2.5):

$$\varepsilon_d = \frac{\Delta d}{d} = \mp\frac{1}{3}K_l F\gamma_{max} \tag{2.27}$$

$$T = \mp\frac{1}{6}K_l \frac{E}{(1+v)}r\gamma_{max} \tag{2.28}$$

$$M = \mp \frac{1}{6} K_l \frac{E}{(1+v)} r^2 \gamma_{max} \qquad (2.29)$$

Where

$$K_l = \frac{12(1+v)}{2F + 5 - 6v} \qquad (2.30)$$

E and v are the Young's modulus and Poisson's ratio of the ground, respectively; r is the radius of the tunnel; γ_{max} is the maximum free-field ground shear strain and F is the flexibility ratio defined in Equation 2-18. K_l is the full-slip lining response coefficient and is determined by Equation 2-30. The relationship between K_l and F is shown in Figure 2.6 (Wang, 1993).

According to this equation and Figure 2.7, a tunnel lining will deform less than the free field when the flexibility ratio is less than one, i.e. a stiff lining in soft soil. As the flexibility ratio increases, the lining deflects more than the free field and may reach an upper limit equal to the deformations of an opening without support.

Einstein and Schwartz (1979) revised the relative stiffness solution of previous authors (Burns and Richard, 1964; Hoeg, 1968; and Peck et al. 1972), by defining the revised compressibility and flexibility ratios as:

$$C^* = \frac{E(1 - v_l^2)r}{E_l t(1 - v^2)} \qquad (2.31)$$

$$F^* = \frac{E(1 - v_l^2)r^3}{E_l I(1 - v^2)} \qquad (2.32)$$

The revised compressibility and flexibility ratios C^* and F^* are derived based on the perforated ground during the calculation of the diametric strain of the free-field ground, while the previous compressibility and flexibility ratios C and Fare derived based on the unperforated ground. The revised compressibility and flexibility ratios C^* and F^* are related to the ratios C and F in the original relative stiffness solution by:

$$C = \frac{(1-v)r}{(1-2v)} C^*$$

(2.33)

$$F = \frac{(1-v)}{6} F^*$$

(2.34)

In the revised relative stiffness solution, Einstein and Schwartz (1979) proposed the displacements, u_r and u_θ, thrust T and moment M in the polar coordinate system, for full-slip, as follows:

$$\varepsilon_d = \frac{pr(1+v)}{E} \left\{ \frac{1}{2}(1+K_0)a_1 - (1-K_0)[(5-6v)a_2 - (1-v)] \cos 2\theta \right\}$$

(2.35)

$$u_\theta = \frac{pr(1+v)}{E} \left\{ \frac{1}{2}(1-K_0)a_1 - (1-K_0)[(5-6v)a_2 - (1-v)] \sin 2\theta \right\}$$

(2.36)

$$T = pr \left\{ \frac{1}{2}(1+K_0)(1-a_1) - \frac{1}{2}(1+K_0)(1-2a_2) \cos 2\theta \right\}$$

(2.37)

$$M = pr^2 \left\{ \frac{1}{2}(1-K_0)(1-2a_2) \cos 2\theta \right\}$$

(2.38)

where the subscripts r and θ denotes the radial and rotational coordinates in a polar coordinate system, respectively; p is the external vertical stress acting on the ground; K_0 is the lateral earth pressure coefficient; $K_0 = -1$ corresponds to pure shear loading; and

$$a_1 = \frac{C^* F^*(1-v)}{C^* + F^* + C^* F^*(1-v)}$$

(2.39)

$$a_2 = \frac{(F^* + 6)(1-v)}{2F^*(1-v) + 6(5-6v)}$$

(2.40)
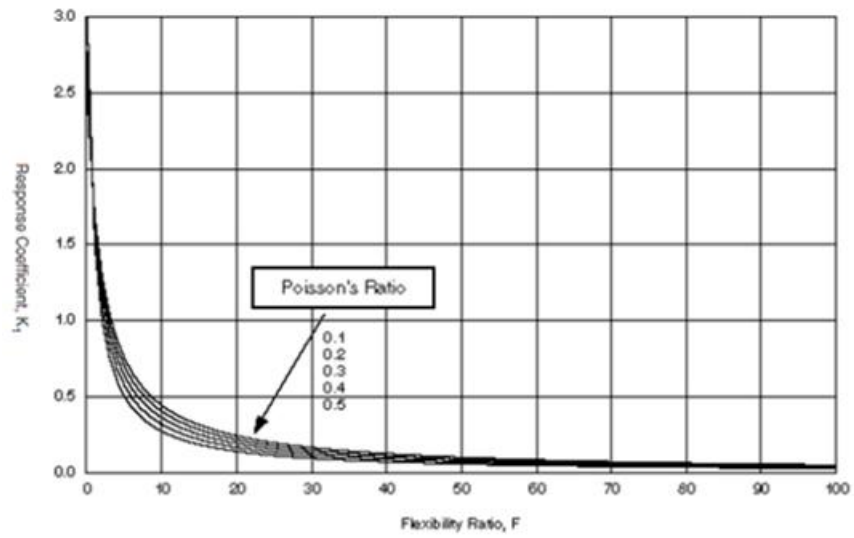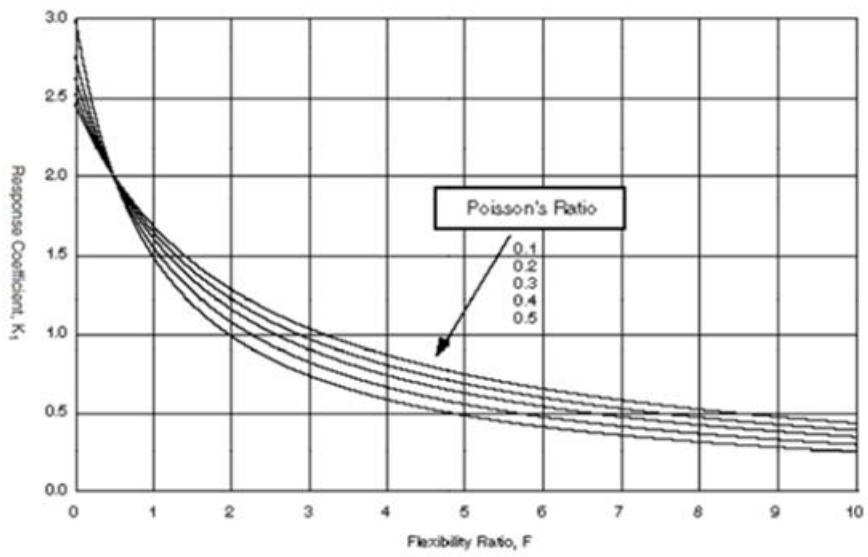
Figure 2.6 Lining response coefficient versus flexibility ratio, full slip interface, and circular tunnel (After Wang, 1993).
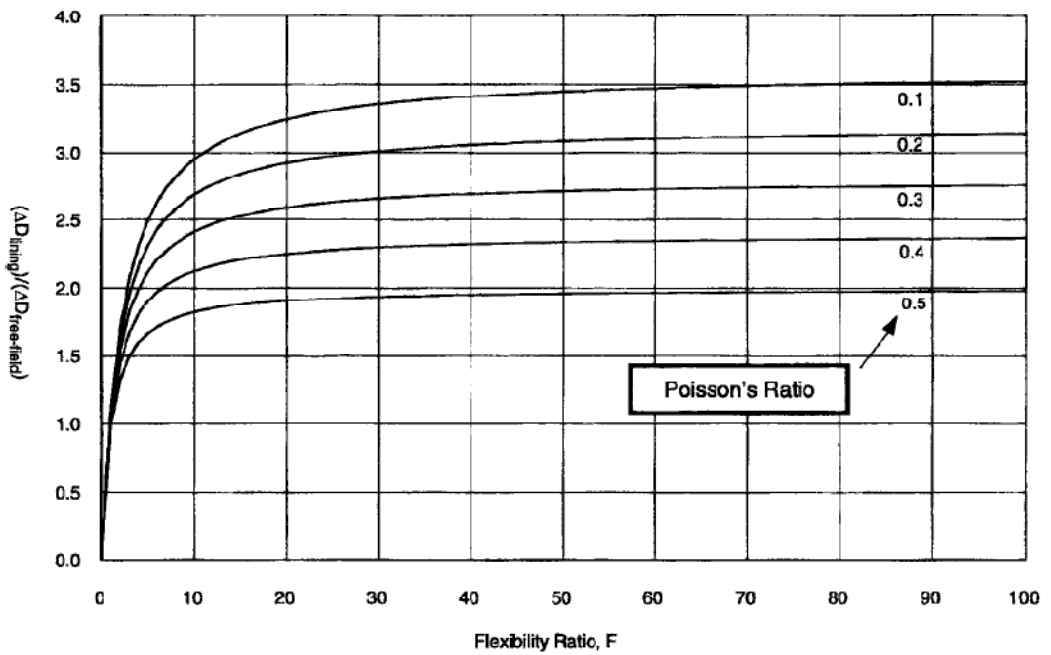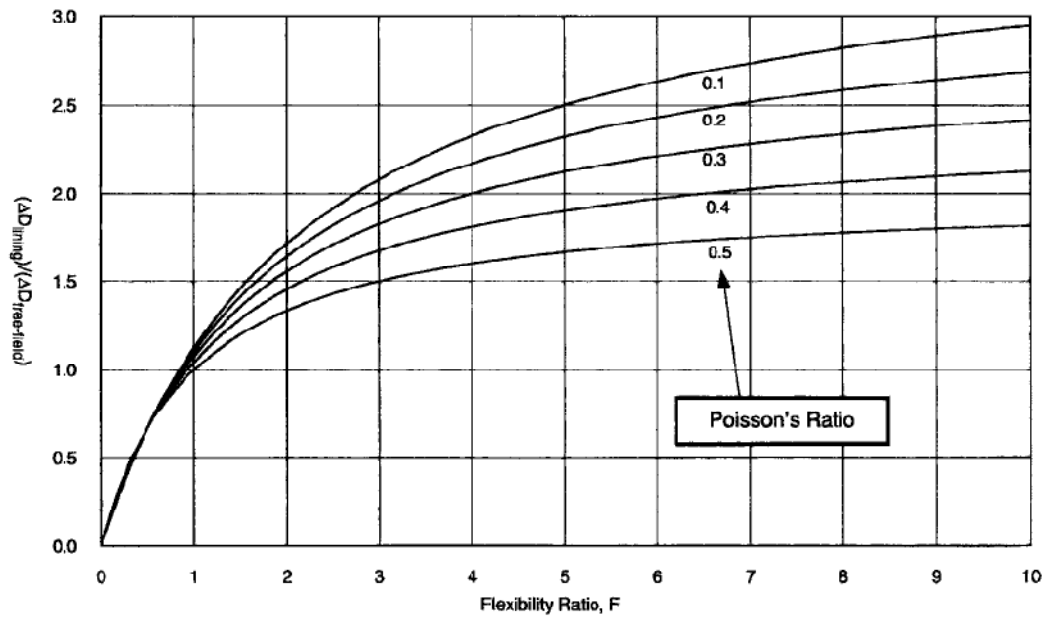
Figure 2.7 Normalized lining deflection vs. flexibility ratio, full slip interface, and circular lining (Wang, 1993).

Penzien and Wu (1998) and Penzien (2000) developed similar closed-form elastic solutions for thrust, shear, and moment for the lining of a circular tunnel. A lining-soil racking ratio was defined as:

$$R = \frac{\Delta_{structure}}{\Delta_{free-field}} \tag{2.41}$$

For circular tunnels, R is the ratio of lining and free-field diametric deformations. Assuming full slip conditions, the thrust, moment, and shear force in a circular tunnel lining are (Penzien, 2000):

$$T(\theta) = -\frac{12E_l I_l \Delta_l}{D^3(1-v_l^2)}\cos 2\left(\theta + \frac{\pi}{4}\right) \tag{2.42}$$

$$M(\theta) = -\frac{6E_l I_l \Delta_l}{D^2(1-v_l^2)}\cos 2\left(\theta + \frac{\pi}{4}\right) \tag{2.43}$$

$$V(\theta) = -\frac{24E_l I_l \Delta_l}{D^3(1-v_l^2)}\sin 2\left(\theta + \frac{\pi}{4}\right) \tag{2.44}$$

where D is the diameter of the liner; E_l and v_l are Young's modulus and Poisson's ratio of the liner, respectively; I_l is the moment of inertia of the liner; θ is the polar coordinate of the point in the liner, with origin in the horizontal direction. The sign convention for the moment and forces is shown in Figure 2.8.

The racking ratio is:

$$R = \mp\frac{4(1-v)}{\alpha+1} \tag{2.45}$$

$$\alpha = \frac{12E_l I_l(5-6v)}{D^3 G(1-v_l^2)} \tag{2.46}$$

where G is the shear modulus of the ground.
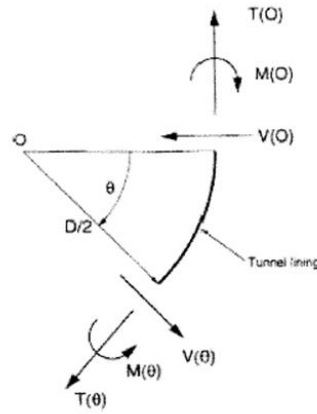
Figure 2.8 Sign convention of the force components in circular lining (After Penzien, 2000).

b)   No-slip conditions

Slip at the interface is only possible for tunnels in soft soils or cases of severe seismic intensity (Hashash et al., 2001). Full-slip assumptions under simple shear may significantly underestimate the maximum thrust. Hoeg (1968) supported this conclusion and recommend that the no-slip assumption is made in assessing the lining response. For no-slip:

$$T_{max} = \mp K_2 r \tau_{max} = \mp K_2 \frac{E}{2(1 + v)} r \gamma_{max} \qquad (2.47)$$

Where,

$$K_2 = 1 + \frac{F[(1 - 2v) - (1 - 2v)C] - \frac{1}{2}(1 - 2v)^2 + 2}{F[(3 - 2v) - (1 - 2v)C] + C\left[\frac{5}{2} - 8v + 6v^2\right] + 6 - 8v} \qquad (2.48)$$

K_2 is defined as the no-slip lining response coefficient. Expressions for deformations and maximum moment were not provided by the author. The relationship between K_2

31

and C is shown in Figure 2.9 (Wang, 1993). The figure shows that seismically-induced thrust increases with decreasing compressibility and flexibility ratios when the Poisson's ratio of the surrounding ground is less than 0.5. As the Poisson's ratio approaches 0.5, the thrust response is independent of compressibility because the soil is considered incompressible (Wang, 1993).

Einstein and Schwartz (1979), in their revised relative stiffness solution, proposed the displacements, u_r and u_θ, thrust T and moment M in polar coordinates, for no-slip, as follows:

$$u_r = \frac{pr(1+v)}{E}\left\{\frac{1}{2}(1+K_0)a_1 - \frac{1}{2}(1-K_0)[4(1-v)a_3 - 2a_2]\cos 2\theta\right\} \quad (2.49)$$

$$u_\theta = \frac{pr(1+v)}{E}\{-(1-K_0)[a_2 + (1-2v)a_3]\sin 2\theta\} \quad (2.50)$$

$$T = pr\left\{\frac{1}{2}(1+K_0)(1-a_1) + \frac{1}{2}(1-K_0)(1+2a_2)\cos 2\theta\right\} \quad (2.51)$$

$$M = pr^2\left\{\frac{1}{4}(1-K_0)(1-2a_2+2a_3)\cos 2\theta\right\} \quad (2.52)$$

where r and θ denote the radial and angular coordinates in polar coordinates, respectively; p is the external vertical stress acting on the ground; K_0 is the lateral earth pressure coefficient; $K_0 = -1$ corresponds to the pure shear loading; and

$$a_1 = \frac{C^* F^*(1-v)}{C^* + F^* + C^* F^*(1-v)} \quad (2.53)$$

$$a_2 = \frac{(F^* + 6)(1-v)}{2F^*(1-v) + 6(5-6v)} \quad (2.54)$$

$$a_3 = \frac{C^*(1-v)}{2[C^*(1-v) + 4v - 6\beta - 3\beta C^*(1-v)]} \quad (2.55)$$

$$\beta = \frac{(F^* + 6)C^*(1-v) + 2F^*v}{3F^* + 3C^* + 2C^* F^*(1-v)} \quad (2.56)$$
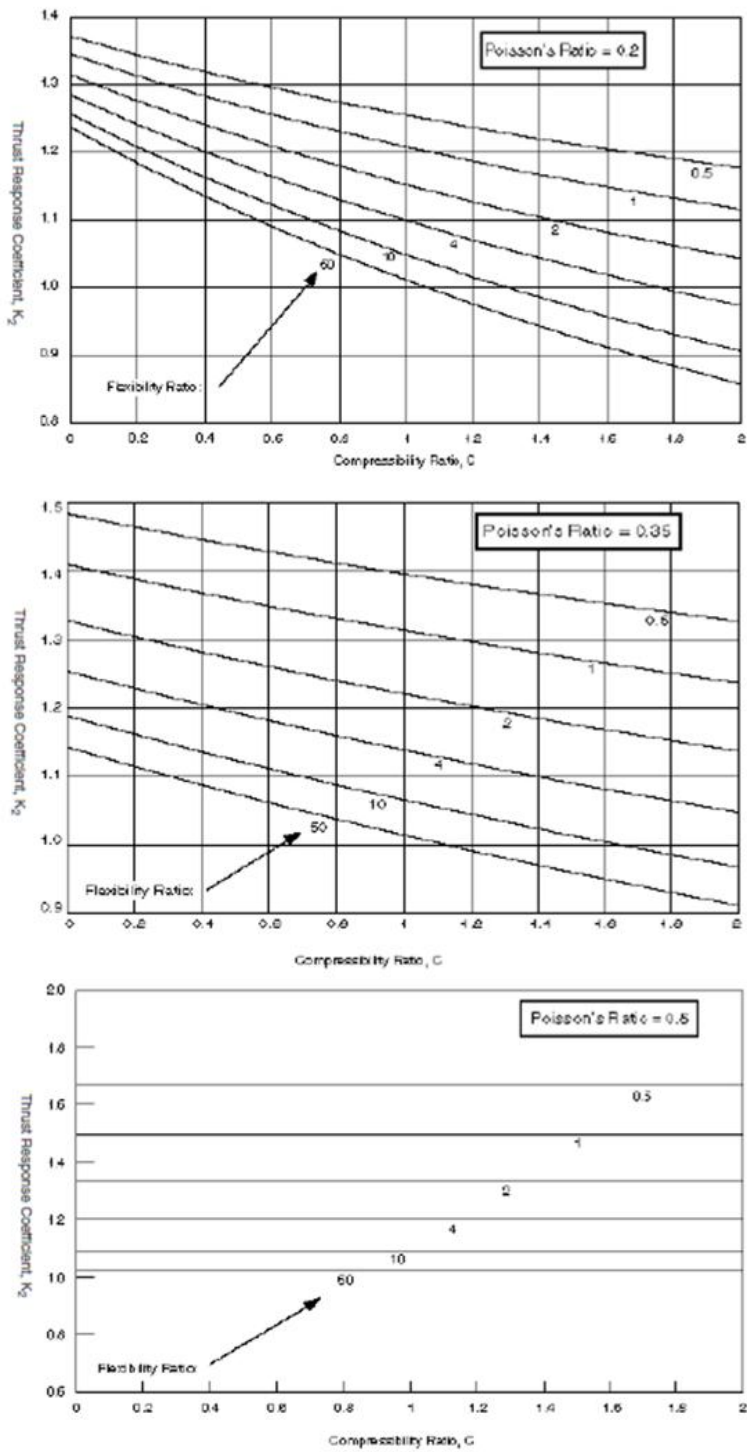
Figure 2.9 Lining (thrust) response coefficient versus compressibility ratio no slip interface for circular tunnel (After Wang, 1993).

33

Penzien (2000) proposed, for no-slip conditions:

$$R = \frac{\Delta_{structure}}{\Delta_{free-field}} \tag{2.57}$$

$$T(\theta) = -\frac{24E_l I_l \Delta_l}{D^3(1 - v_l^2)}\cos 2\left(\theta + \frac{\pi}{4}\right) \tag{2.58}$$

$$M(\theta) = -\frac{6E_l I_l \Delta_l}{D^2(1 - v_l^2)}\cos 2\left(\theta + \frac{\pi}{4}\right) \tag{2.59}$$

$$V(\theta) = -\frac{24E_l I_l \Delta_l}{D^3(1 - v_l^2)}\sin 2\left(\theta + \frac{\pi}{4}\right) \tag{2.60}$$

where,

$$R = \mp\frac{4(1 - v)}{\alpha + 1} \tag{2.61}$$

$$\alpha = \frac{24E_l I_l(3 - 4v)}{D^3 G(1 - v_l^2)} \tag{2.62}$$

CHAPTER 3

A CASE STUDY ON SEISMIC BEHAVIOR OF BOLU TUNNELS

3.1 Introduction

Bolu Tunnels form crucial part of the Trans European Motorway (TEM) connection between İstanbul and Ankara. These tunnels are located between Asarsuyu Valley and Elmalık Village in stretch-II of the Gümüşova-Gerede section of the Anatolian Motorway, which interconnects Turkey to Europe (Figure 3.1). The twin tunnels are more than 3 km in length and designed to carry three-lane directional traffic. The vehicular clearance is 5.0 m and the width of the tunnel is determined through the requirements of three lanes, each 3.75 m wide and the safety walks, each 0.75 m wide for each tube. These high standards necessitate an excavation of cross-section in excess of 200 m^2 for each tube (Figure 3.2). The tunnel excavation geometry is an arc section with 15 m height and 16 m length in cross-sectional direction. A 40 m wide rock pillar separates both tubes. Vehicular and pedestrian cross adits at regular distances connect the tubes.
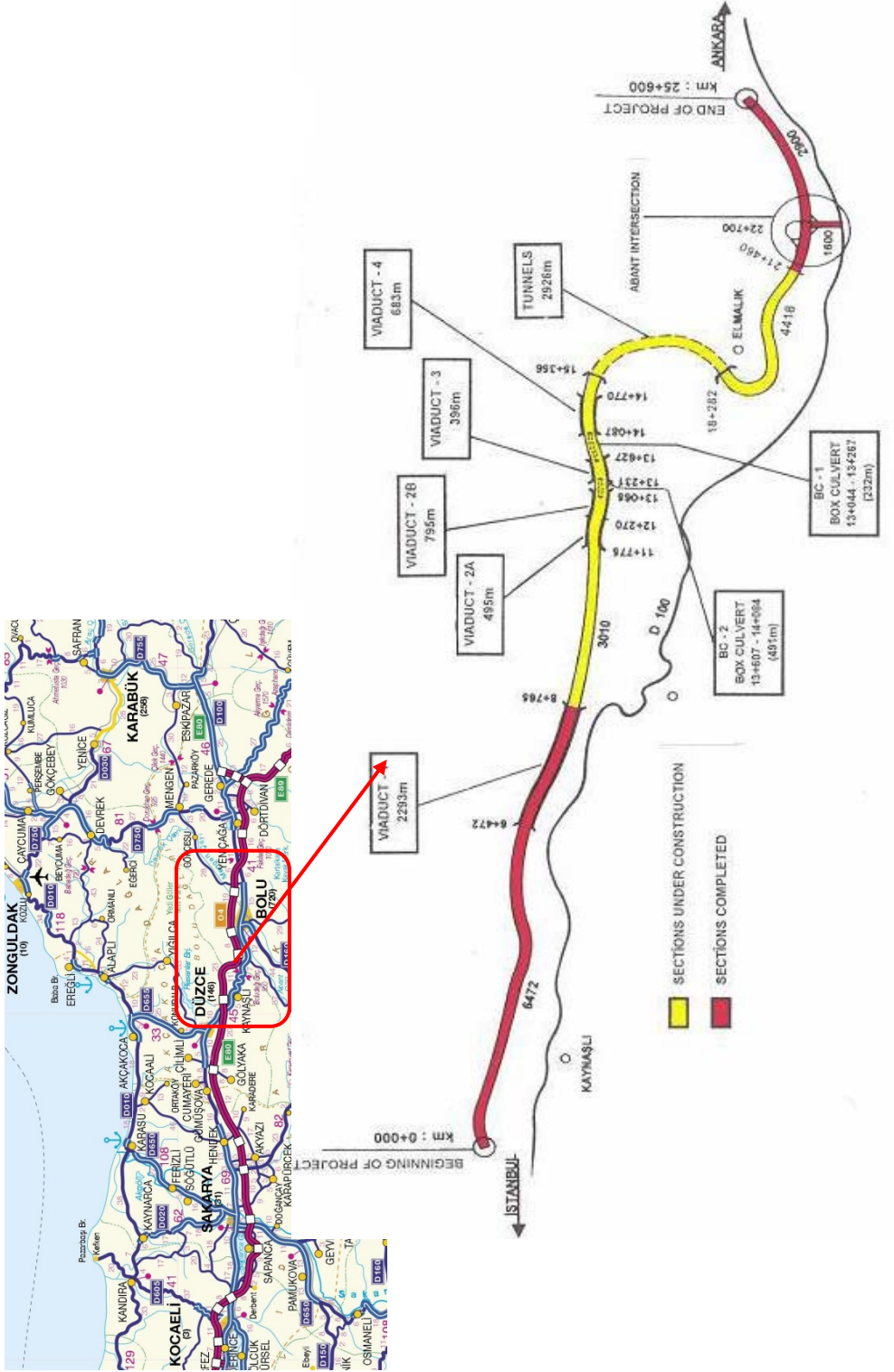
Figure 3.1 Project Location (Yüksel Project Co.).
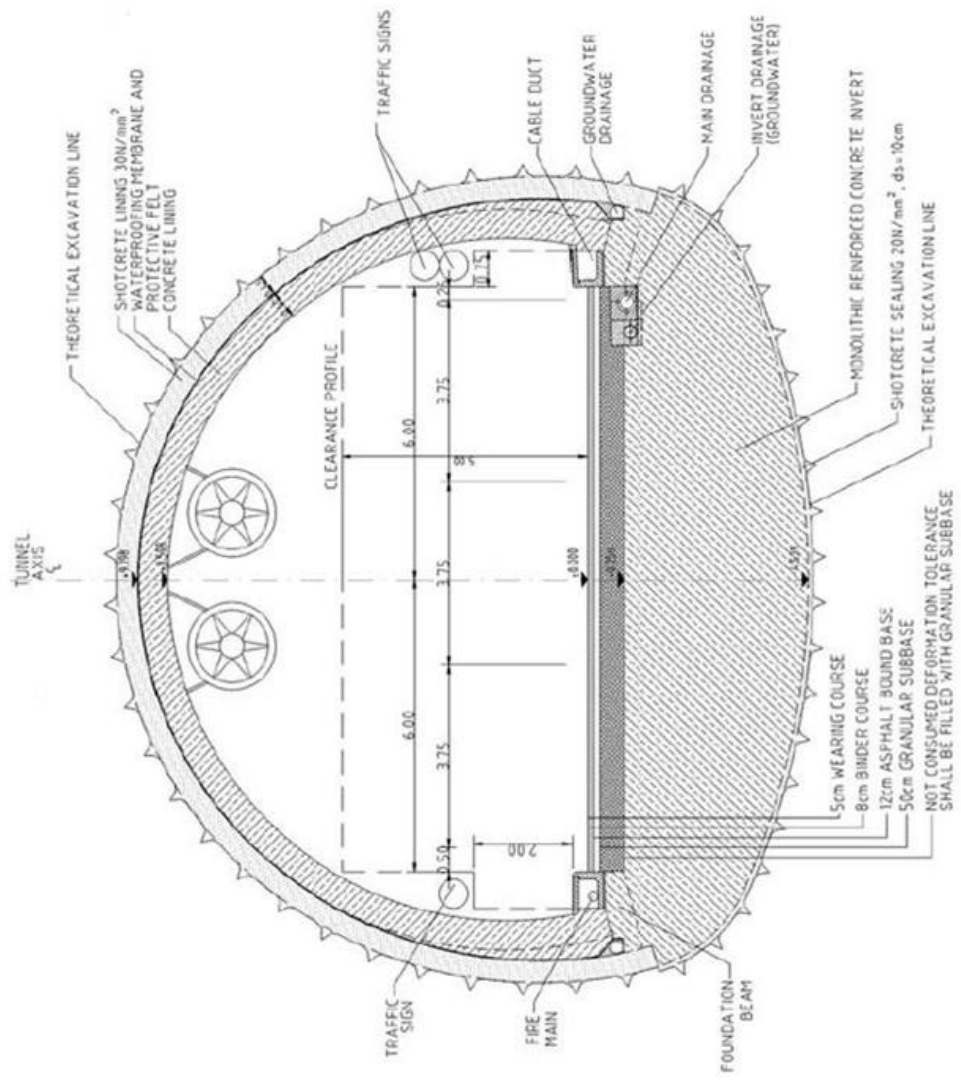
Figure 3.2 A typical cross section of the Tunnel section (Technical Drawing TN/TUG/D/LO/208 Rev.1).

3.2 History of the Bolu Tunnels project

Tunnel excavation started in 1993 from the Asarsuyu portal in the west and 1994 from the Elmalık portal in the east. NATM principles according to Austrian standard ÖNORM B2203 with some modifications, to overcome the local difficulties, are used in the design. For rock, five support classes were considered (A1, B1, B2, C1 and C2), for the portal stretches two (L1 and L2). Bolu Tunnels are excavated using conventional backhoes and other earth moving equipment.

The excavation was characterized by large, constant movements, which could only be stopped or at least reduced after ring closure. More than 1 m deformations of shotcrete lining brought extensive reprofiling. Repeated invert heave stood the replacement of the installed shotcrete invert by a deep monolithic concrete invert. During 1996, the first major low angle fault gouge was encountered at the excavation from the Elmalik side, after approximately 300 m of advance. This zone could be crossed with the right tube, although with significant difficulties. Excavation of the left tube in this fault gouge zone caused massive movements and damaged the already excavated right tube. Correspondingly, the excavation in the fault gouge zone was decided to be led by a short pilot tunnel. Severe cracking of the shotcrete lining was monitored in the pilot tunnel lining, in the time of excavation of the main tube top heading. Approximately similar problems were experienced when following the top heading excavation with bench and invert. Failure of the top heading temporary invert followed cracking of the top heading shotcrete. Collapse was avoided with backfilling the top heading. Then, this region was remined by using two 5 m diameter circular pilot tunnels per tube at bench level. After the excavation of these two bench pilot tunnels, they were backfilled with reinforced B40 concrete to provide abutments for the main tunnels' top heading. Finally, to complete the tunnels, a 70 cm shotcrete top heading lining was excavated and the ring closed by following 15 m with a massive monolithic invert. In this manner, the fault gouge zone could be passed successfully until early 1998.

Severe invert heave was encountered in the first tube for a stretch extending up to 200 m backwards from the face in the late 1997. Simultaneously, radial deformations at the face exceeded 1.2 m. As a result, further advance of the two Elmalik drives was stopped and a comprehensive review of excavation and support methods was carried out.

3.3 Investigation Program

Before the new design solutions could be developed, it was considered as important to obtain more distinctive geological description of the sections to be excavated. A 4.6 m inner diameter pilot tunnel was advanced both from Elmalik and Asarsuyu sides to clarify the geological formations. Moreover, several surface investigation boreholes were drilled and an extensive laboratory testing program was performed, including soil classification, shear box tests (CU and CD) including residual strength measurement, triaxial tests (UU and CU) plus pore water pressure measurement, consolidation tests as well as swelling potential and swelling pressure measurements. Pressuremeter and dilatometer tests were carried out both inside of the pilot tunnel and in the excavated sections of the main drives for the determination of stiffness parameters. Various monitoring stations consisting of pressure cells, shotcrete strain meters, piezometers and extensometers were set up in the pilot tunnel. The results of this extensive investigation program provided for a detailed classification of rock mass into distinct lithological units and determination of the design parameters associated with each unit.

3.4 Post Earthquake Condition of the Tunnels

The advance of Elmalik drives began again, after the investigation program and the determination of design solutions for the difficult ground conditions. The two major earthquakes of 17 August 1999 Marmara and 12 November 1999 Düzce occurred before the tunnels completed.
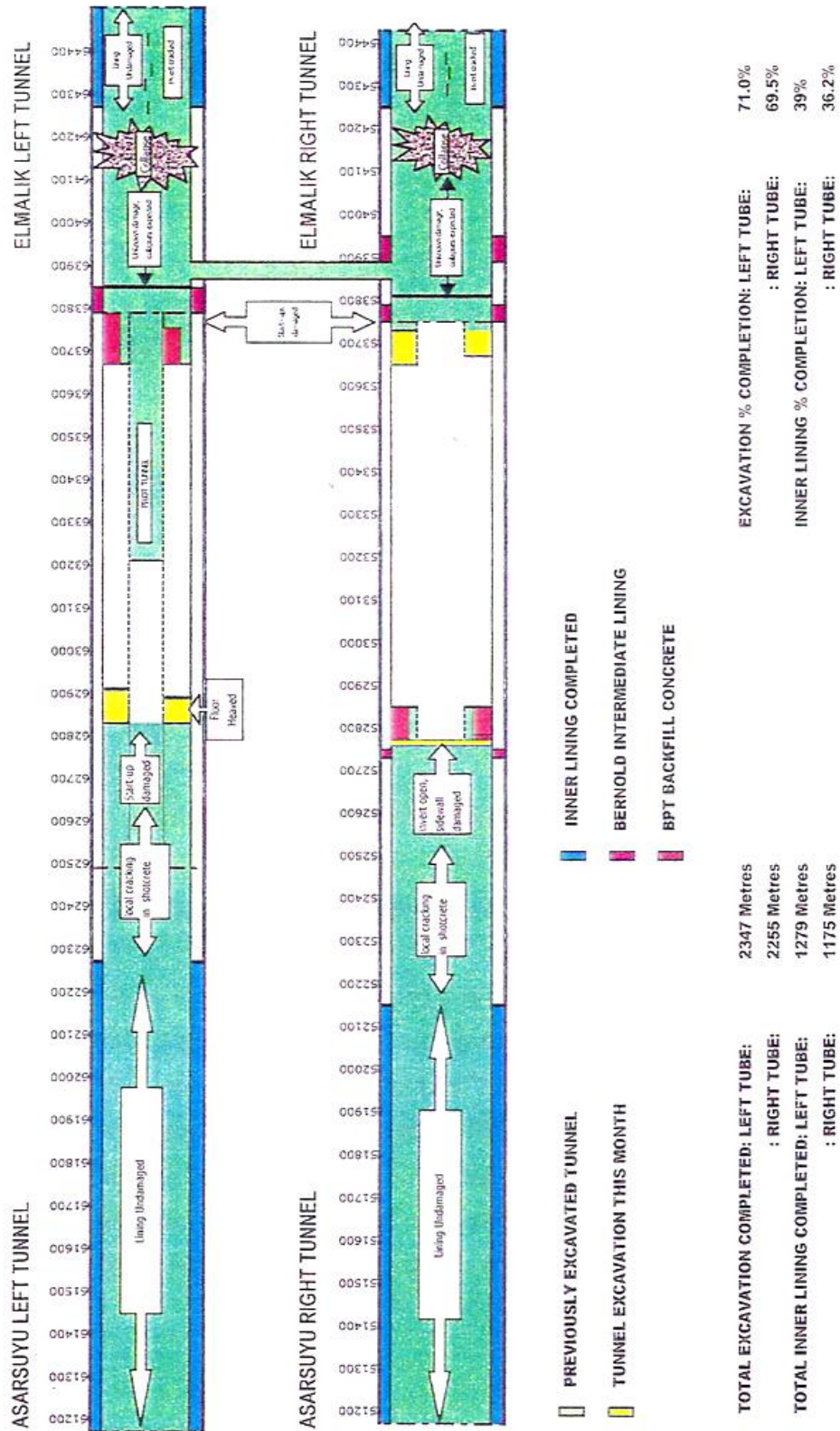
Figure 3.3 Bolu Tunnels after Earthquake Collapse (Çakan, 2000)

The first earthquake, August 17, 1999, was reported with a magnitude of $M_w = 7.4$ have had minimal effect on the Bolu Tunnels. The epicenter of the earthquake was located about 150 km west of the construction site and very close to İzmit. The closure rate of one monitoring station was reported to have temporarily increased to an accelerated rate for a period of approximately 1-week, and then become stable again. Additionally, several hairline cracks, which had previously been observed in the final lining, were continuously monitored. However, no additional movements due to earthquake were observed (Çakan, 2000).

The second earthquake, November 12, 1999, was reported with a magnitude of $M_w = 7.2$ caused the collapse of both tunnels starting at 300 m from their eastern portal (Figure 3.3). Epicenter, Düzce, is only about 20 km far from the site. At the time of the earthquake, an 800 m section had been excavated, and a 300 m section of unreinforced concrete lining had been completed. The collapse took place, in clay gouge material in the unfinished section of the tunnel. The section was supported with shotcrete and bolt anchors (Çakan, 2000). Cracks of various widths and patterns were observed in other parts where inner liner was constructed.

Although several mechanisms have been proposed to explain the collapse of the tunnel including strong motion, displacement across the gouge material, and landslide, further and detailed studies are required to determine the actual reason of collapses.

The excavations began again in late 2001 with the realigned route after further studies (Figure 3.4). In the middle of 2005, excavation was completed in both tunnels.
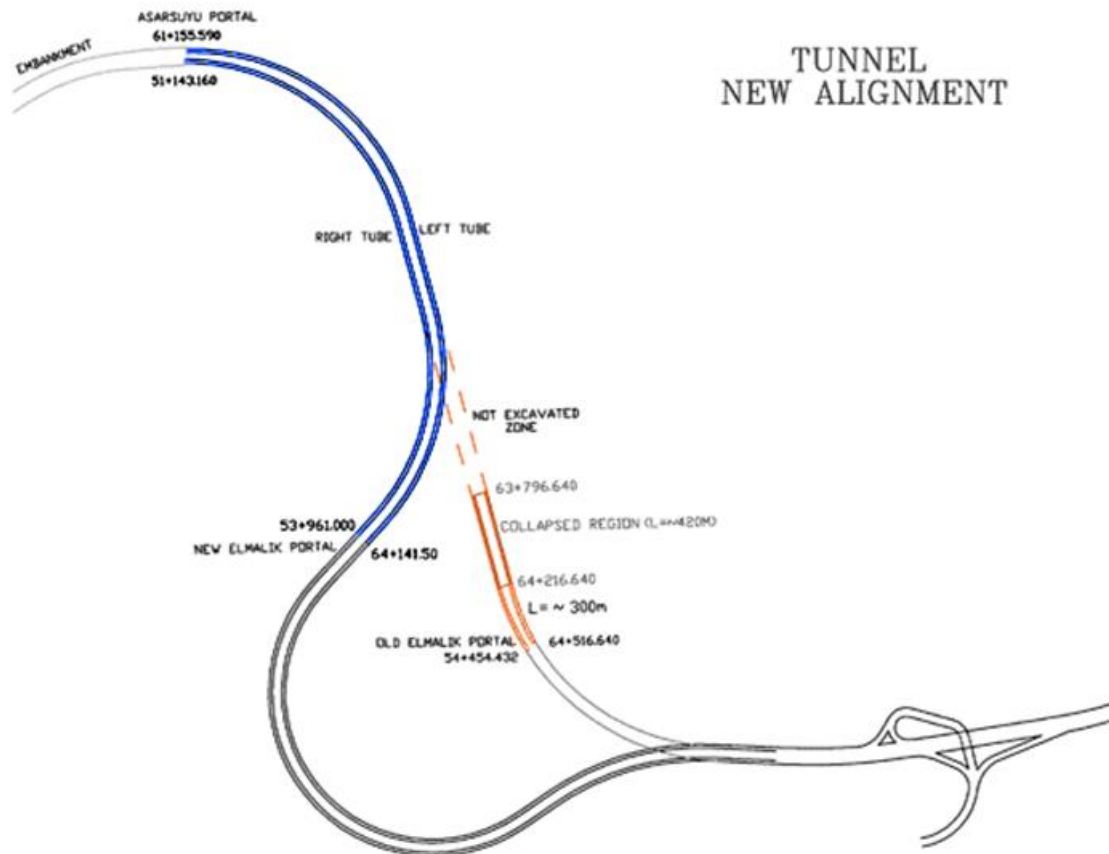
Figure 3.4 New Tunnel Alignment (Aşçıoğlu, 2006).

3.5 **Geology of the Area**

The project lies about 10 km north of the main branch of North Anatolian Fault Zone (NAFZ), which is the plate tectonic boundary between the Eurasian plate on the north and the Anatolian block on the south (Figure 3.5). The fault is described by steep, E-W striking strike-slip faults crossing the tunnel alignment. The fault is active with movements of approximately 15 mm per year in the Bolu region (Unterberger, W. and Brandl, H., 2000). The tectonic environment was characterized by thrust faulting. This lead to the formation of low-angle fault gouge zones, some of them up

to 300 m wide. The rock mass consists of conglomerates, arkoses, sandstones and marly shales, limestones and dolomitic limestones. Tectonic movement have sheared and displaced the various rock types, such that one unit rarely can be found continuously over a stretch exceeding a few hundred meters in length.

Following steps have been performed in the course of geological and geotechnical studies:

i)   Fault zones and landslides are determined and evaluated stereoscopically with using a scale of 1:10000

ii)   Geological mapping carried out by using a scale of 1:5000 for the whole corridor. All natural rock outcrops have been inspected and evaluated on lithology, weathering, discontinuities etc.

iii)   A subsurface investigation program has been set up following the results and the interpretation of the previous two steps. In the course of this program 33 investigation drillholes with a total length of 2200 m performed with continuous coring has been executed between summer 1990 and winter of 1991. Many of the boreholes were in very difficult access conditions. Also, difficult ground conditions exist in the field due to the heavy tectonism in the vicinity of the NAFZ. In the portal locations some of the drillholes have been equipped with inclinometer tubes to allow the monitoring of possible movements and their change in time. Also, many of the drillholes were equipped with open standpipe type piezometers to allow long term water level monitoring.(Üçer, 2006)

Figure 3.5 Tectonic setting of Turkey (Bogaziçi University, 2000) (Modified after Nafi Toksoz of MIT/ERL).

Over the NAFZ, the Anatolian block moves westward relative to the Eurasian plate. The general geological situation (after Niehof, 1976) is as follows:

The basis is built up by the Northern Anatolian polymetamorphic crystalline basement. Its age is considered to be most probably Precambrian.In the Silurian, Devonian and Carboniferous ages conglomerates, arcoses, sandstones, greywackes and marly shales, limestones and dolomitic limestones have developed.The crystalline basement rocks consist predominantly of granites, granodiorites, quartzdiorites and diorites and metamorphic rocks of the amphibolite fazies as migmalites, gneisses and amphibolites. This ridge of crystalline basement rocks has

been uncovered in the older Palezoic, in the younger Palezoic it divided a northern continental basin from a southern marine basin.This development has been affected by a variscian low grade metamorphism (greenshist fazies) so that the former sediment cover has been changed to marbles, phyllites, schists etc.In the Tertiary age further conglomerates, breccias, sandstones, marls, limey marls, siltstones and nummulithic limestones have been deposited, as well as evaporates as gypsum have been generated. Miocene dykes and local tuffites have developed.

All these rocks have been heavily affected by the North Anatolian Fault Zone, which in the section of Yeniçağa-Gerede shows a post Pliocene right lateral total strain of about 35 km, being an average of 3.5 to 7.0 mm each year. On the Elmalik side of the tunnel alignment as a result of heavy faulting, the more competent rock mass blocks (crystalline basement, meta-sediment rock series and the competent parts of the flyschoid sequence) do rarely exceed a few hundreds of meters in length, being "embedded" in fault gouges as a kind of large scale matrix. Geological profile for the tunnel is given in Figure 3.6.

3.5.1   Engineering Geology

The whole area of the tunnel alignment is heavily affected by the North Anatolian Fault Zone as mentioned before. Discontinuity data (orientation of bedding planes, schistosity, joints and slickensides) have been collected during the geological field mapping campaign from natural rock outcrops along the tunnel alignment. Five different homogeneous areas concerning structural features have been distinguished by statistical evaluation of these discontinuity data (Geoconsult, Elmalik Tunnel Final Design Geological Report). Proceeding from North to South these are:

In the first homogeneous area the prevailing schistosity shows a steeply inclination towards north to north-northwest and displays fold structures with occasional overturned limbs. Three major joint sets have been identified. The first trends to WSW, the second trends to WNW and the third trends N-S, all of them dipping very steeply to vertically. Two sets of slickensides occur, one of them trends to NE

dipping steeply to almost vertically, the second one trends E-W with almost vertical dipping.

The second homogeneous area is located in the metasediment series. The bedding displays a mean strike direction from WNW to ESE with almost vertical dip angles. The joint distribution shows irregular trends however with steep dip angles in general. Slickensides show almost vertical dip and trend WNW to NW.

The third homogeneous area is located in the northern part of the "flyschoid sequence" (sedimentary rock series). The bedding shows various minor maxima with medium steep to quite gentle dip angles striking in different directions. The jointing varies between gentle to almost vertical dip angles with irregular trends. Slickensides usually approximately trend in NE-SW directions with steep to vertical dip angles.

The fourth homogeneous area is situated in the southern area of the "flyschoid sequence". The bedding shows a strict trend in E-W directions and has steep to very steep dip angles towards north and south since being folded. Three joint sets are distinguished. One of them strikes SW, the second towards NW, and the third in N-S direction. All three sets have very steep to vertical dip angles. Two sets of slickensides have been identified, one of them striking WNW, the second trends NE-SW. Dip angles vary from steep to vertical.
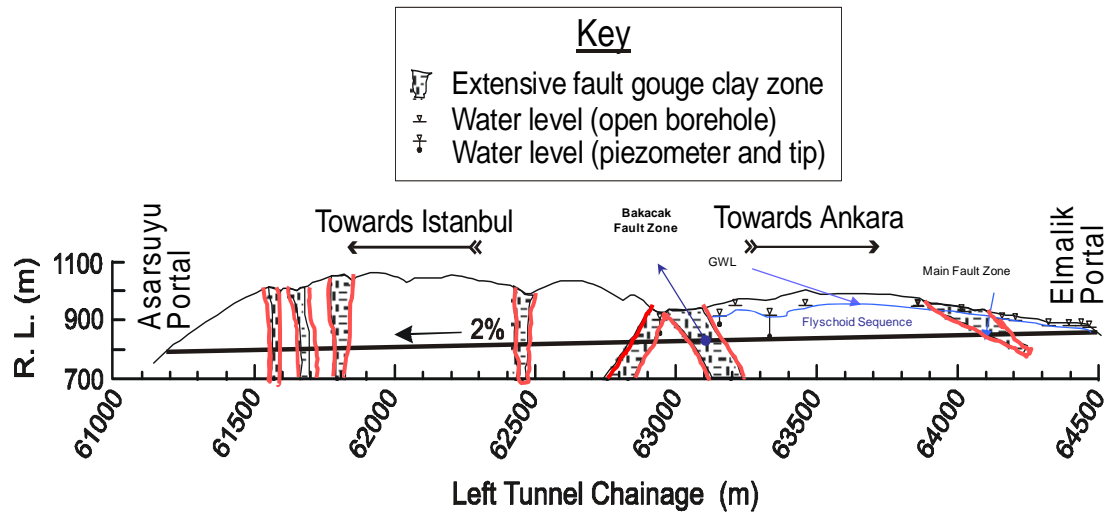
Figure 3.6 Geological profiles along the tunnels (Yüksel Project Co., 2004).

The fifth homogeneous area is in the more competent rocks of the "flyschoid sequence" which are frequently surrounded by fault gouge material. The bedding plane means dips gently to medium steeply towards NE. Two joint sets have been monitored, one of them dips medium steeply towards NW, the second dips medium steeply towards SW. The evaluation of the slickenside data did not lead to a significant maximum.

3.5.2 **Fault Gouge**

Faults are shear planes and commonly contain the debris from the frictional contact of the two surfaces. In strong rocks, material is fragmented to create a zone of crushed rock or fault breccias. In weaker rocks, the material in the fault plane can be reduced to a very fine clay-size infill known as fault gouge. Over time, crushed rock can react with subsurface fluids to produce a variety of other secondary minerals, many of them in the "clay" family. Often, fault gouge is a mixture of crushed rock and several of these fine-grained alteration minerals. However, some fault gouge may be composed of finely-ground particles of just one principle type of mineral.

47

The "gouge zone", where the grinding and shearing takes place, may be up to a kilometer wide in large faults.

Gouge is very significant in engineering terms, since the shear strength of the discontinuity is that of the weak gouge rather than the wall rock. From the engineering point of view, the properties of fault gouge are similar to soft soil in soil mechanics.

CHAPTER 4

ANALYSES FOR C2 SECTION

4.1 Finite Element program PLAXIS 2D

The finite element software PLAXIS, which is utilized in the analyses performed in this study, has been developed specifically for the analysis of deformation and stability in geotechnical engineering applications. The simple graphical input procedures enable a quick generation of complex finite element models, and the enhanced output facilities provide a detailed presentation of computational results. The calculation itself is fully automated and based on robust numerical procedures. Soils and structures are often subjected not only to static loads due to constructions in and on the ground surface but to dynamic loads as well. With the PLAXIS dynamic analysis module the effects of vibrations on soils can be analyzed. In modeling the dynamic response of an earth structure, the inertia of the subsoil and the time dependence of the load are considered. Also, damping due to material and/or geometry is taken into account. Initially the Linear-elastic model can be utilized for the simulation of the dynamic effects, but in principle any of the available soil models in PLAXIS can be used.

4.2 Limitations of the Study

The seismic response of the Bolu Tunnels is analyzed with 2-D plane strain finite element model. To be able to represent the 3-D structural response reasonably in a 2-D model, the so called relaxation factors are to be used in modeling the section. Use of relaxation factors involve reduction of stiffness of a certain part of the material within the tunnel section in order to represent 3-D stress state in 2-D. Because the study is actually related to the seismic response of the tunnel section, these factors are selected without performing any axisymetric analyses. Some minor faults crossing the tunnel in longitudinal direction, which could possibly have affected the seismic behavior of the tunnel, are not considered in 2-D analyses. Also, the model is

generated with a single tube tunnel section. Hence, the possible interaction effects between the two tunnels are not taken into consideration when analyzing the section.

The soil response is modeled using Mohr-Coulomb soil model. The elastic-plastic Mohr-Coulomb model in PLAXIS requires five input parameters: E and ν for soil elasticity, φ and c for soil plasticity and ψ as the angle of dilatancy. This Mohr-Coulomb model represents a 'first-order' approximation of soil or rock behavior. It is recommended to use this model for an initial analysis of the problem considered. For each element a constant average stiffness is calculated. Due to this constant stiffness, computations tend to be relatively fast.

Although the increase of stiffness with depth can be taken into account, the Mohr-Coulomb model does neither include stress dependency nor stress-path dependency of stiffness or anisotropic stiffness. In general, stress states at failure are quite well described using the Mohr-Coulomb failure criterion with effective strength parameters φ´ and c´.

4.3 Analyzed Case of Bolu tunnels

In the analyses, the section which aligns in Asarsuyu left tunnel, km: 62+050, called C2 was considered (Figure 4.1). At this part of the tunnel, lining remained undamaged following 17 August 1999 Marmara and 12 November Düzce earthquakes.

CLASS C2
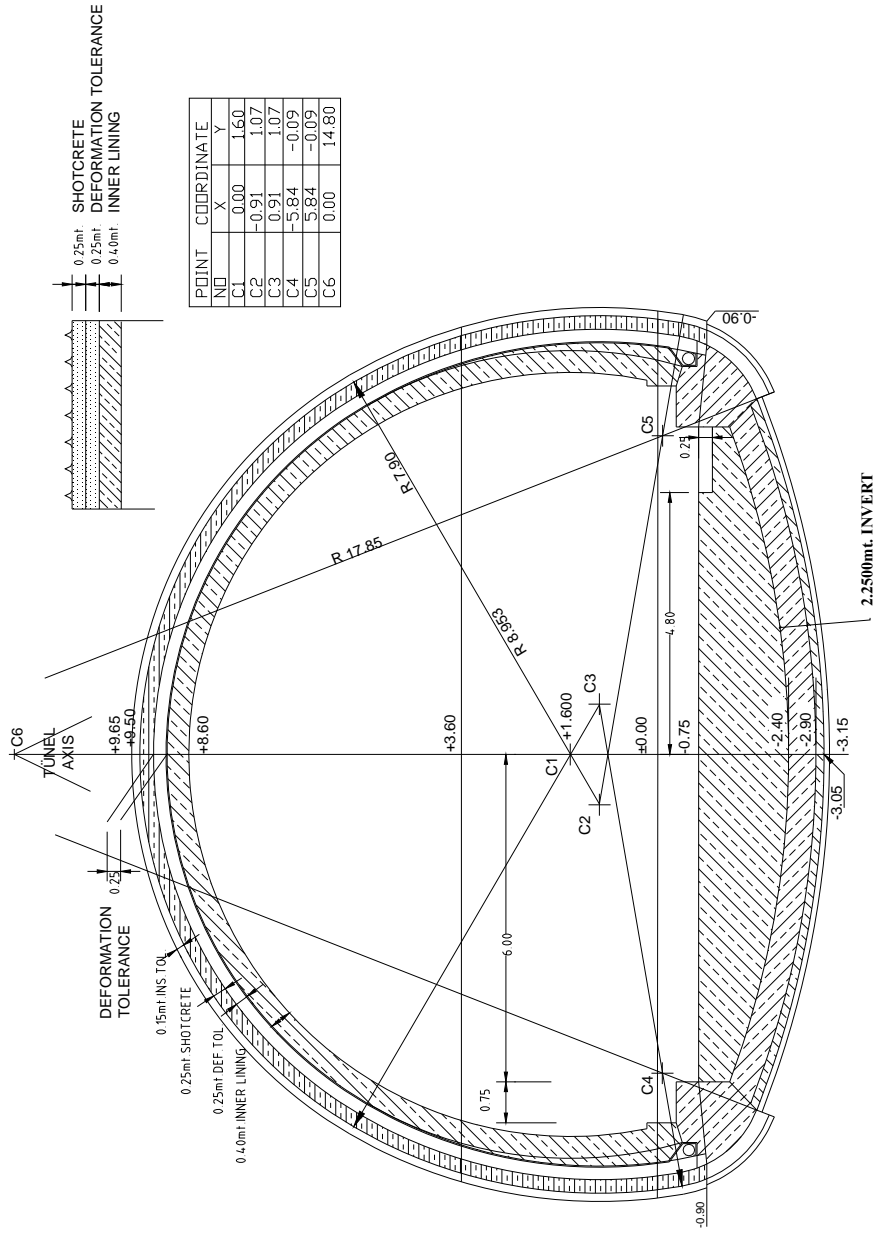
Figure 4.1 Cross-section of section C2 (Yüksel Project Co., 2000).

51

In the modeled section, the thickness of cover is about 225 m above the tunnel section. According to the piezometric and surface borehole readings, maximum groundwater level over the crown is 80 m (Üçer, 2006).
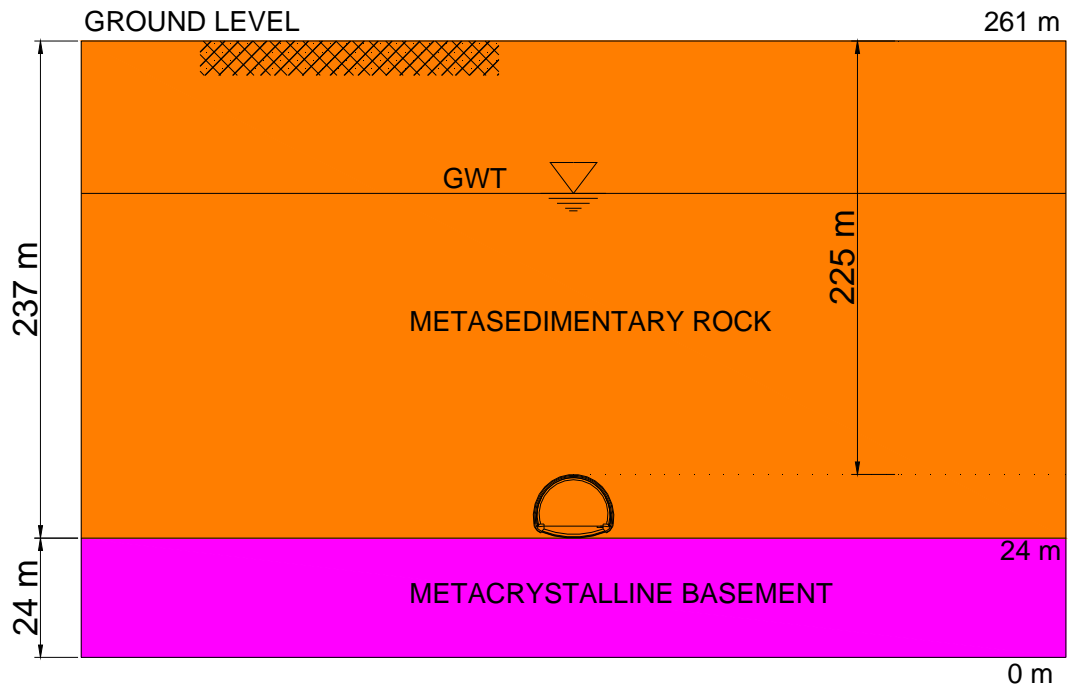
Figure 4.2 Modeling definition of the selected section Km: 62+050 (not to scale).

The geological profile of the given section and modeling geometry are defined as given in Figure 4.2. As can be observed from the figure, the upper part of the profile mainly consists of metasedimentary rock and below there exists metacrystaline formation. Geological definitions of these formations are:

Metasedimentary Rock: Highly to completely weathered, heavily slickensided, folded, crushed, bedded and locally laminated complex metasediments sequence consisting of grey to black coloured soft clay, shale and phyllite fault gauge matrix

sub-rounded slightly weathered strong fragment of whitish to black coloured of metasediment fragments.

Metacrystaline Basement: Slightly to completely weathered, fractured very weak to strong, crushed and meta-quartzdiorite, meta-granite and amphibolites, slickensided. Water conditions are dry to damp.

The tunnel section remained within the metasedimentary rock which consisted of saturated soft clay material and fault clay gauge zone. Thus, the analyses were performed with the assumption of undrained behavior of the medium. This assumption is also utilized for the dynamic analyses.

4.4 Input Parameters for the Analyses

The parameters which are used in the analyses are taken from various sources including Aygar, 2000, Şimşek, 2001 and the report which is prepared by Geoconsult (2002).

The section of the Bolu Tunnels selected for the case study here is bored through the Metasediment formation and the basement is Metacrystaline. The following relevant key material parameters are defined for these lithological units in literature:

For Metasedimentary Rock:

$\gamma = 20$ kN/m^3
$\gamma_{sat} = 22$ kN/m^3
Friction angle, $\varphi = 25 - 39^o$
Cohesion, $c = 25 - 63$ kPa
$E = 0.2\sigma_v$ Mpa

For Metacrystaline Basement:

$\gamma = 20 - 21$ kN/m^3
$\gamma_{sat} = 22 - 23$ kN/m^3
Friction angle, $\varphi = 15 - 25^o$

Cohesion, c = 25 – 200 kPa

E = 250 – 600 Mpa

Geotechnical parameters used in the analyses considering undrained behavior are listed below:

For Metasedimentary Rock:

$\gamma = 20$ kN/m^3

$\gamma_{sat} = 22$ kN/m^3

$\varphi = 28^o$

$\psi = 5^o$

c = 50 kPa

E = $0.2\sigma_v$ Mpa

$\nu = 0.3$

For Metacrystaline Basement:

$\gamma = 20$ kN/m^3

$\gamma_{sat} = 22$ kN/m^3

$\varphi = 18^o$

$\psi = 5^o$

c = 50 kPa

E = 533 Mpa

$\nu = 0.3$

Shotcrete:

Thickness = 25 cm

E = 4 000 000 kPa (Fresh Concrete)

E = 15 000 000 kPa (Hard Concrete)

$\gamma = 24$ kN/m^3

Inner lining:

Thickness = 40 cm

E = 30 000 000 kPa

γ = 24 kN/m^3

ν = 0.4

Monolithic concrete invert:

E = 27 500 000 kPa

γ = 24 kN/m^3

ν = 0.4

Bolts :

IBO R32S type

P_{ult} = 360 kN

EA = 9.802E+04

SN type

P_{ult} = 370 kN

EA = 1.062E+05

4.5 Model Definition and Geometry

The geometry of the section modeled in this study is shown in Figures 4.1 and 4.2. As mentioned before, only one of the twin tunnels is modeled to estimate the seismic response during the Düzce earthquake. The ground cover over the tunnel section is not modeled as a whole, but the part of overburden is applied to the model as a uniform distribution of pressure of 1440 kPa (Figure 4.3). This approach will not only reduce the model dimension, but also decrease the solution time particularly in analyzing the dynamic response of the section. Mesh dimensions should be appropriately defined, to prevent the boundary effects on the model response.

Meissner (1996) recommended model dimensions for 2-D modelling of tunnels. Accordingly, it was suggested to use (4 - 5) diameter (D) from the tunnel centerline to the vertical boundaries, and (2 – 3) D from tunnel center line to the bottom of the model. Based on these suggestions, the dimensions of the geometry are fixed as 190 m in vertical direction and 200 m in lateral direction.

Mesh size is selected as coarse to decrease the run time in the model, but it is refined to provide sufficient sensitivity in the surrounding of the tunnel where stress concentration are expected to occur. As seen from the Figure 4.4, mesh size becomes finer from outside towards inside of the model, approaching to the tunnel section. The generated mesh of the models composed of the 6-noded triangular elements to decrease run time in dynamic analysis, instead of 15-noded elements. PLAXIS uses Gaussian integration scheme within the triangular elements. For the 6-noded elements the integration is based on 3 sample points (PLAXIS 2D Scientific Manual, version 8.2). In the model, shotcrete, inner lining as well as the monolithic concrete invert are modeled with 6-noded triangular element types.

At the model boundaries, except the top of the model, standard fixities were applied. Top boundary of the model is left free with the uniform surcharge load being applied. Besides these assignments, the prescribed acceleration time history is defined at the bottom of the boundary to impose the earthquake shaking.

As indicated in the previous section, Mohr-Coulomb model is used for the geological properties of the medium. Bolts are modeled as geogrid material with elastoplastic model. Next, linear elastic continuum material model is assigned to the shotcrete and monolithic concrete invert sections to simulate the concrete behavior. Finally, for modeling the inner lining, elastoplastic plate elements are used with 0.25 m equivalent lengths to represent the tunnel section.
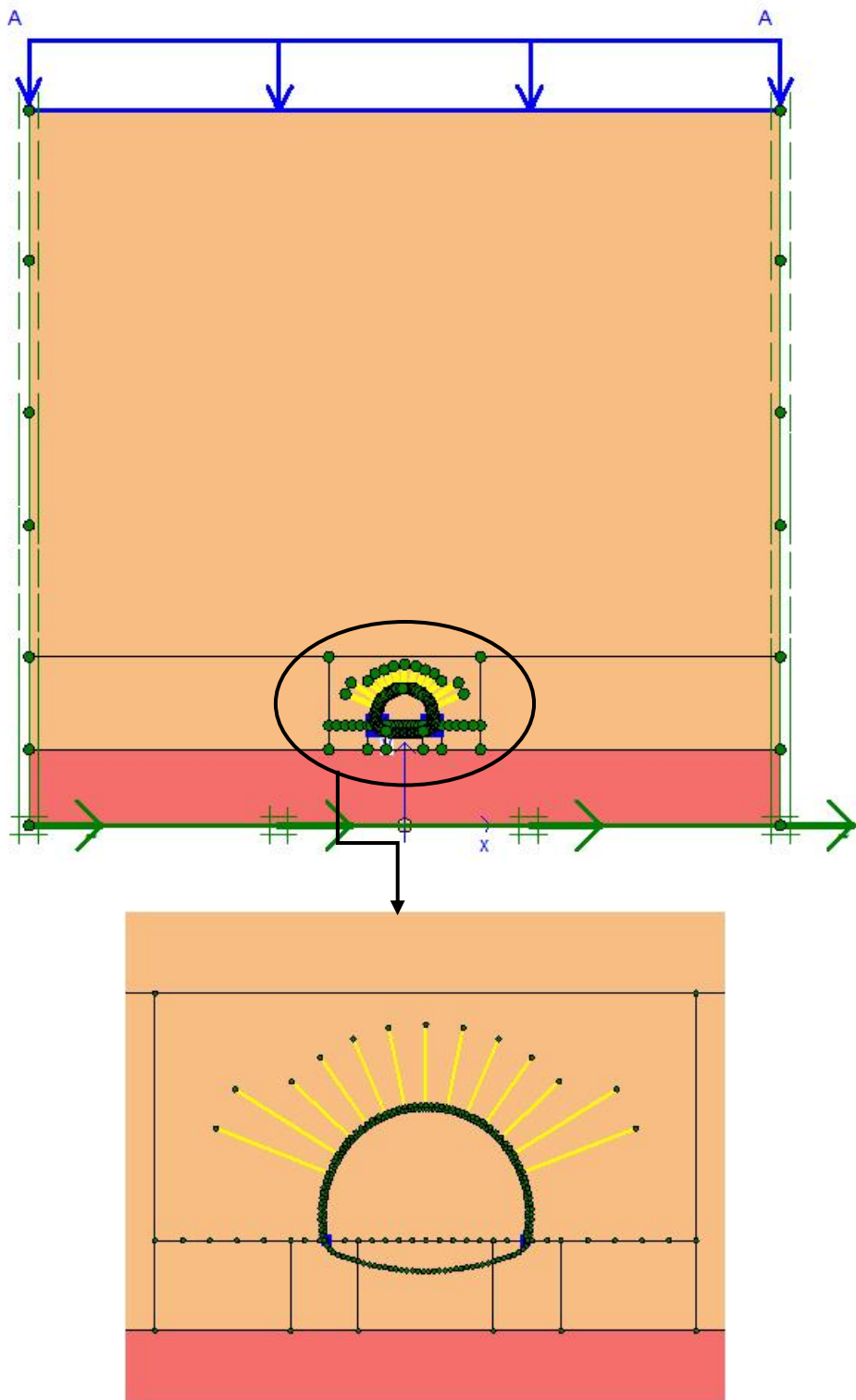
Figure 4.3 Model view of the C2 Section
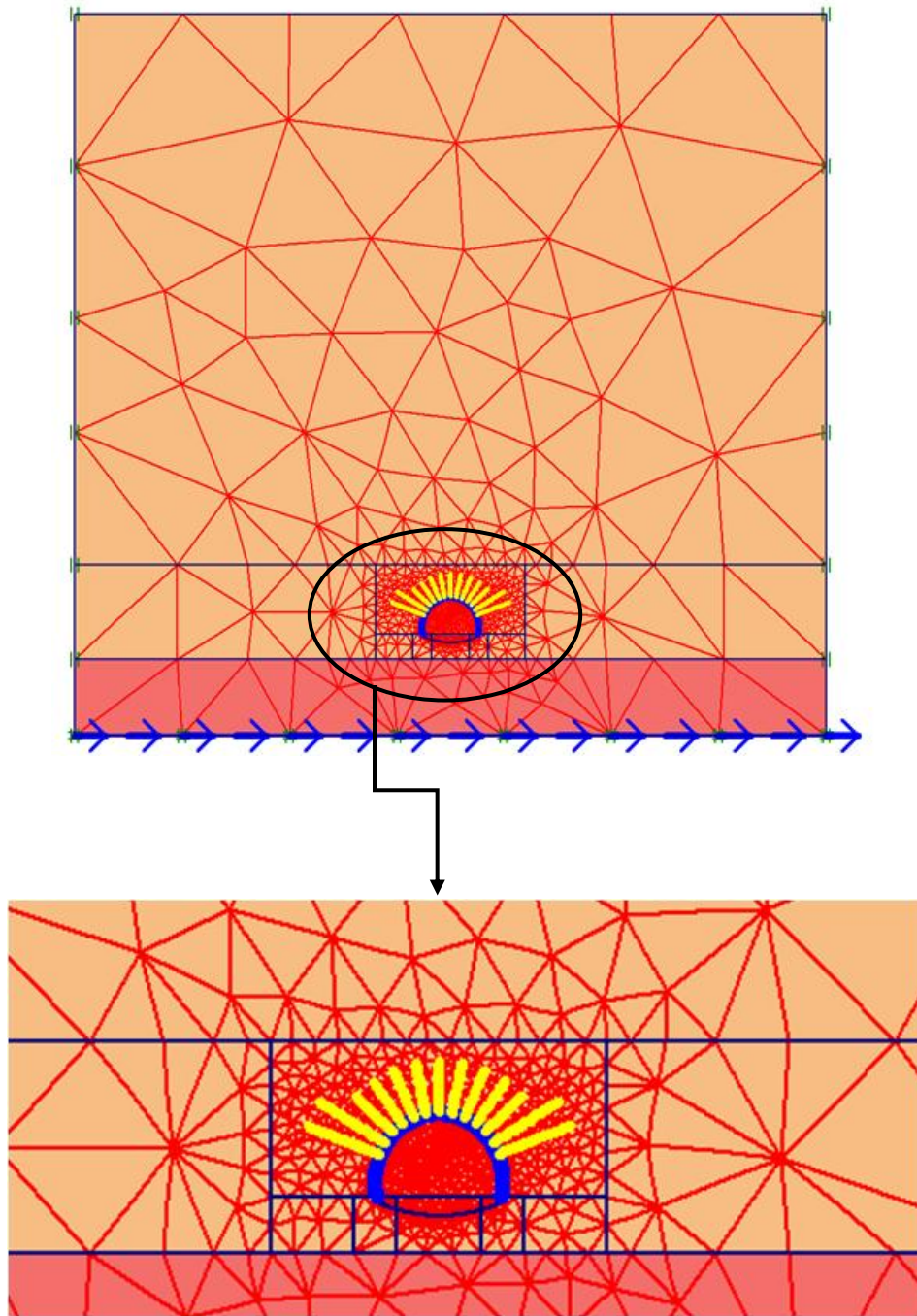
Figure 4.4 Model Mesh Generation.

4.6 Definition of Excavation and Dynamic Analyses Stages

Following the formation of the model in PLAXIS 2D software, the stages are defined to represent the construction sequence and the subsequent dynamic shaking. Support class C2 is utilized under heavy pressures exerted over the support system. The geological material is characterized under such conditions by the development of deep failure zones, rapid and significant movements of the rock mass into cavity and deformations which decrease very slowly. Hence, the support elements are generally overstressed.

A subdivision into top heading, bench and invert is imperative during construction. Maximum round length was 1.2 meters in the top heading and 2.0 meters in the bench. Excavation is carried out by smooth blasting or by tunnel excavator. Shotcrete sealing is required immediately. A dense support pattern at all exposed surfaces is needed. Special features such as deformation slots in the shotcrete or highly deformable support elements might be required. The support elements should maintain the triaxial stress state of the rock mass. All tunnel supports are applied systematically and immediately after excavation. The ring closure of the invert arch may be required as short as 25 to 50 meters behind the top heading face. Forepoling is required over the whole roof section. In accordance with the observed trend of deformations, shortening of the round lengths, increase in forepoling length, large central support body at the top heading face, further subdivision of the face, widening of the lining foot, bolting and grouting of the abutment shotcrete zone or temporary invert arches may become necessary.

Since the aim of the study is to investigate the seismic behavior of the analyzed section, the excavation was defined in two steps, for simplicity: top heading and invert. In PLAXIS, excavations and analysis options are defined in 19 sequential construction stages. The details of these stages are given in the following.

1. Initial stress state generation of the medium with the additional overburden pressure 1440 kPa.
2. 50% relaxation of the top heading

3. 100% relaxation of the top heading and 25 cm thick shotcrete installation (fresh)

4. Installation of the bolts

5. 50% relaxation of the invert and hardening of the shotcrete

6. 100% relaxation of the invert and installation of monolithic concrete invert

7. Installation of the inner lining

8. Relaxation of the soil medium overlying the tunnel section due to creep deformation with a relaxation factor of 1.2

9. Relaxation of the soil medium overlying the tunnel section due to creep deformation with a relaxation factor of 1.4

10. Relaxation of the soil medium overlying the tunnel section due to creep deformation with a relaxation factor of 1.6

11. Relaxation of the soil medium overlying the tunnel section due to creep deformation with a relaxation factor of 1.8

12. Relaxation of the soil medium overlying the tunnel section due to creep deformation with a relaxation factor of 2.0

13. Relaxation of the soil medium overlying the tunnel section due to creep deformation with a relaxation factor of 2.2

14. Relaxation of the soil medium overlying the tunnel section due to creep deformation with a relaxation factor of 2.4

15. Relaxation of the soil medium overlying the tunnel section due to creep deformation with a relaxation factor of 2.6

16. Relaxation of the soil medium overlying the tunnel section due to creep deformation with a relaxation factor of 2.8

17. Relaxation of the soil medium overlying the tunnel section due to creep deformation with a relaxation factor of 3.0

18. Assigning the unrelaxed material properties for dynamic stage

19. Dynamic Analysis

4.7 Definition of the Earthquake Time History for the Analyzed Case

As it was mentioned earlier in Chapter 3, Bolu Tunnels were damaged during the Düzce Earthquake. Hence, the record captured by the Bolu Station is used in the analyses, following the necessary modifications, since this was the closest station to the tunnels. The seismograph was located at the first floor of the Public Works and Settlement Directorate building. The location of the station is shown in Figure 4.5.
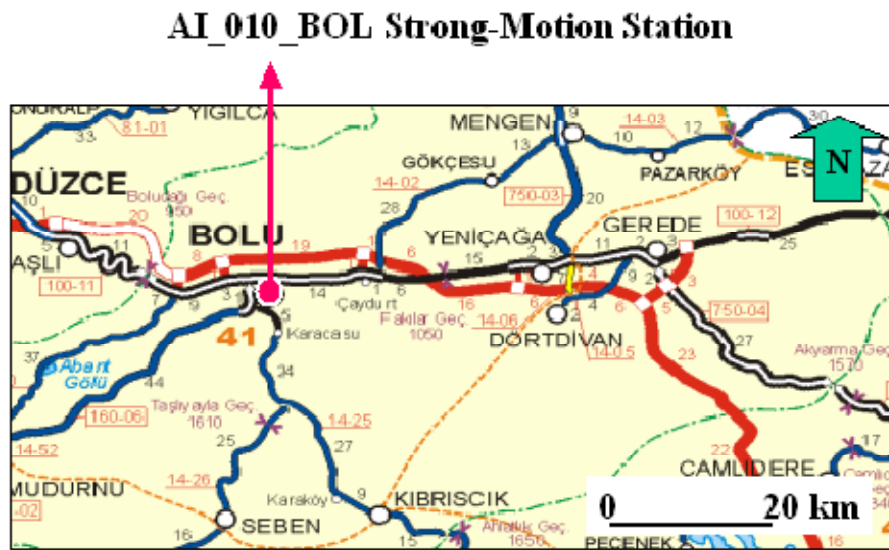
Figure 4.5 Location of the Bolu Strong Motion Station

The characteristics of the earthquake and the record are the following:

Earthquake: Düzce, Turkey 1999-11-12

Magnitude: 7.14

Hypocenter Latitude: 40.7746, Longitude: 31.1870, Depth: 10.0 (km)

Fault Rupture Length: 46.8 (km), width: 20.3 (km)

Average Fault Displacement: 169.4 (cm)

Station: ERD 99999 Bolu

Latitude: 40.74635, Longitude: 31.60755

Preferred V_{s30}: 326.00 (m/s)

Epicentral Distance: 41.27 (km)

Hypocentral Distance: 43.58 (km)

Joyner-Boore Distance: 12.02 (km)

Campbell R Distance: 12.41 (km)

RMS Distance: 32.27 (km)

Closest Distance: 12.04 (km)

PGA: 0.7662 (g)

PGV: 59.6800 (cm/sec)

PGD: 17.6900 (cm)

Being approximately perpendicular to the cross-section of the Bolu tunnels, east-west component of the record is utilized in the dynamic analyses. In order to simulate the ground motion realistically at the tunnel site, the record was carried to the site using appropriate procedures. The procedures applied to obtain the site motion are explained in Figure 4.6.
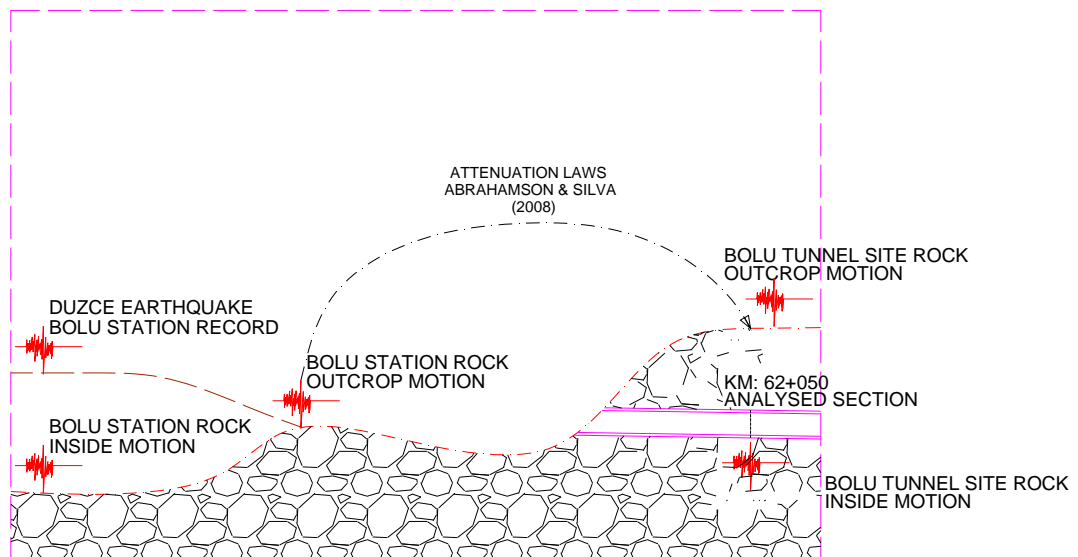
Figure 4.6 Procedures used for obtaining the record at analyzed section.

A computer program for equivalent-linear earthquake site response analyses of layered soil deposits (EERA) is used to simulate the amplification or deamplification of the motion in the ground. EERA implements the well-known concepts of equivalent linear earthquake site response analysis. A summary of the applied procedures is given in the following:

1. Firstly, E-W component of the Bolu Station record (Figure 4.7) is deconvolved to obtain the bedrock motion (Figure 4.8). Shear wave velocity profile and soil profile, obtained from site specific borehole data shown in Figure 4.9, are idealized to the depth of 30.45 m. However, the available depth of the available profile did not reach to the bed rock at the site of the station. Assuming $V_s > 700$ m/s in the bedrock, values given in Table 4.1 were used for the variation of shear wave in the analyses (Başokur, A. T., 2005).

Table 4.1 Shear wave velocity profile (Başokur, A. T., 2005).

Depth, (m)	V_s, (m/s)
0-11	255
11-27	440
27-64	502
≥64	1000
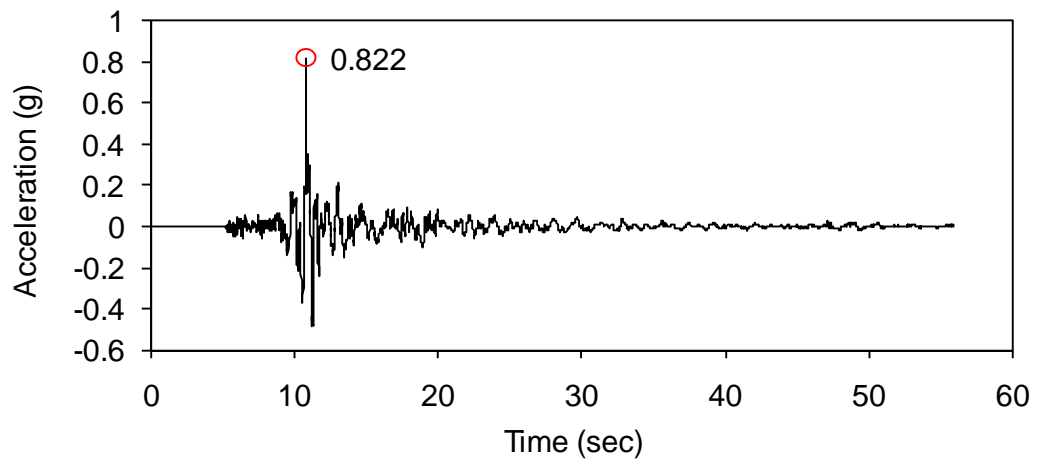
Figure 4.7 E-W component of the Bolu Station record of Düzce Earthquake.
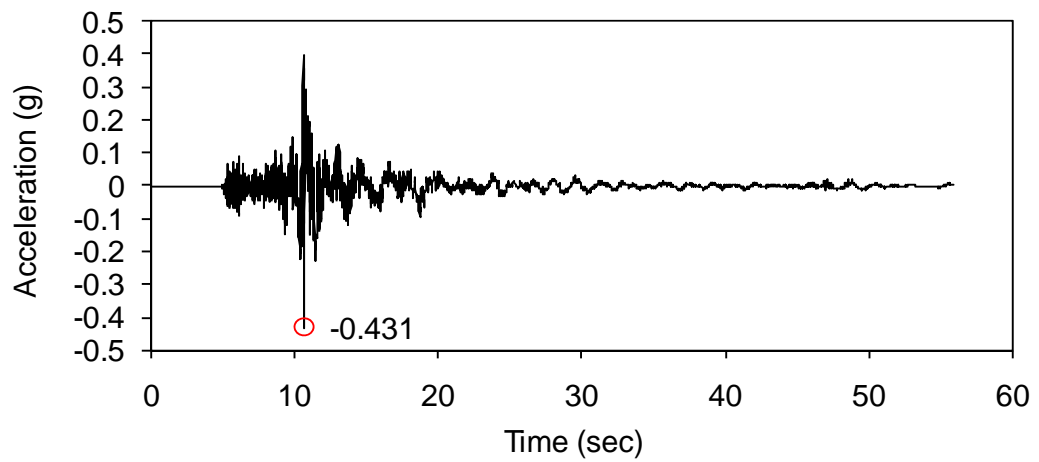
Figure 4.8 Bedrock motion of the Bolu Station record of Düzce Earthquake.
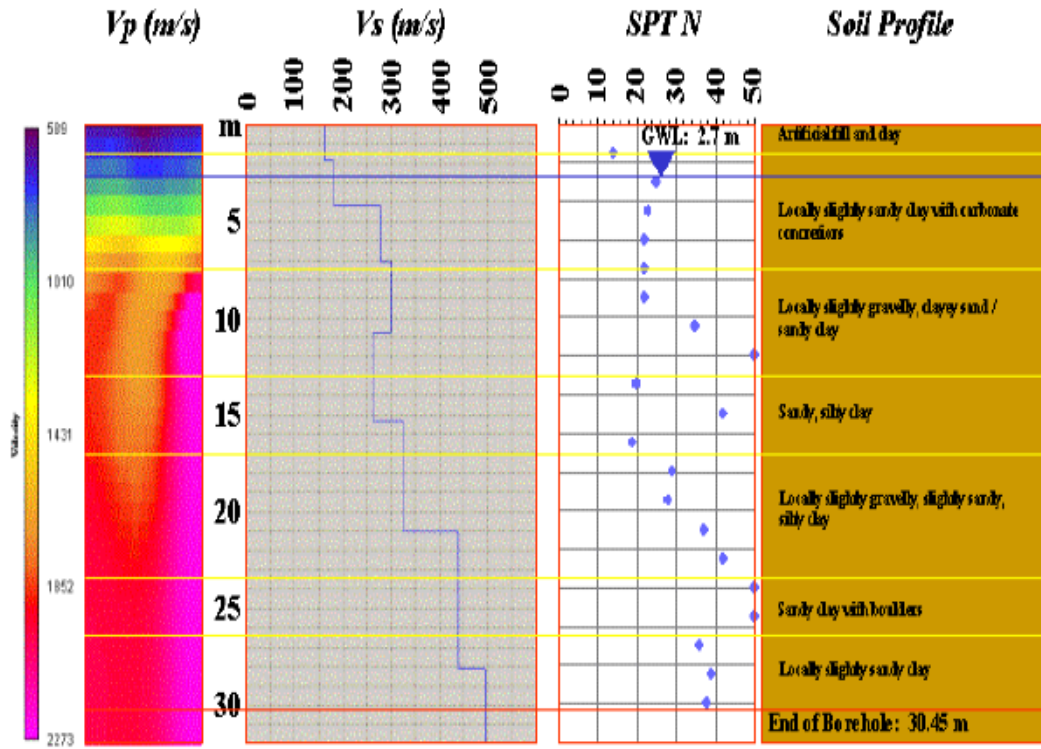
Figure 4.9 from left to right: P-wave velocity-depth model; the S-wave velocity-depth profile; uncorrected SPT N values measured at 1.5-m intervals; and the simplified form of the soil profile from the geotechnical borehole. The yellow horizontal lines define the layer boundaries within the soil column based on the geotechnical borehole log, the blue horizontal line represents the groundwater level (GWL), and the red horizontal line represents end of the borehole. GWL has not been observed over a long duration. (TÜBİTAK Research Project, No. 105G016, 2006).

2. Secondly, Bolu Station rock outcrop motion was generated by using the soil profile given in stage 1 (Figure 4.10).
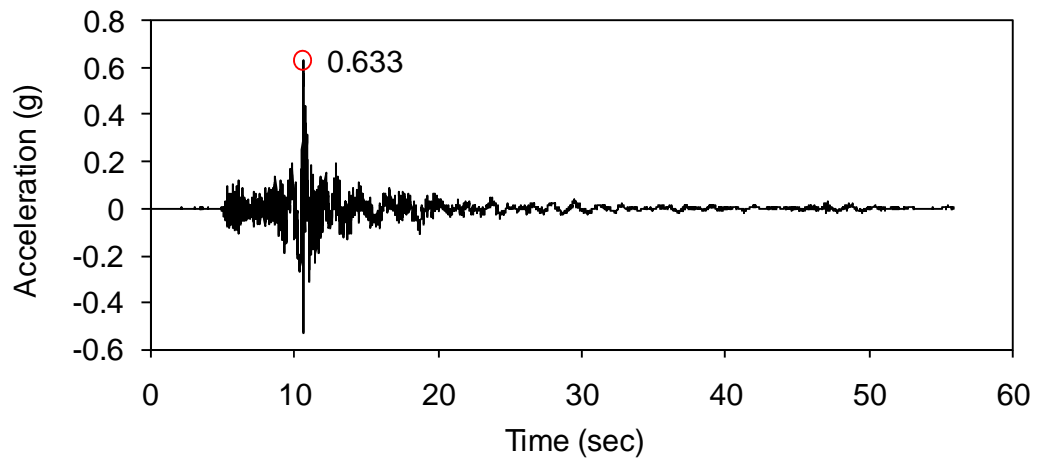
Figure 4.10 Rock outcrop motion of the Düzce Earthquake.

3. The acceleration time history was then transferred to the Bolu Tunnels site by using attenuation formulation proposed by Abrahamson and Silva (2008) (Figure 4.11). A spreadsheet was used for these calculations, which was prepared by Linda Al Atik, PEER – Sep., 2009. The explanatory variables for the attenuation model are listed in Table 4.2.

Table 4.2 Explanatory variables for the attenuation model.

	Record Site	Tunnel Site
M	7.14	7.14
R_{RUP} *(km)*	12.04	4.00
R_{JB} *(km)*	12.02	4.00
R_X *(km)*	-12.02	-4.00
U	0	0
F_{RV}	0	0
F_{NM}	0	0

Table 4.2 (cont'd). Explanatory variables for the attenuation model.

	Record Site	Tunnel Site
F_{HW}	0	0
Z_{TOR} (km)	0.00	0.00
δ	54	54
V_{S30} (m/sec)	1000	1000
$F_{Measured}$	0	0
$Z_{1.0}$ (m)	DEFAULT	DEFAULT
$Z_{2.5}$ (km)	DEFAULT	DEFAULT
W (km)	20.3	20.3
F_{AS}	0	0
HW Taper	0	0

Definitions of parameters in Table 4.2 are given in the following:

M = Moment magnitude

R_{RUP} = Closest distance to coseismic rupture (km), used in AS08, CB08 and CY08.

R_{JB} = Closest distance to surface projection of coseismic rupture (km).

R_X = Horizontal distance from top of rupture measured perpendicular to fault strike (km), used in AS08 and CY08.

U = Unspecified-mechanism factor: 1 for unspecified; 0 otherwise, used in BA08

F_{RV} = Reverse-faulting factor: 0 for strike slip, normal, normal-oblique; 1 for reverse, reverse-oblique and thrust

F_{NM} = Normal-faulting factor: 0 for strike slip, reverse, reverse-oblique, thrust and normal-oblique; 1 for normal

F_{HW} = Hanging-wall factor: 1 for site on down-dip side of top of rupture; 0 otherwise, used in AS08 and CY08

Z_{TOR} = Depth to top of coseismic rupture (km), used in AS08, CB08 and CY08

δ = Average dip of rupture plane (degrees), used in AS08, CB08 and CY08

V_{S30} = Average shear-wave velocity in top 30 m of site profile

$F_{Measured}$ = Vs30 Factor: 1 if VS30 is measured, 0 if Vs30 is inferred, used in AS08 and CY08

$Z_{1.0}$ = Depth to 1.0 km/sec velocity horizon (m), used in AS08 and CY08. Enter "DEFAULT" in order to use the default values or enter your site specific number

$Z_{2.5}$ = Depth of 2.5 km/s shear-wave velocity horizon (km), used in CB08. Enter "DEFAULT" in order to use the default value or enter your site specific number

W = Fault rupture width (km), used in AS08

F_{AS} = Aftershock factor: 0 for mainshock; 1 for aftershock, used in AS08 and CY08

HW Taper = To choose the hanging wall taper to be used in AS08. Enter 0 to use the hanging wall taper as published in Abrahamson and Silva (2008), or enter 1 to use the revised hanging wall taper

Table 4.3 Resulting PGA values obtained from Abrahamson and Silva (2008) Attenuation Laws.

	Record Site	Tunnel Site
PGA (g)	0.184	0.354

Ratio= $PGA_{Record\ Site}$ / $PGA_{Tunnel\ Site}$ = 1.924 from Table 4.3.

Before the final stage the resulting earthquake record data is scaled with this ratio.
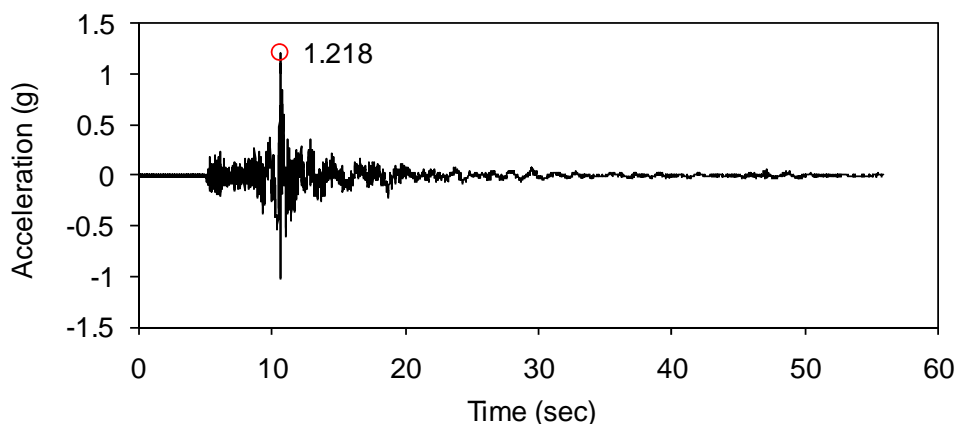
Figure 4.11 Rock outcrop motion of Düzce Earthquake at the location of Bolu Tunnels.

4. After applying attenuation laws to the rock outcropping motion, the bed rock motion was obtained at the tunnel site. In the derivation of the record, shear modulus values were computed by using Figure 4.12 assuming zero shear strain. This record, illustrated on Figure 4.13, was then used in the dynamic analyses of the selected section of the tunnels for the case study.
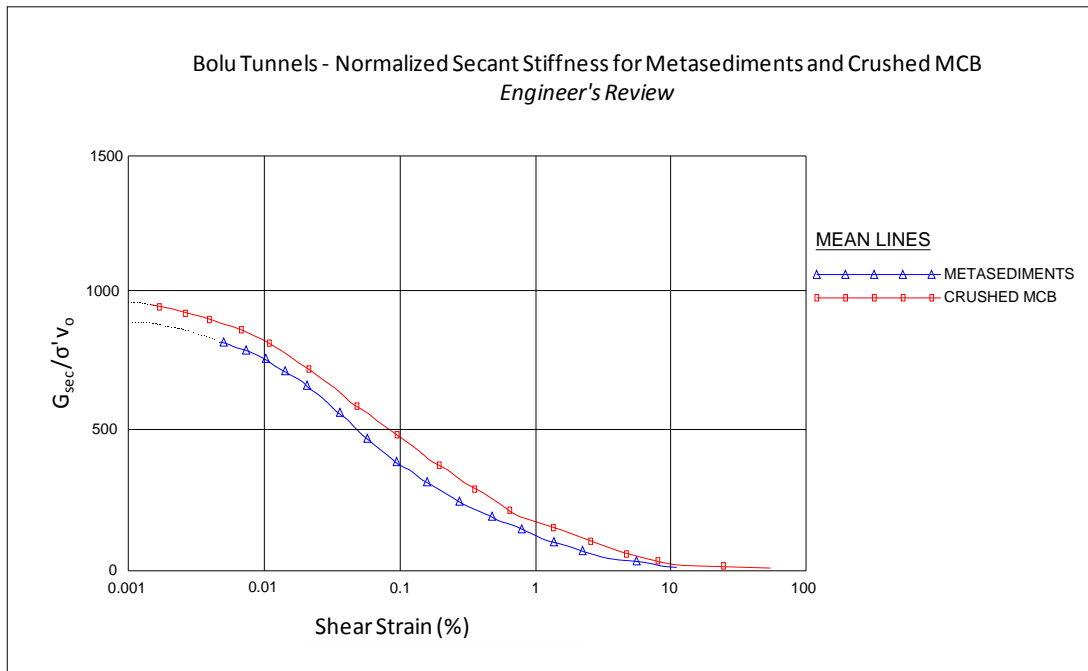
Figure 4.12 Bolu Tunnels - normalized secant stiffness for Metasediments and Crushed Metacrystaline Basement (MCB) (Report No: 45.110/R/2251, Astaldi, 2000).
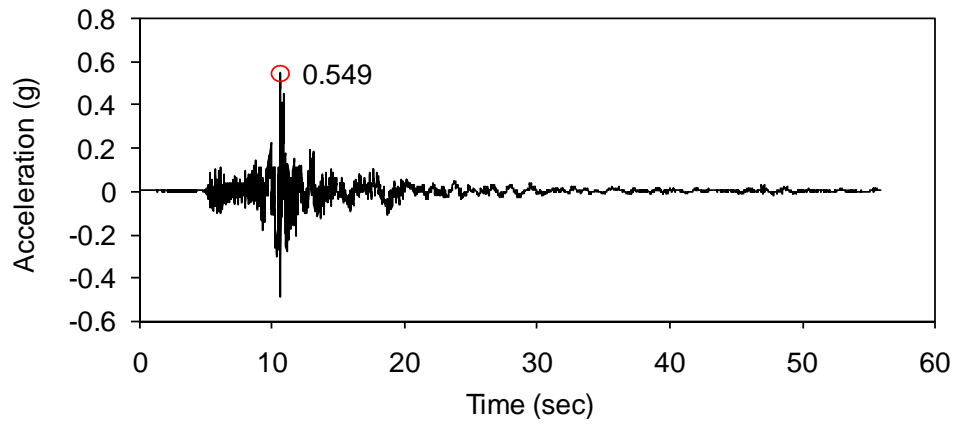
Figure 4.13 Bedrock motion of the Düzce Earthquake at the location of Bolu Tunnels.

CHAPTER 5

RESULTS AND DISCUSSION

In this chapter, the results obtained from the analyses to simulate the seismic effects of the Düzce earthquake on the analyzed section are presented and discussed. The results including the displacements and stresses in the vicinity of the tunnels as well as the shear forces and moments of the liners are presented in Figures 5.1 through 5.12.

In Figure 5.1, the maximum displacements that occur on the soil medium are presented following the seismic shaking. From Figure 5.2 through Figure 5.4 the maximum displacements of the medium surrounding the tunnels due to seismic shaking are illustrated only to give an idea about the levels of deformations imposed by the Düzce Earthquake. The resulting stresses that occur following the seismic excitation are given in Figures 5.5 and 5.6. It is seen that the maximum stresses take place around the bottom of the invert as it would be expected. Figure 5.7 presents the total displacement of the tunnel inner lining after the earthquake. The deformation of the lining caused by seismic shaking is shown in Figure 5.8. The displacements obtained from the analyses indicate that the deformation tolerance of the analyzed section is not exceeded (Figure 4.1). The forces and moments which are illustrated in Figures 5.9 through 5.12, which are the main interest of this study, are compared with the site recorded data. Locations of the gauges installed over the tunnel liners are given in Figure 5.13.

The calculated results in dynamic analyses are compared with the site measured gauge readings in Figures 5.14 through 5.17, in terms of the strength capacities of the analyzed section. In the comparisons, interaction diagrams were used to check whether the capacity of the section was exceeded or not. Comparisons of the liner forces based on site measurements with those that are calculated in the analyses are given in Figures 5.14 and 5.15.

It is mentioned before that the inner lining of the tunnel was modeled by using uniform length plate elements of 25 cm. For the sake of completeness, the capacities of whole inner lining elements, apart from the gauge point locations were also checked to observe whether the available capacity was sufficient. Capacity calculations of the tunnel liners based on the forces determined from the analyses are presented in Figures 5.16 through 5.19. Figures 5.16 and 5.17 show the capacity calculation of the entire tunnel lining. It is observed that the capacities were sufficient for all parts of the liners and that the tunnel should remain stable after the earthquake. These results are consistent with the post earthquake site measurements and visual observations.

In addition to the forces representative of the post earthquake situation of the section, PLAXIS keeps track of the maximum and minimum forces during the history of loading in all subsequent calculation phases. These maximum and minimum forces up to the current calculation step can be viewed in the form of force envelopes. Figures 5.18 and 5.19 illustrate the capacity calculations relating to such forces that occur during the seismic analyses including the previous stages forces.

Time histories of the site measured strains, stresses, forces and moments as well as pressure cell readings are given in Figures 5.20 through 5.26. Figures 5.20 through 5.23 represent the recorded inner and outer strains at each instrumented section. The forces and moments calculated based on the site recorded data are shown in Figures 5.24 and 5.25. It is observed that the internal forces of the inner lining display a trend of increase, which is most probably due to the creep deformations in the surrounding medium. To simulate this trend in the analyses of the section, relaxation factors are applied to the ground in the stages previous to the seismic analysis until the forces indicated by the recorded data are approximately reached. For the gauge points 1 and 7, the results obtained from analyses immediately after the earthquake are very similar to the site recorded data as can be observed from Figures 5.24 and 5.25. In contrast, there exist deviations between the recorded data and the analyses results for the gauge points 2, 4, 5 and 6 in terms of the liner normal forces and moments. The results obtained from the analyses are compared to the data recorded from

measurements of the relevant gauges installed over the tunnels are summarized in Table 5.1.

In order to check the consistency of the analyses results with the post earthquake observations (Figure 3.3), crack widths that occur during the dynamic analyses are calculated according to the procedure defined by AASHTO LRFD 4th Edition, 2006. In Figure 3.3, it is observed that the lining remains undamaged at the analyzed section. The critical force envelopes were used in calculation of the crack widths for liner thicknesses of 650 mm (near top heading) and 850 mm (near invert), as shown in Tables 5.2 and 5.3. The calculation results show that all of the section remains in compression in the case of 650 mm thick section, which means no cracks occur near the top heading. Whereas for the inner lining sections near the invert, crack width did not exceed the indicated limit according to the calculation results. Crack width of the section for the force envelopes is calculated as 0.018 mm and the corresponding limit was 0.324 mm near the invert. These findings are in well agreement with the post earthquake observations of the analyzed section.

Table 5.1 Analyses results compared with the recorded site data.

Gauge Points	Analyses Results		Calculated Site Data from Gauge Points	
	P	M	P	M
	kN/m	kN-m/m	kN/m	kN-m/m
1	4763.80	149.34	4996.21	177.09
2	4340.93	87.47	3698.01	-388.10
3	5283.07	164.95	2459.79	189.08
4	3741.19	-470.53	1191.11	-302.52
5	5139.06	-336.98	1374.78	-250.11
6	11782.46	1589.36	11563.16	-1511.97
7	13802.84	332.75	13893.78	321.56

Table 5.2 Control of cracking for b=650mm, h=1000 mm.

Control of Cracking for b=650 mm, h=1000 mm

Service Load Analysis (cracked section - triangular concrete stress)

Material Properties

Concrete f'$_c$ =	30 MPa		Steel	f$_y$ =	420 MPa
fcf = 0.6√f'c =	3.286 MPa			E$_s$ =	200000 MPa
E$_c$ =	25136 MPa			n = E$_s$/E$_{ct}$ =	7.96
Creep factor, C$_t$ =	0				
Long term concrete E$_{ct}$ = E$_c$/(1+C$_t$) =	25136 MPa				

Reinforcing Details

Bar diameter, db = 60 mm
Bar spacing, s = 100 mm
Concrete cover to bar in tension, clr = 50 mm

Service Loads:

P =	5597 kN	(positive for compression)
M =	787 kN-M	(positive for tension on the bottom)

Uncracked concrete section stresses

Section Properties	Concrete	Reinforcing steel	Transformed to Ect
Area, A =	650000	1095	657617
Moment inertia, I =	54166666667	109494000	54928371845
Centroid from bot.Yb =	500	500	500

Elastic concrete stresses
stress at tension fibre = -1.347 MPa (Bottom)
stress at compression fibre = -15.675 MPa (Top)
Neutral axis from compression fibre = 1094.0 mm (From top)
Concrete area in tension, Act = -61116 mm²   α = 0 rad

Cracked section analysis

Dist. to N.A. from compression edge, c$_{NA}$ =	1000.0 mm	
Max. stress in tensile reinforcement, f$_s$ =	0.0 **MPa**	**Full section is in Compression**
Concrete stress, f$_c$ =	-15.67 MPa	
Area of steel in tension, Ast =	497.70 mm²	
Tensile steel located from: Bottom, yb =	200.00 mm	
Compress. edge, ds =	800.00 mm	

Table 5.3 Control of cracking for b=850mm, h=1000 mm.

Control of Cracking for b=850 mm, h=1000 mm

Service Load Analysis (cracked section - triangular concrete stress)

Material Properties

Concrete f'c =	30 MPa	Steel	fy =	420 MPa
fcf = 0.6√f'c =	3.286 MPa		Es =	200000 MPa
Ec =	25136 MPa		n = Es/Ect =	7.96
Creep factor, Ct =	0			
Long term concrete Ect = Ec/(1+Ct) =	25136 MPa			

Reinforcing Details

Bar diameter, db =	60 mm
Bar spacing, s =	100 mm
Concrete cover to bar in tension, clr =	50 mm

Service Loads:

P =	16300 kN	(positive for compression)
M =	3164 kN-M	(positive for tension on the bottom)

Uncracked concrete section stresses

Section Properties	Concrete	Reinforcing steel	Transformed to Ect
Area, A =	850000	1095	857617
Moment inertia, I =	70833333333	109494000	71595038512
Centroid from bot. Yb =	500	500	500

Elastic concrete stresses		
stress at tension fibre =	3.090 MPa	(Bottom)
stress at compression fibre =	-41.103 MPa	(Top)
Neutral axis from compression fibre =	930.1 mm	(From top)
Concrete area in tension, Act =	59439 mm²	α = 0 rad

Cracked section analysis

Dist. to N.A. from compression edge, c_{NA} =	930.1 mm	
Max. stress in tensile reinforcement, f_s =	17.9 MPa	
Concrete stress, f_c =	-30.0 MPa	
Area of steel in tension, Ast =	99.54 mm²	(3 bars)
Tensile steel located from: Bottom, yb =	0.0 mm	
Compress. edge, ds =	1000.0 mm	

Maximum bar spacing by AASHTO LRFD 4th Edition, 2006

β_s = 1+(clr+db/2)/[0.7(h-clr-db/2)] =	1.124	
Exposure factor, γ_e =	0.75	Class 1 exposure γ_e = 1.00, Class 2 γ_e = 0.75)
Corresponds to crack limit width =	0.324 mm	
Calculated crack width, **wk** =	0.018 mm	
Smax = 122600γ_e/($\beta_s f_s$) - 2(clr+db/2) =	4397.4 mm	(5.7.3.4-1)
Check maximum bar spacing S ≤ Smax	**100 mm ≤ 4397.4 mm**	**OK**

Figure 5.1 Total displacements of the tunnel section following the seismic shaking.

Extreme Total Displacement
$176.77*10^{-3}$ m

Extreme Total Displacement
78.13*10^{-3} m
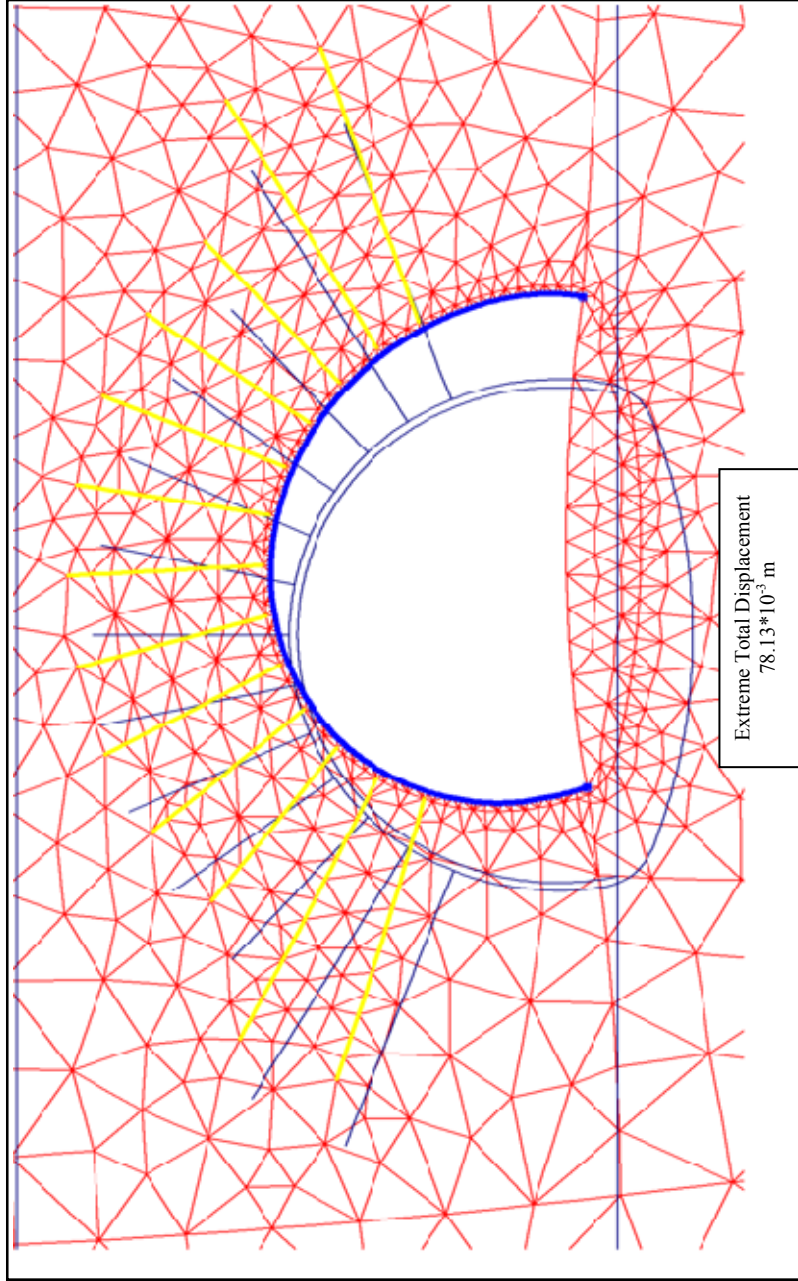
Figure 5.2 Displacements of the tunnel section due to seismic shaking only.
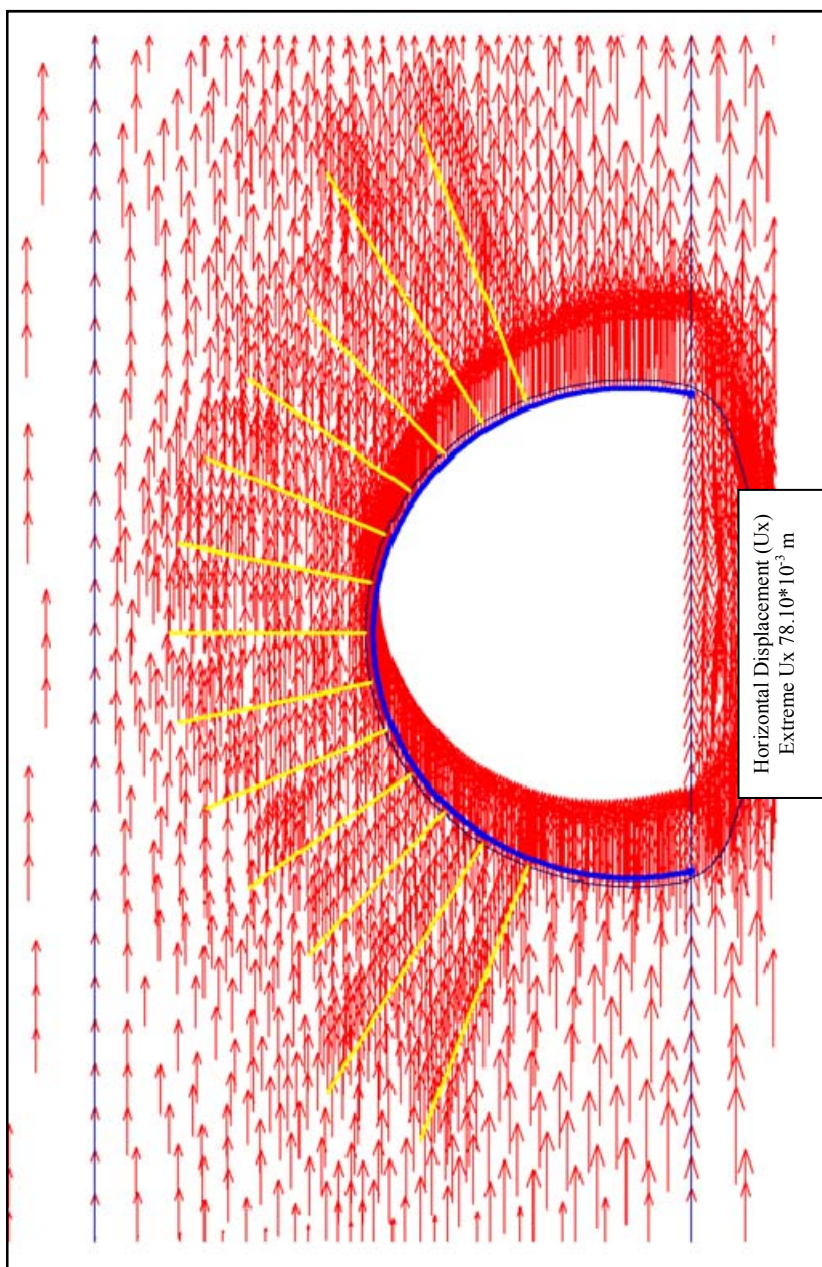
Figure 5.3 Horizontal displacements of the tunnel section due to seismic shaking only.

Vertical Displacement (Uy)
Extreme Uy 78.10*10^{-3} m
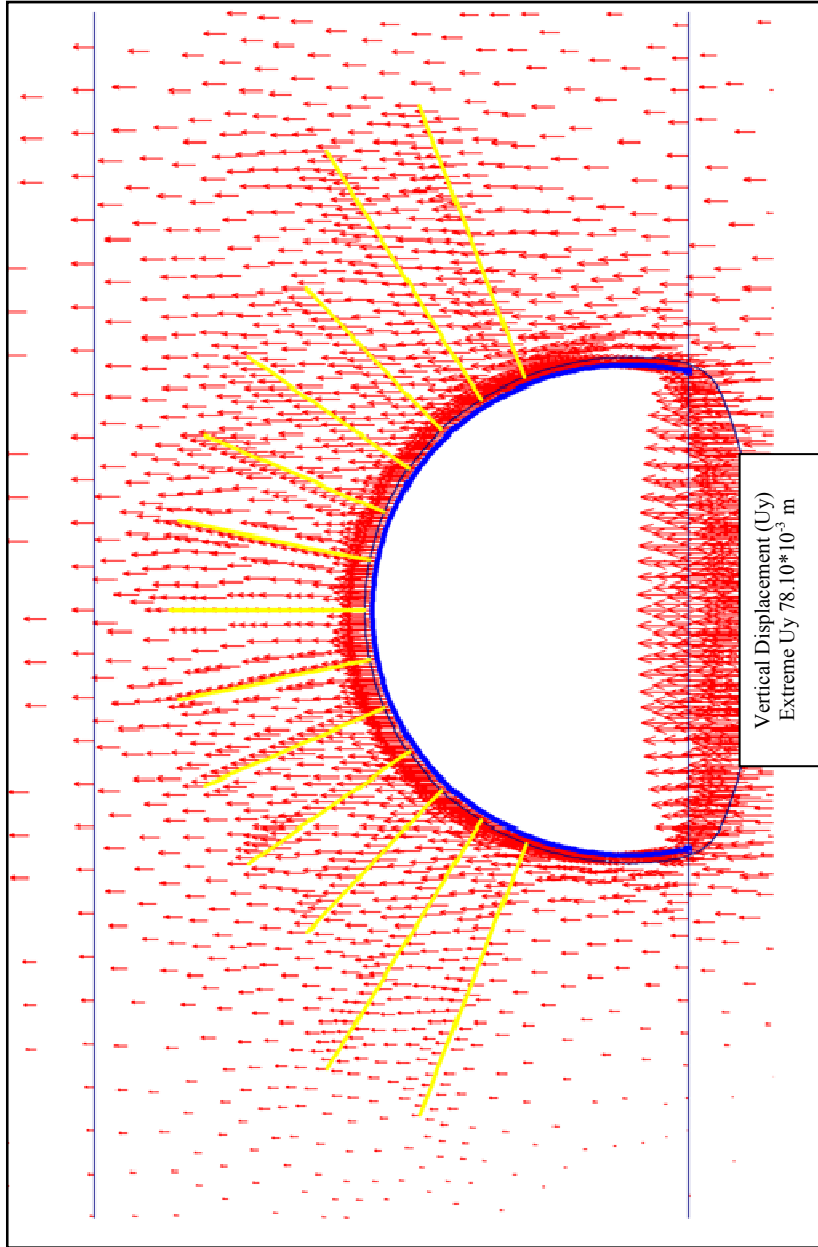
Figure 5.4 Vertical displacements of the tunnel section due to seismic shaking only.
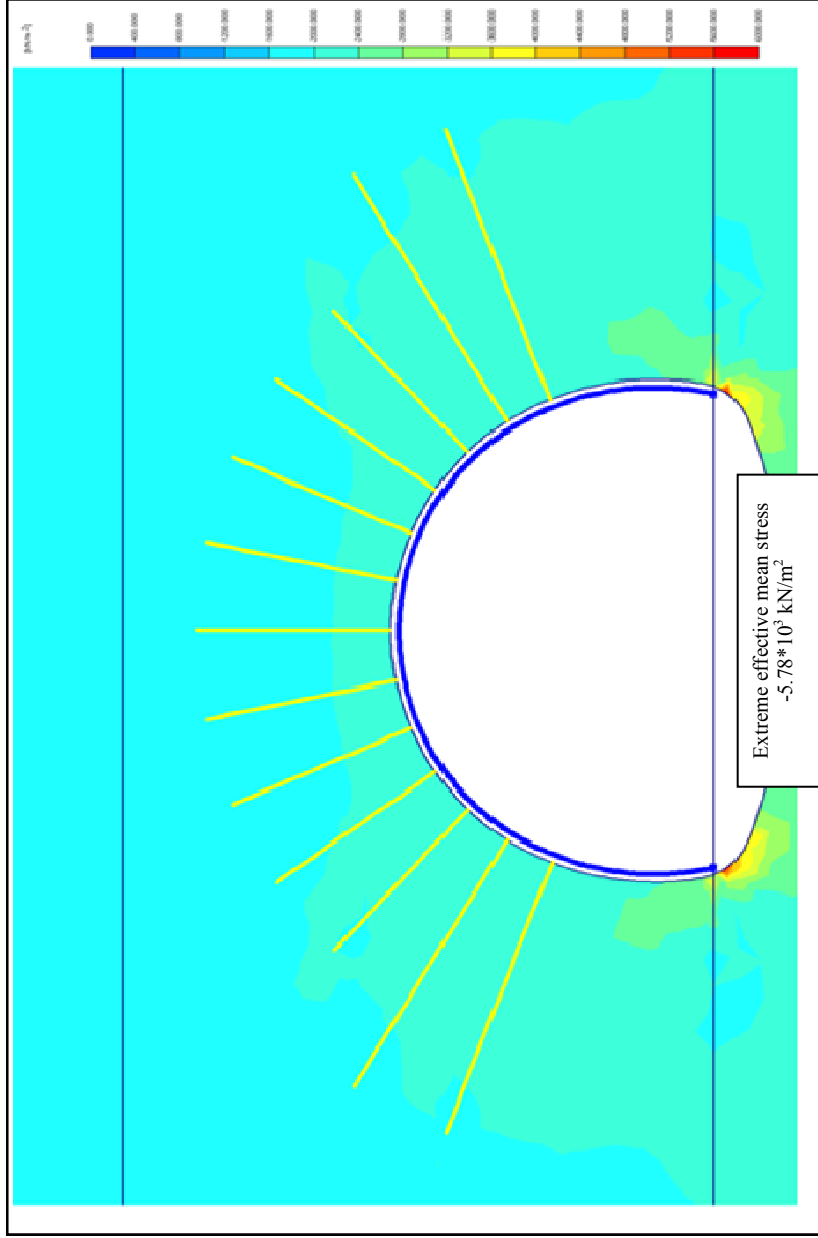
Figure 5.5 Effective mean stresses of the tunnel section following the seismic shaking.
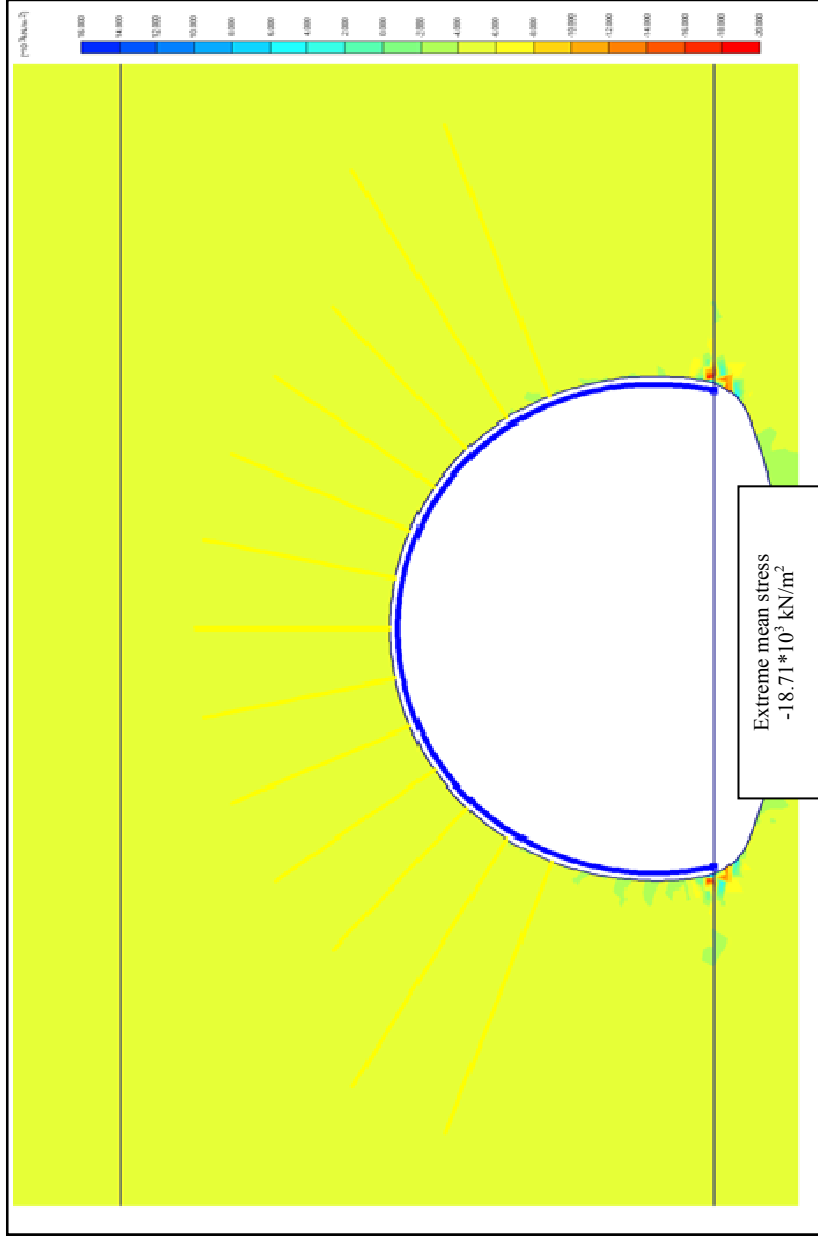
Figure 5.6 Total mean stresses of the tunnel section following the seismic shaking.
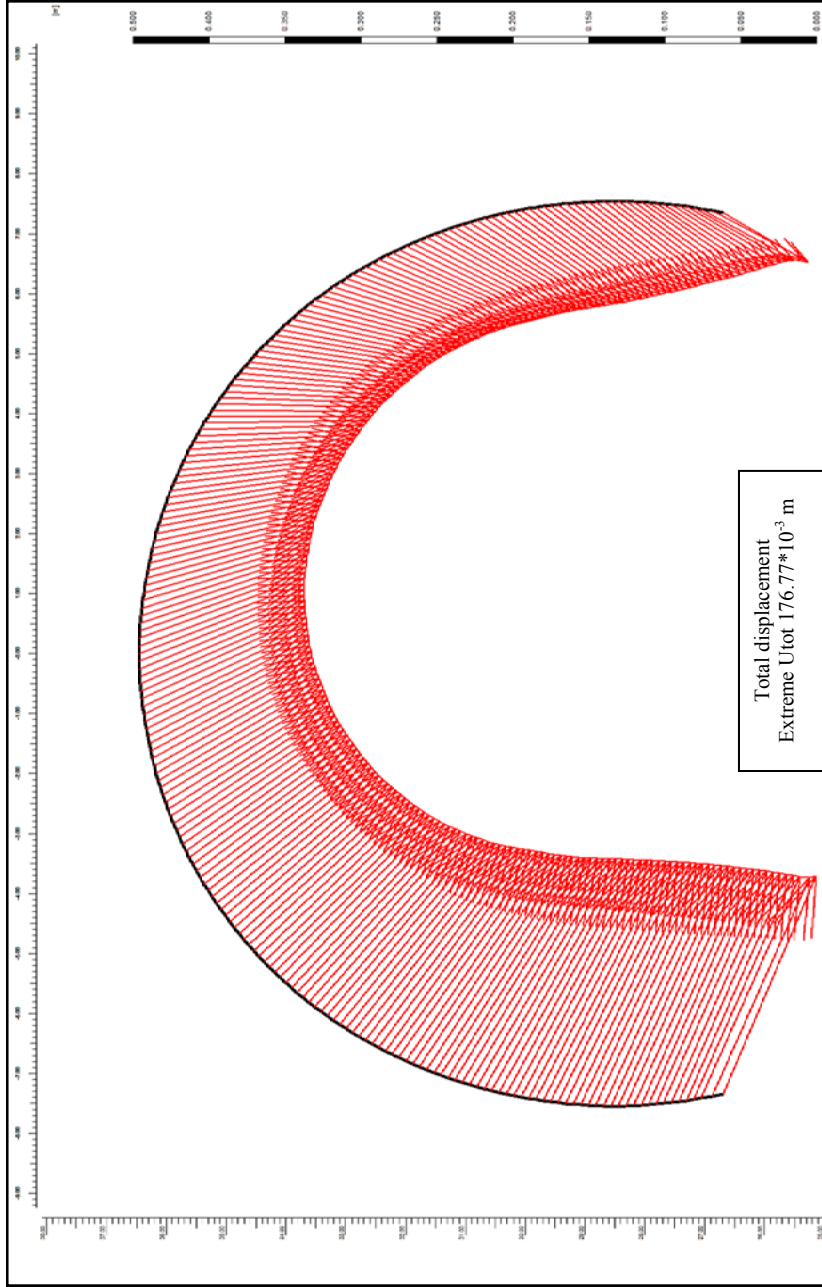
Figure 5.7 Total displacements of the inner lining of the analyzed section following the seismic shaking.

Total displacement
Extreme Utot 62.73*10⁻³ m
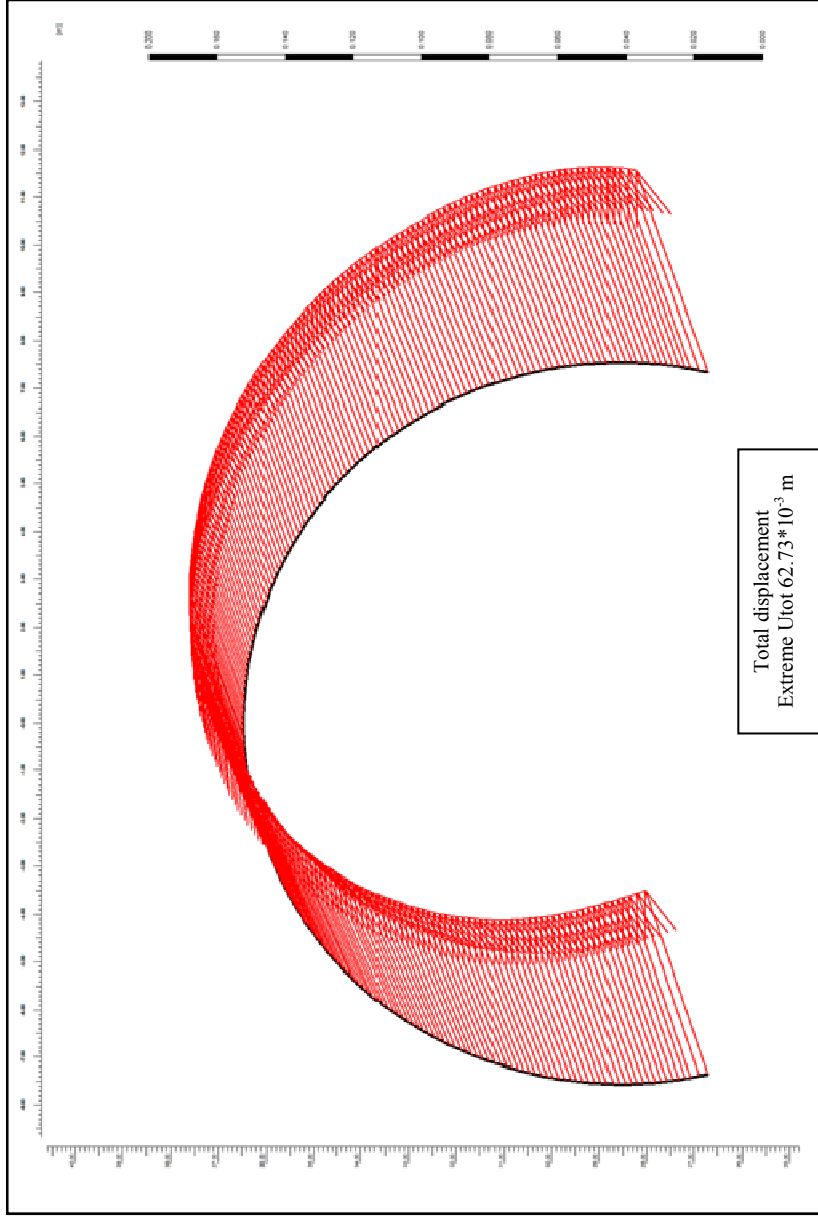
Figure 5.8 Displacements of the inner lining of the analyzed section due to seismic shaking only.
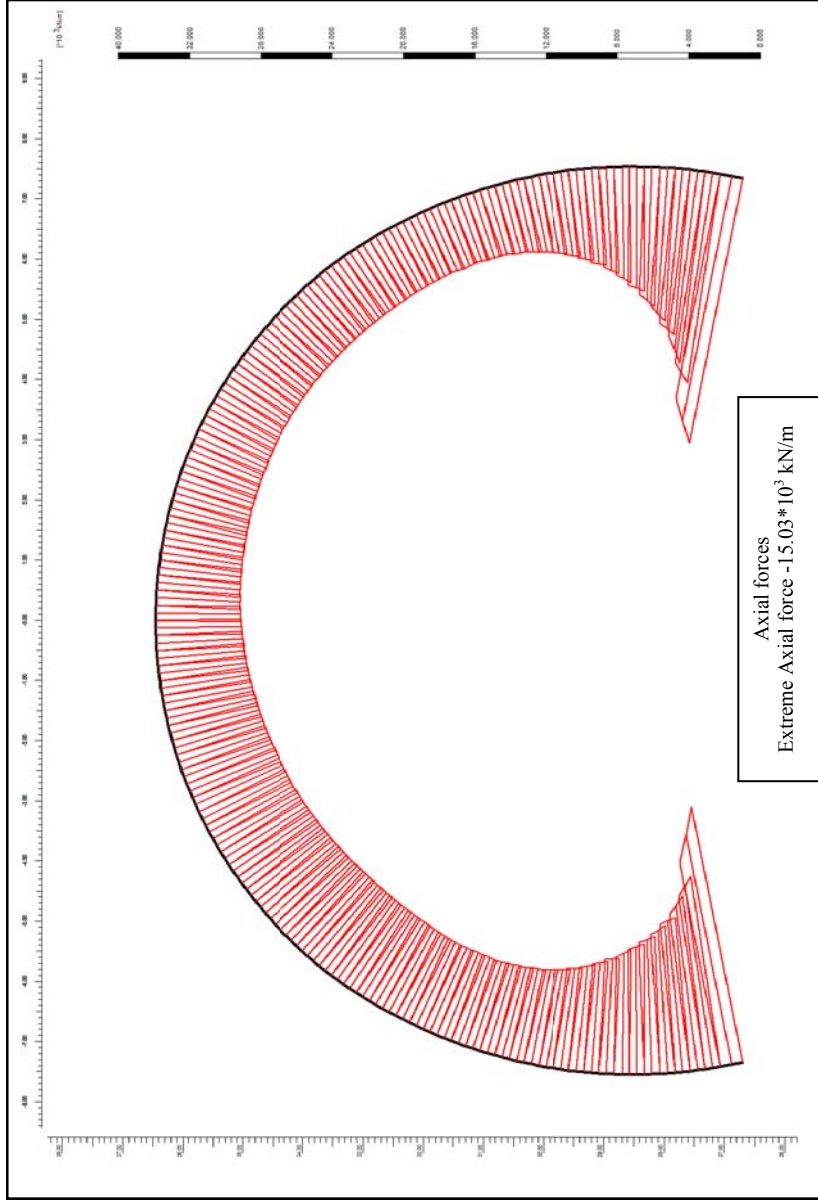
Figure 5.9 Axial forces of the inner lining of the analyzed section following seismic shaking.
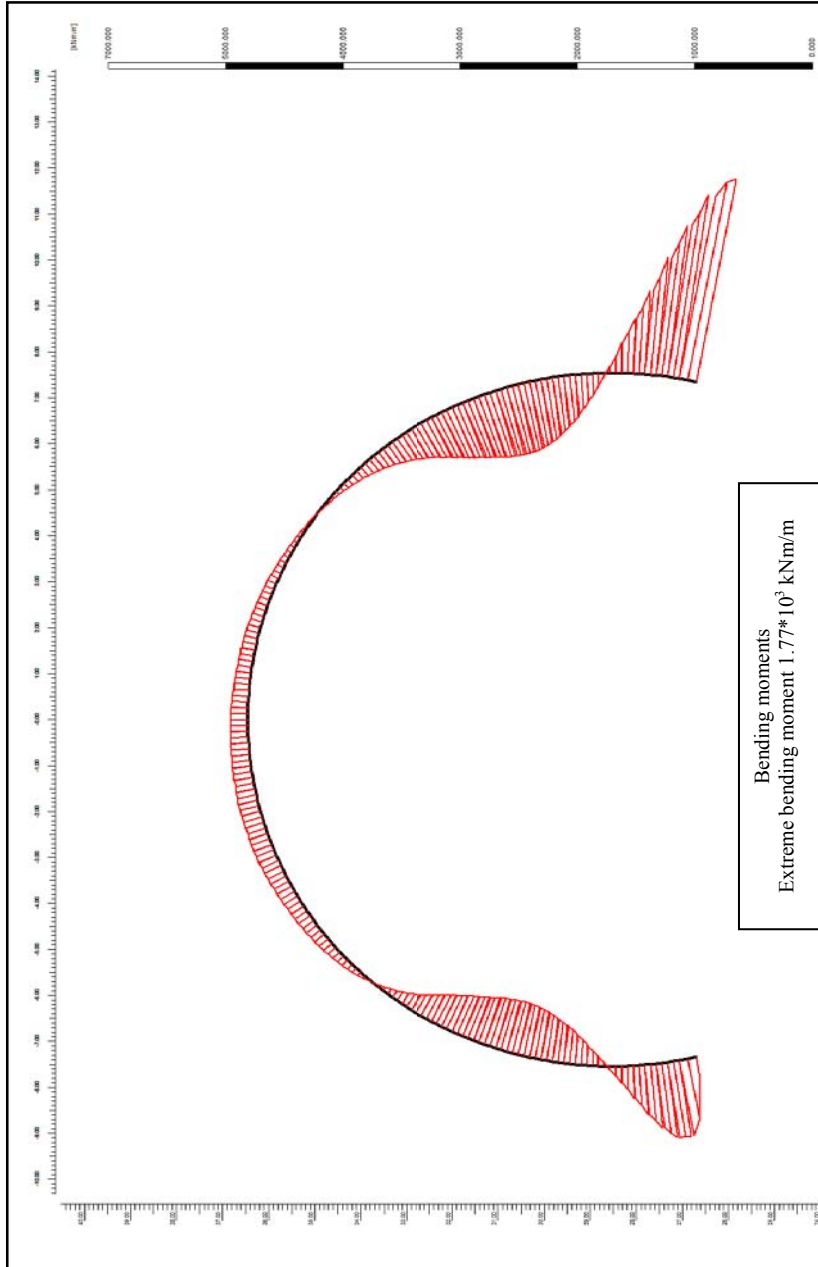
Figure 5.10 Bending moments of the inner lining of the analyzed section following seismic excitation.
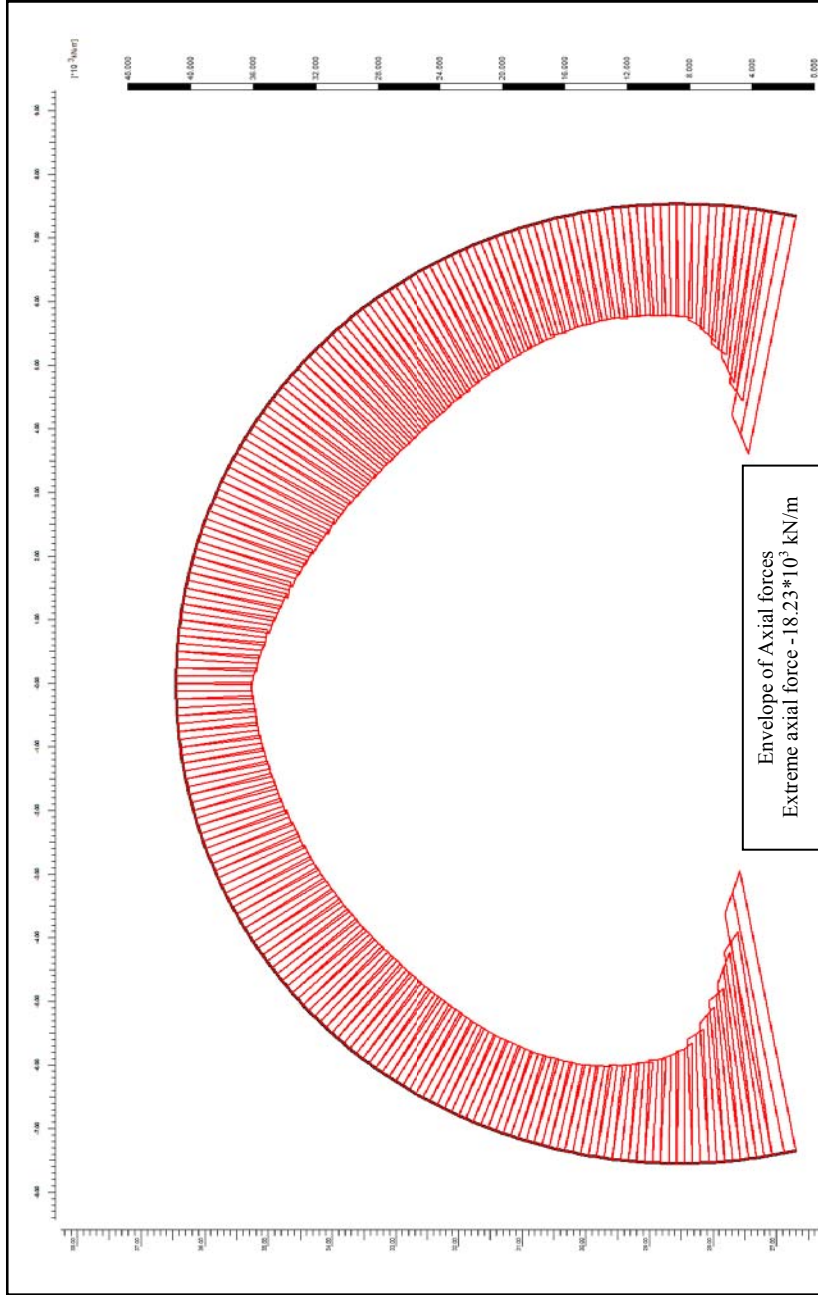
Figure 5.11 Envelope of the axial forces of the inner lining of the analyzed section during seismic shaking including previous stages.
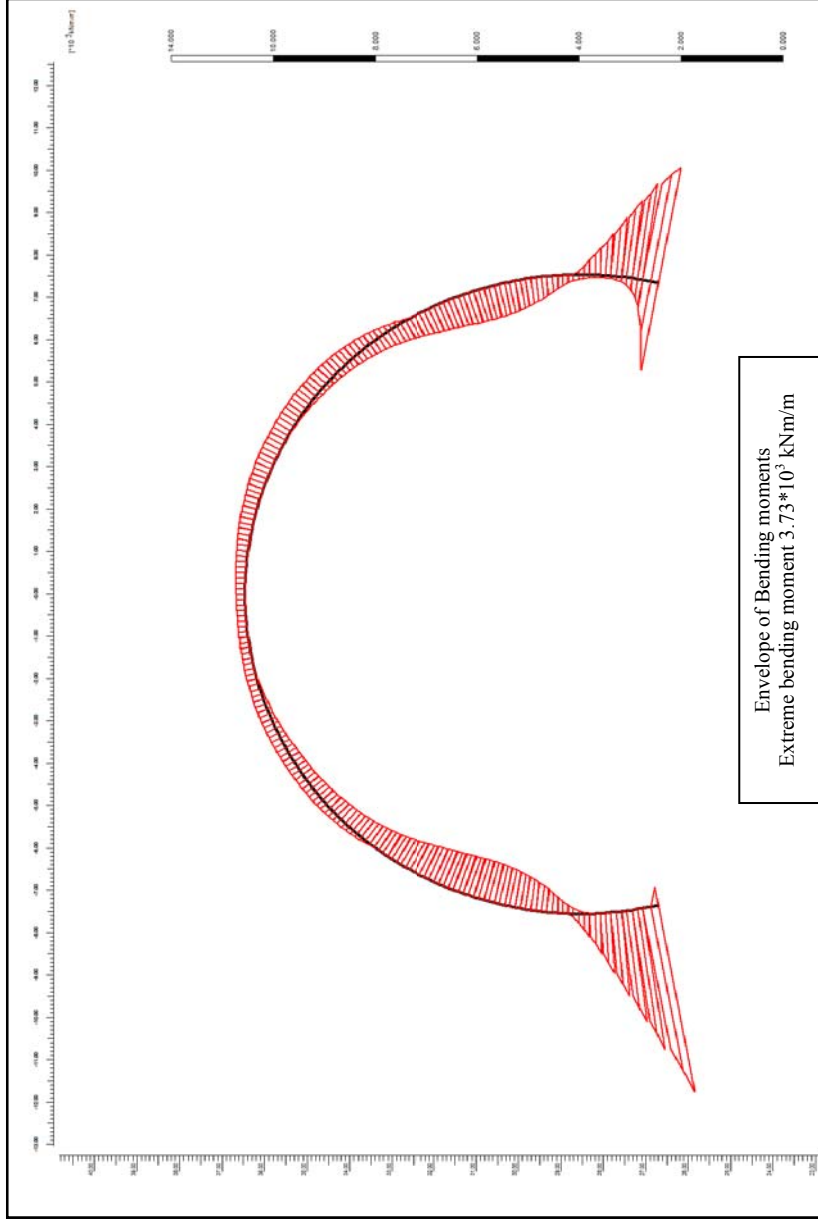
Figure 5.12 Envelope of the bending moments of the inner lining of the analyzed section during seismic shaking including previous stages.
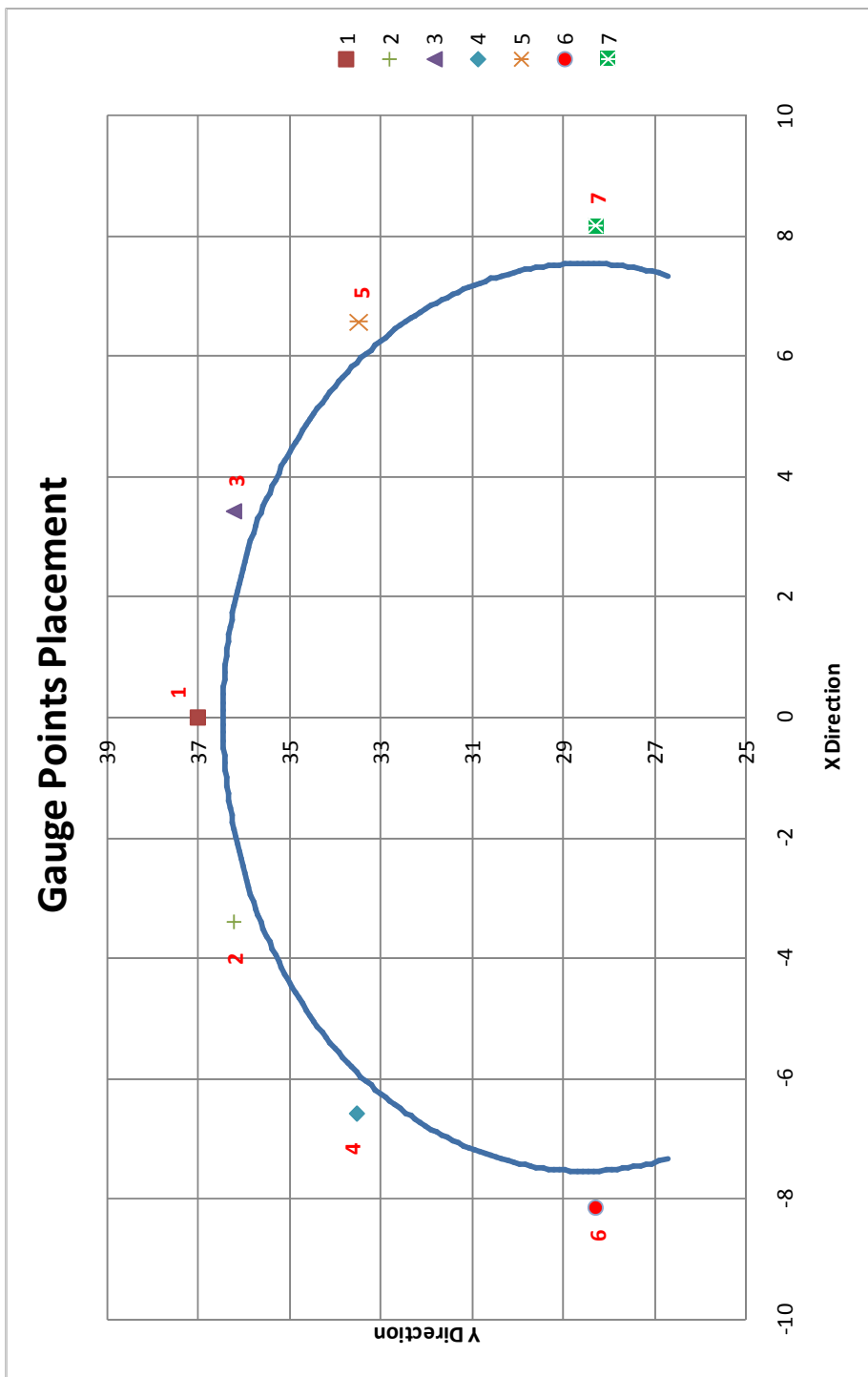
Figure 5.13 Location of the gauge points at the analyzed section (block 62).
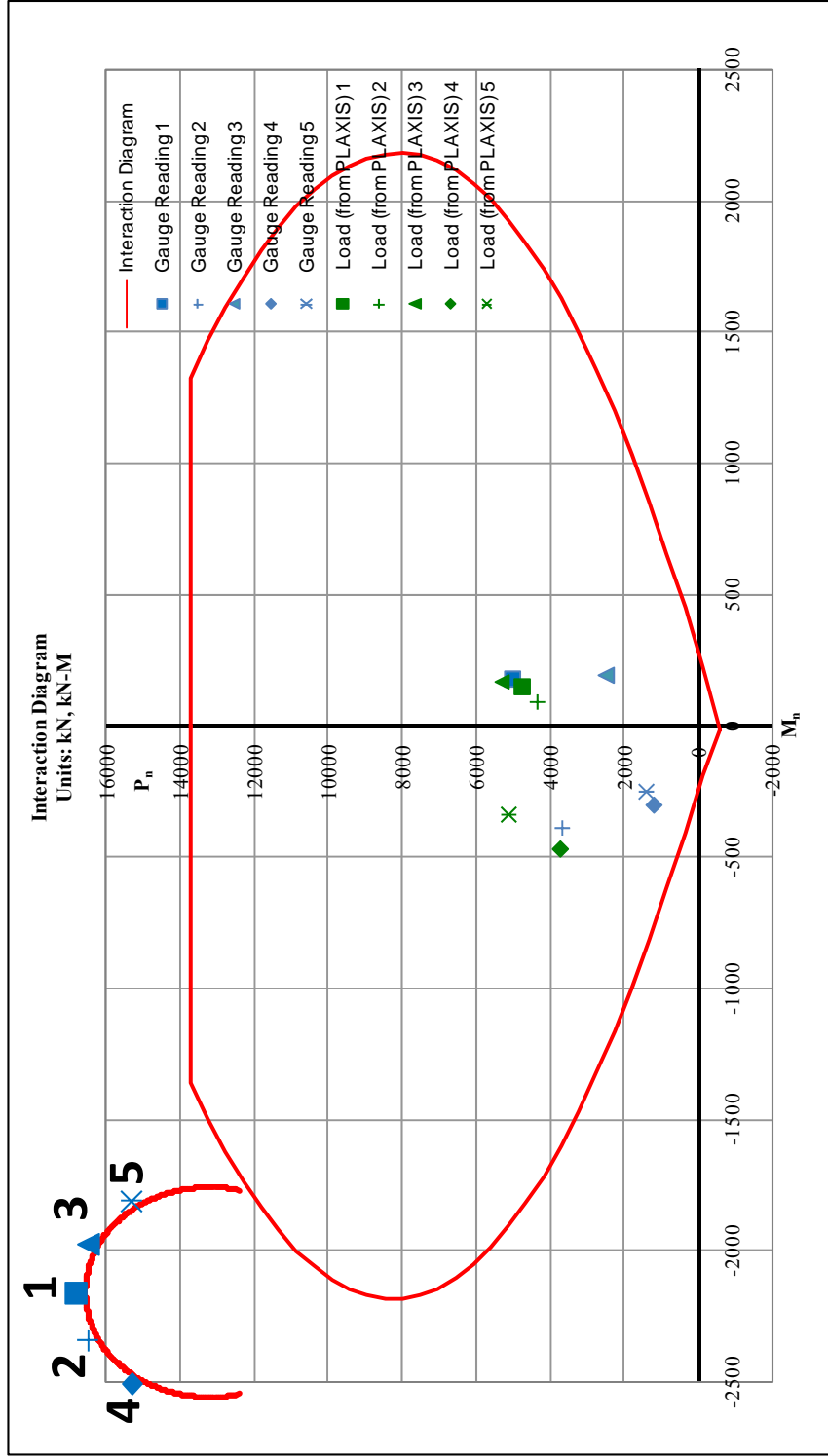
Figure 5.14 Comparison of the forces based on measurements at gauge points 1, 2, 3, 4 and 5 with analyses results using M-N interaction diagram (h=1000 mm, b=650mm) following seismic shaking.
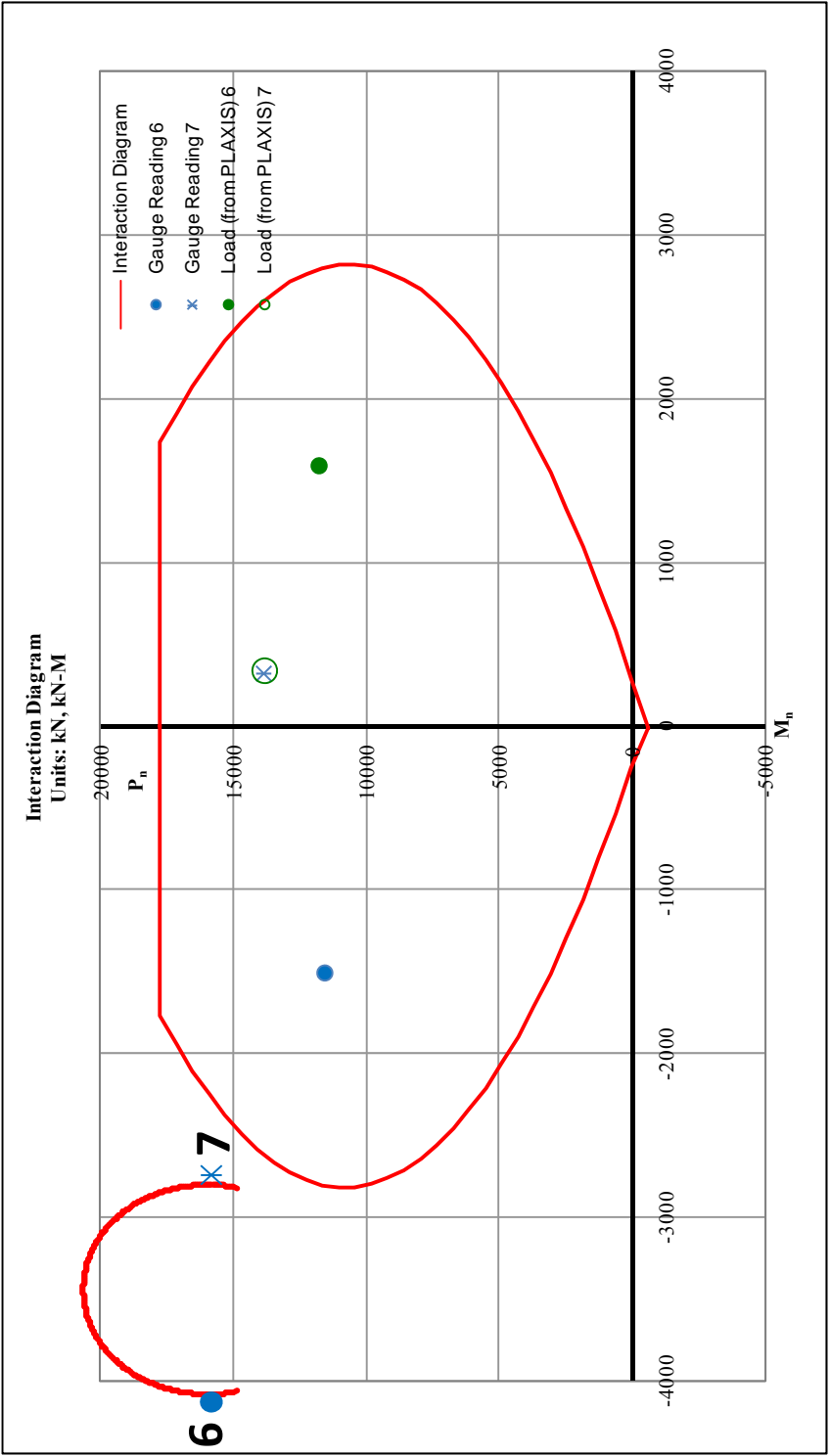
Figure 5.15 Comparison of the forces based on measurements at gauge points 6 and 7 with analyses results using M-N interaction diagram (h=1000 mm, b=850 mm) following seismic shaking.
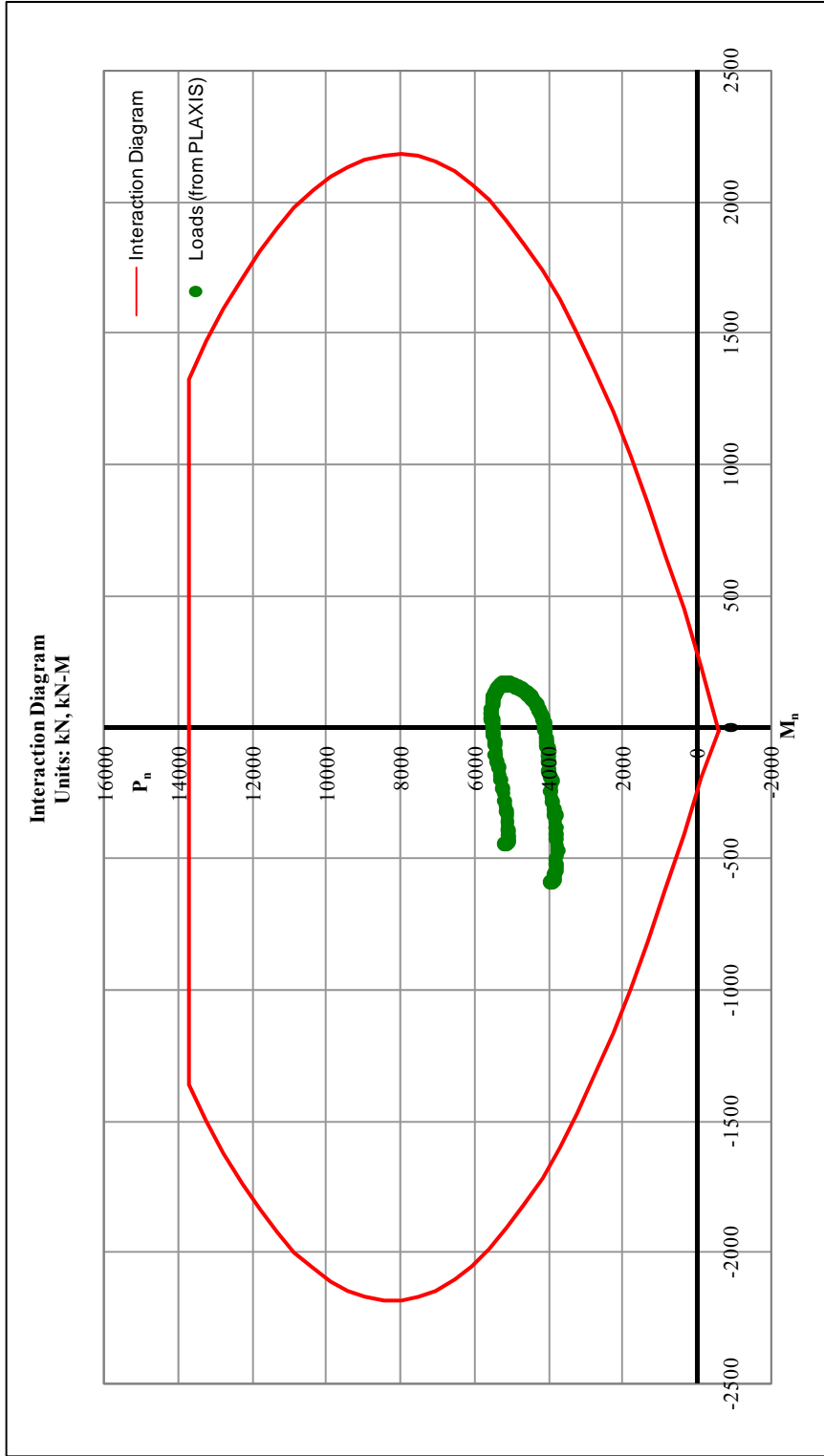
Figure 5.16 Capacity calculations for all of the section based on analyses results using M-N interaction diagram (h=1000 mm, b=650mm) following the seismic shaking.
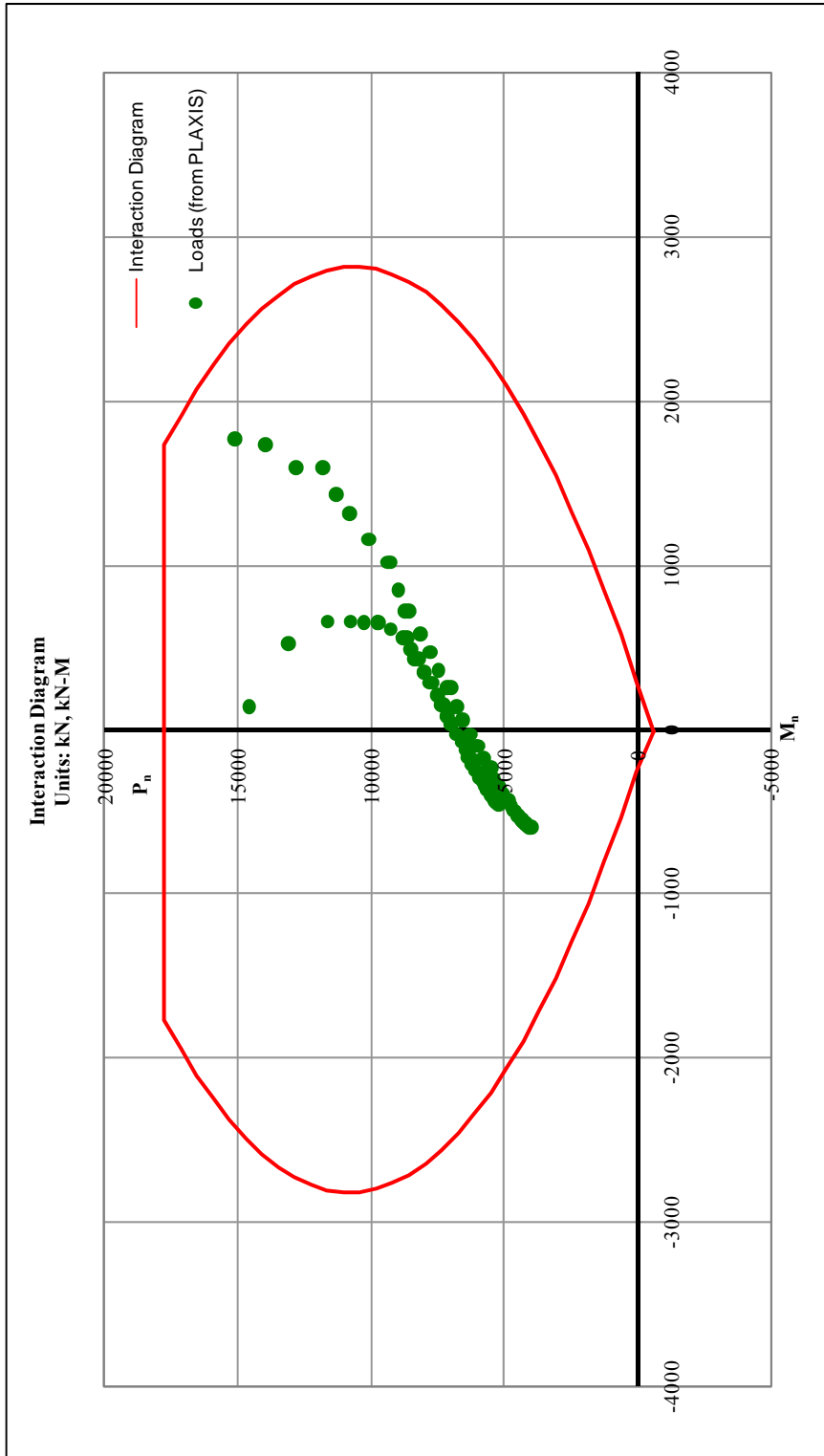
Figure 5.17 Capacity calculations for all of the section based on analyses results using M-N interaction diagram (h=1000 mm, b=850 mm) following the seismic shaking.
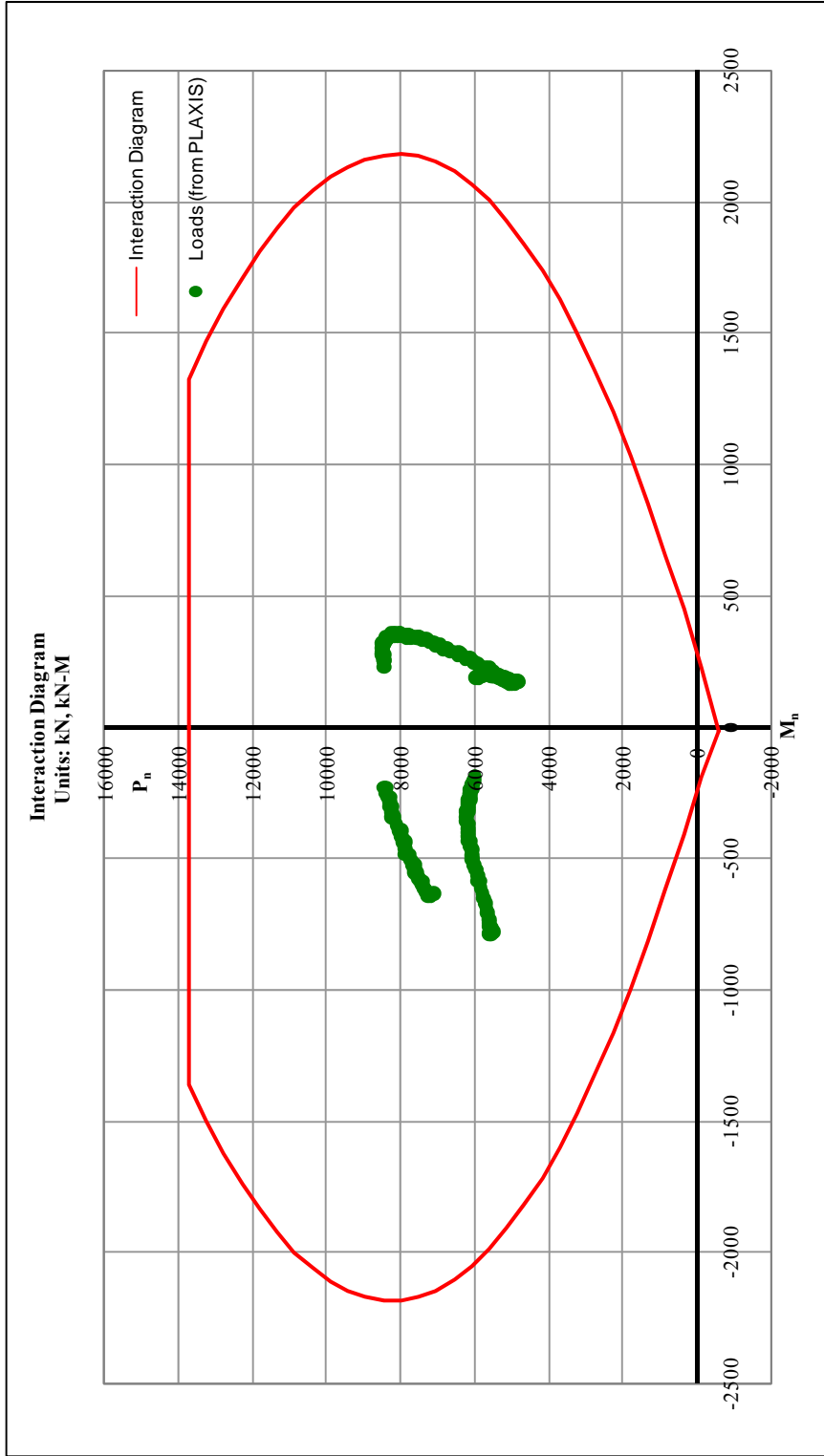
Figure 5.18 Capacity calculations based on analyses results relating to the force envelopes using M-N interaction diagram (h=1000 mm, b=650mm) during seismic shaking.
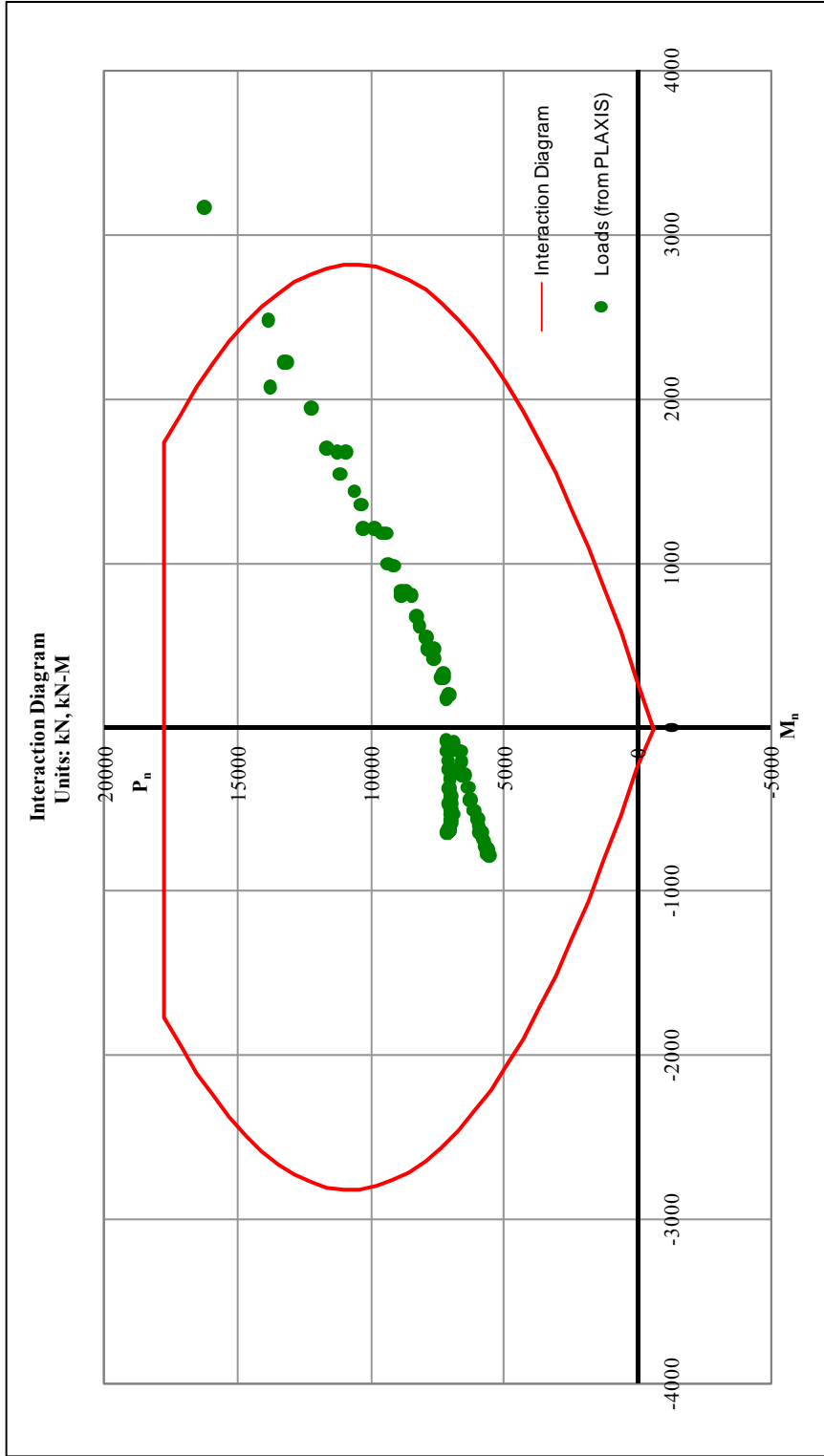
Figure 5.19 Capacity calculations based on analyses results relating to the force envelopes using M-N interaction diagram (h=1000 mm, b=850 mm) during seismic shaking.
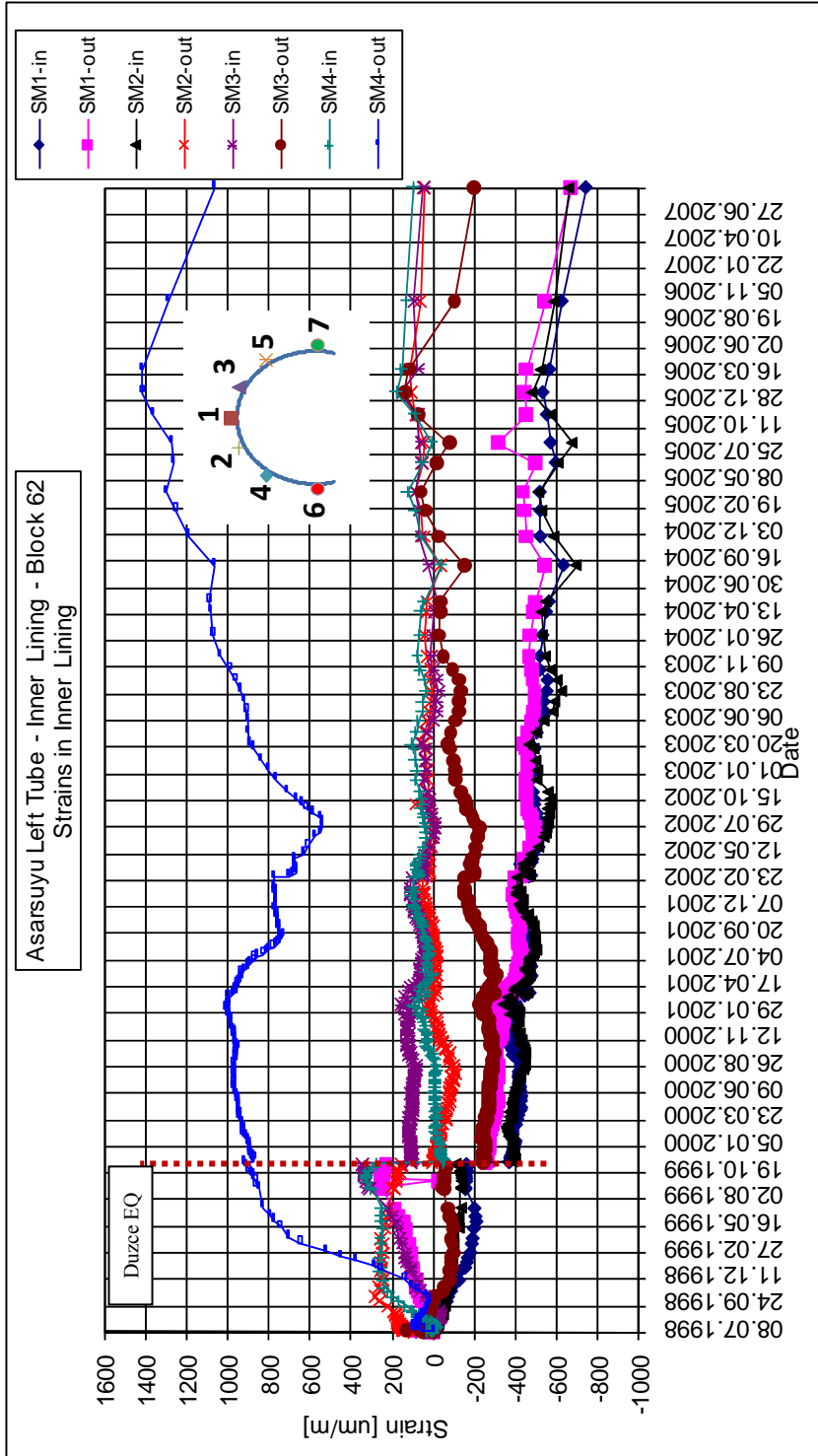
Figure 5.20 Variation of measured inner lining strains at the analyzed section (block 62) in time.
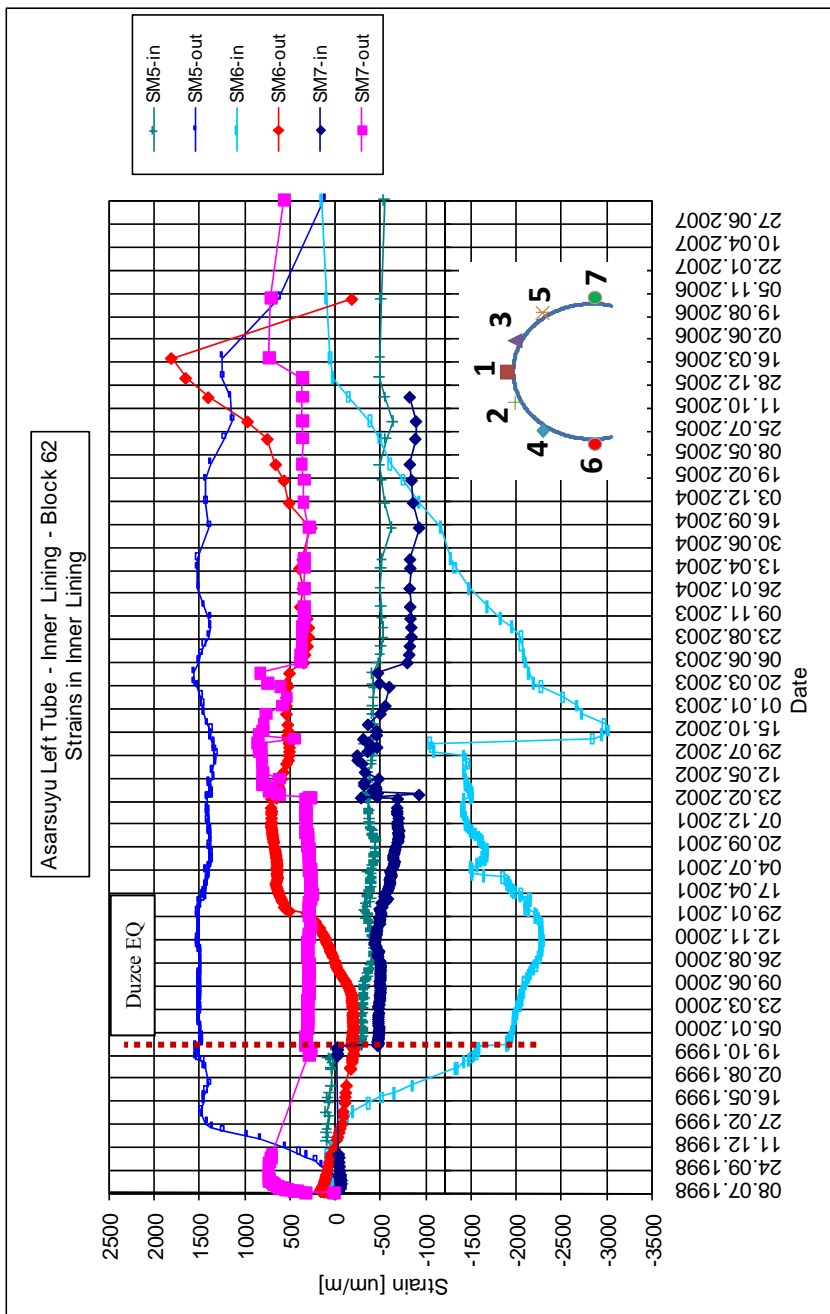
Figure 5.21 Variation of measured inner lining strains at the analyzed section (block 62) in time.
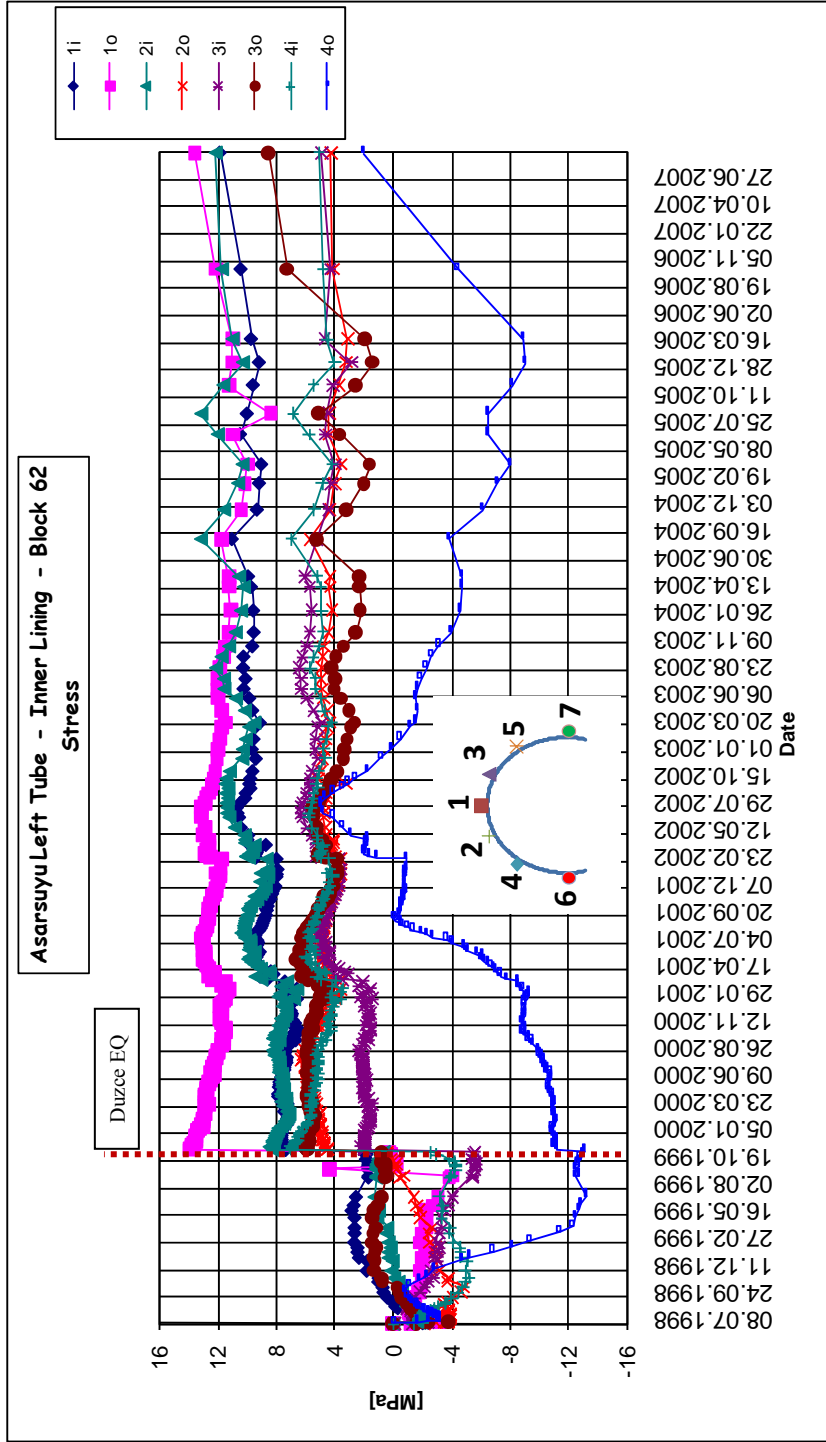
Figure 5.22 Calculated inner lining stresses at the analyzed section based on field measured strains (block 62).
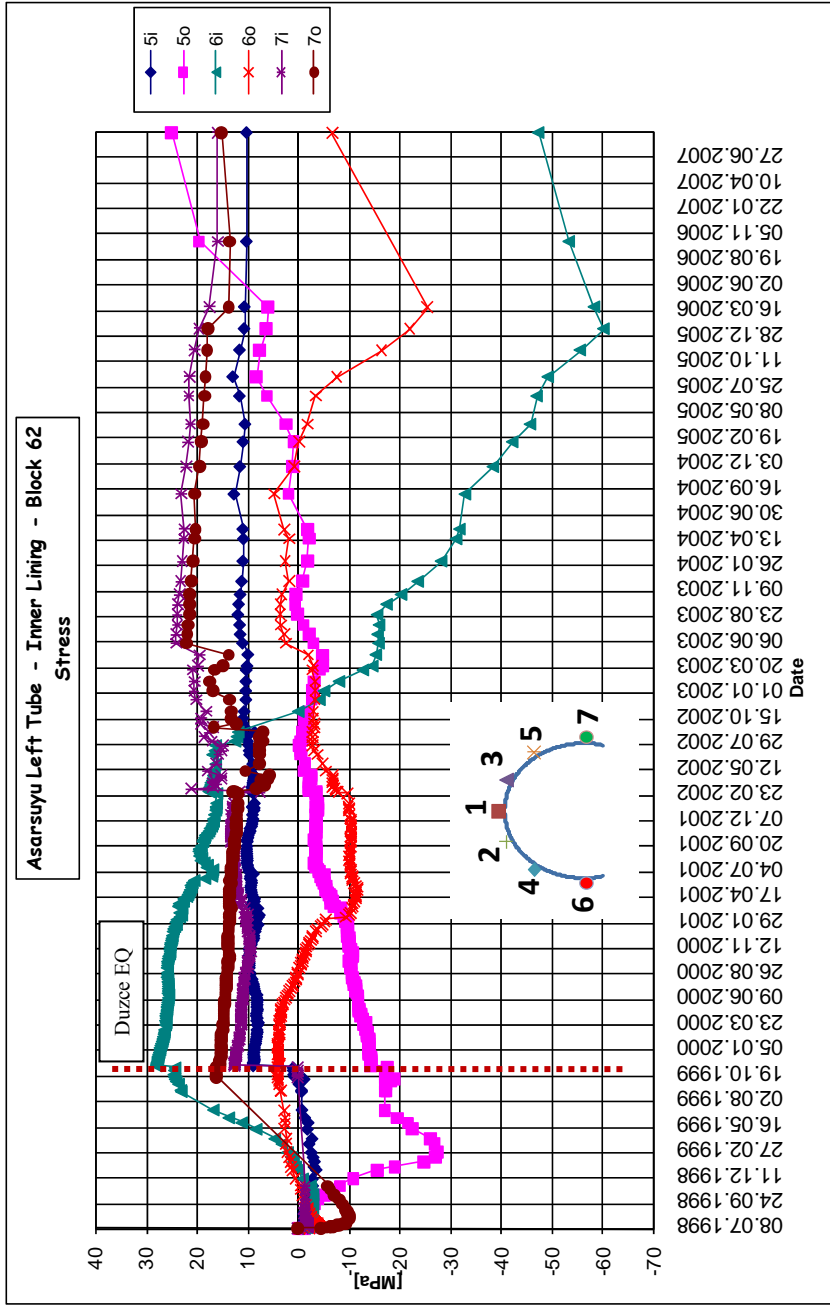
Figure 5.23 Calculated inner lining stresses at the analyzed section based on field measured strains (block 62).
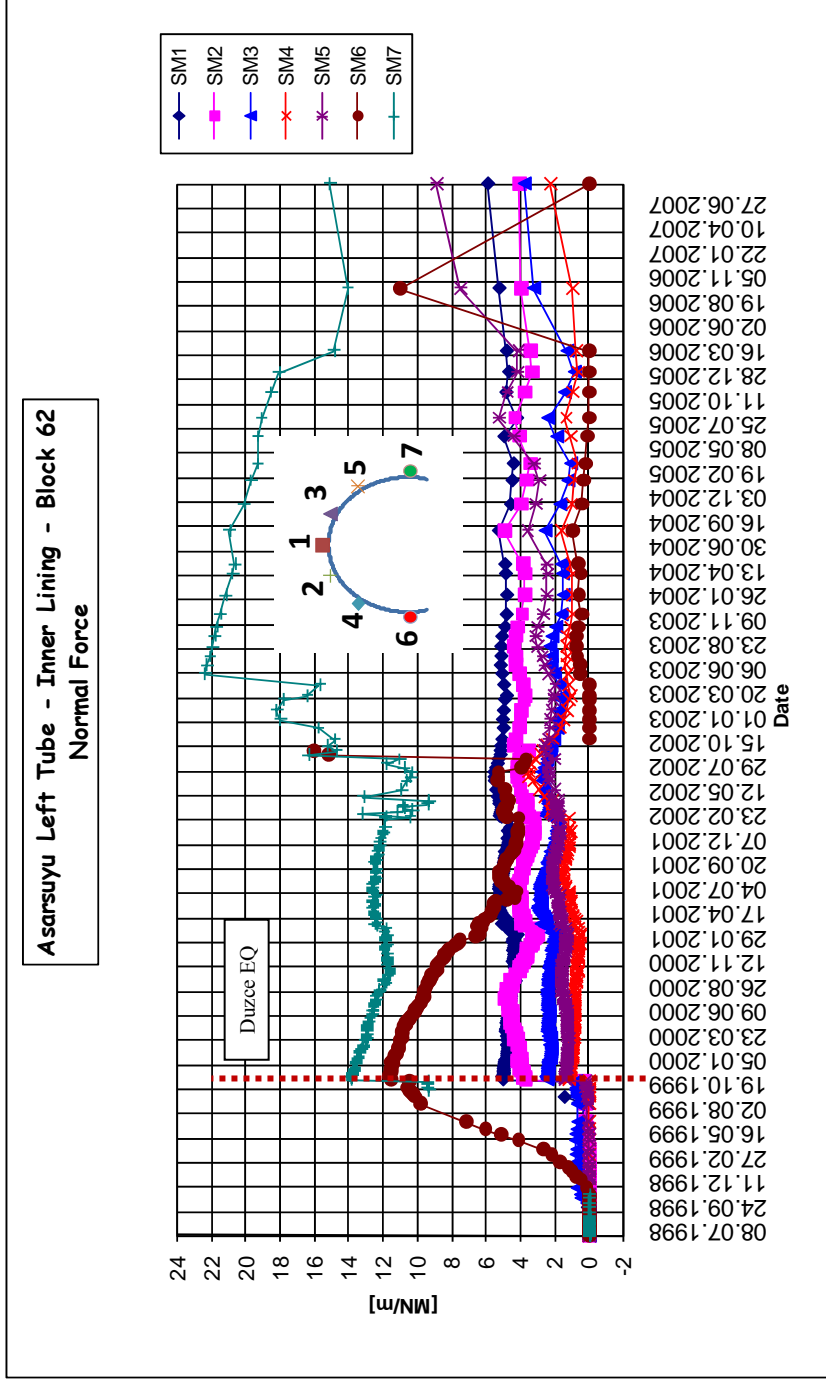
Figure 5.24 Calculated normal forces at the analyzed section based on field measurements (block 62).
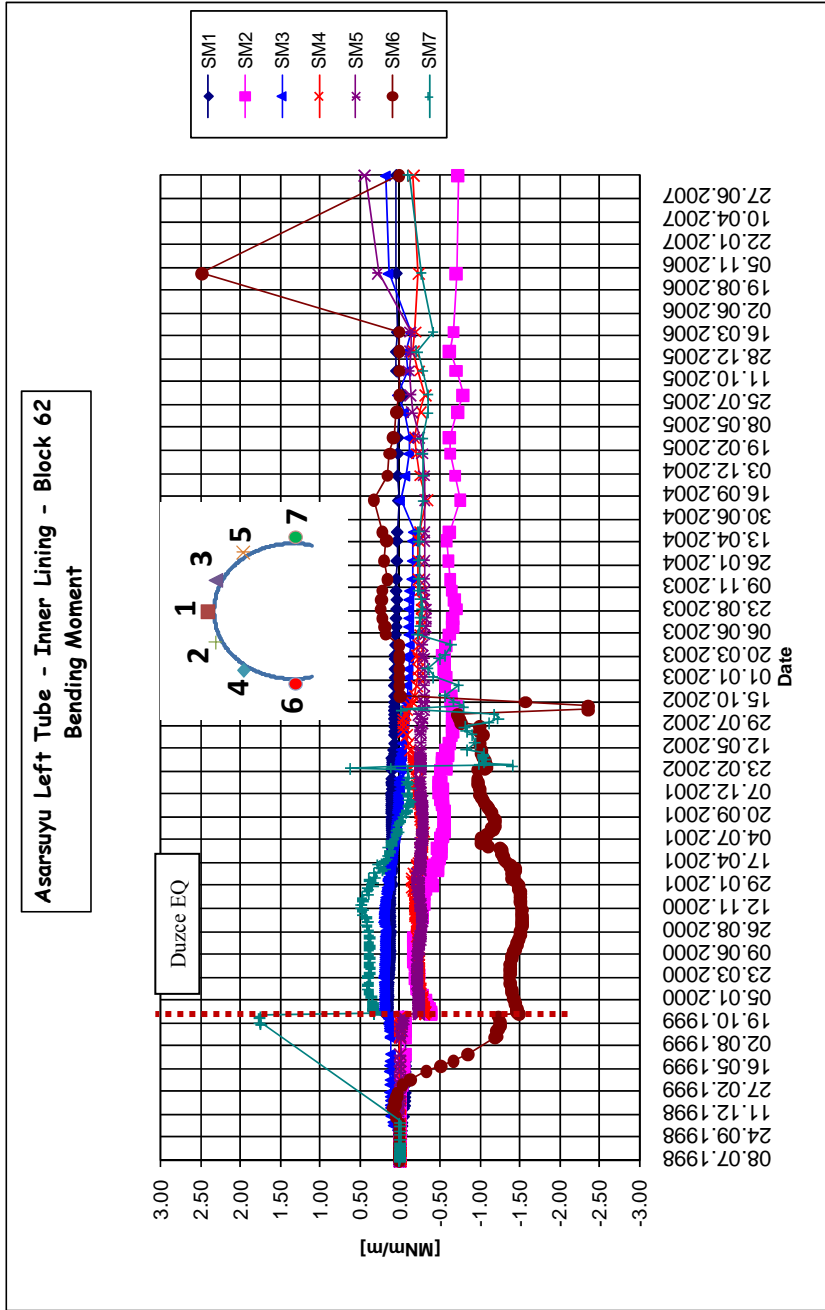
Figure 5.25 Calculated moments at the analyzed section based on field measurements (block 62).
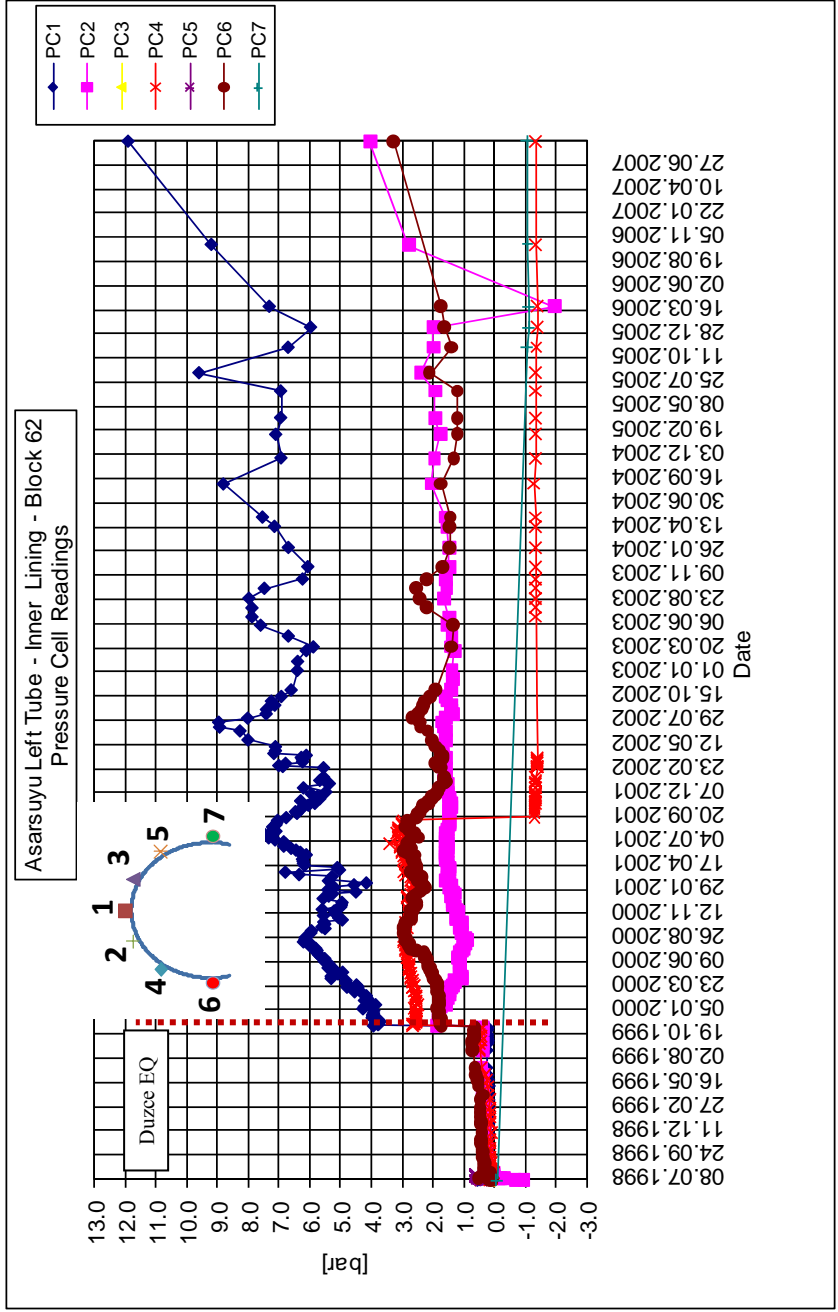
Figure 5.26 Pressure cell readings at the analyzed section (block 62).

CHAPTER 6

CONCLUSIONS AND RECOMENDATIONS FOR FUTURE STUDIES

6.1 Conclusions

Bolu Tunnels were quite well documented and subjected to various forms of damage during the Düzce earthquake. A section of the tunnels is modeled and response during the seismic shaking is simulated through detailed dynamic analyses. The conclusions reached are the following:

1. Pressure cell readings show that the geological medium surrounding the tunnels is subject to long term creep deformations. This phenomenon, which is simulated in the model with relaxation of the medium previous to the dynamic analyses, results in rather high axial forces over the upper part of the lining.

2. The levels and locations of the maximum stresses and corresponding forces and moments are generally in agreement with the available site measurements from pressure cell readings.

3. The capacities calculated with the 2-D model using the presently available analyses methods show that the analyzed section of the tunnel was sufficient in terms of strength against the seismic loading exerted during the Düzce earthquake. That is, collapse was not expected due to the earthquake, which is consistent with the post earthquake condition of the analyzed tunnel section.

6.2 Recommendations for Future Studies

The presented study is based on several assumptions and approximations which can be improved through further research. These topics, which involve detailed site data collection and comprehensive 3D modeling, are the following:

1. The tunnel liners are assumed to respond linearly elastic in this study. Nonlinear or elastoplastic behavior of such elements can be utilized in the analyses.

2. Effect of the ground water on seismic response of the tunnel can be implemented in the analyses.

3. Although the modeling would be much more complicated and computation time would increase drastically, 3 D modeling of the tunnel can be useful to simulate the actual behavior more closely.

4. The effects of the faulting and the directivity effects over the ground motion at the site of the tunnels can be examined in detail.

5. The soil and rock properties at the recording station and site of tunnels can be studied further.

6. The interaction of the twin tunnels can be incorporated in the model.

7. More realistic creep models can be utilized to model the time dependent deformations.

REFERENCES

AASHTO LRFD, (2006) American Association of State Highway and Transportation Officials, Standard Specification for Highway Bridges, 4th Edition., Washington D.C..

Abrahamson, N. A., and W. J. Silva (2008), Summary of the Abrahamson & Silva NGA Ground-Motion Relations, *Earthquake Spectra*, 24(1), 67-97.

Astaldi S.p.A., 1993-2006; Anatolian Motorway Gümüşova Gerede Section - Strecth 2 Bolu Tunnel Bypass Drawings Album; Astaldi *S.P.A. Turkey Branch Technical Office*.

Astaldi S.p.A., (2000). Anatolian Motorway Gümüşova Gerede Section - Strecth 2 Bolu Tunnel – Seismic Design, Seismic Screening, *Report No: 45.110/R/2251*, Astaldi *S.P.A. Turkey Branch Technical Office*.

Aşcıoğlu G. (2007). Analysis of Support Design Practice at Elmalık Portals of Bolu Tunnel; *M.Sc. Thesis, Department of Mining Engineering, METU*.

Aygar E. (2000). A Critical Approach To The New Austrian Tunneling Method In Bolu Tunnels; *M. Sc. Thesis, Institute Of Natural Sciences, Hacettepe University*.

Aygar E. (2007). Investigation of the Bolu Tunnel Stability by means of Static and Dynamic Analysis; *PhD Thesis, Institute Of Natural Sciences, Hacettepe University*.

Bardet, J.P., Ichii, K., and Lin, C. H., "EERA (2000). A Computer Program for Equivalent-linear Earthquake site Response Analyses of Layered Soil Deposits", University of Southern California.

Başokur, A. T. (2005). Determination of Shear Wave Velocity Profile by the Application of Remi Method, 4-9.

Burns, J.Q. and Richard, R.M. (1964). Attenuation of Stresses for Buried Cylinders. *Proceedings of the Symposium on Soil-Structure Interaction*, University of Arizona at Tempe, Arizona.

Çakan, A. G. (2000). Analysis of Tunnel Advance in Soft Ground Using Finite Element Method – A Case Study on Bolu Tunnels, *M.Sc. Thesis, Department of Civil Engineering, METU.*

Dowding, C.H., Rozen, A. (1978). Damage to rock tunnels from earthquake shaking, *Journal of Geotechnical Engineering Division*, ASCE 104 (GT2), 175-191.

Einstein, H.H. and Schwartz, C.W. (1979). Simplified Analysis for Tunnel Supports, *Journal of Geotechnical Engineering Division*, ASCE, GT4, pp.499-518.

Electric Power Research Institute (EPRI) (1993). Guidelines for determining design basis ground motions, *Electric Power Research Institute Technical Report EPRI TR-102293.*

Hartzell, S., Bonilla, L. F., and Williams, R. A., (2004). Prediction of Nonlinear Soil Effects, *Bulletin of the Seismological Society of America*, Vol. 94, No. 5, pp. 1609–1629.

Hashash, Y.M.A., Hook, J.J., Schmidt, B., Yao, J.I. (2001). Seismic Design and Analysis of Underground Structures, *Tunneling and Underground Space Technology*. 16, pp. 247-293.

Hoeg, K. (1968). Stresses Against Underground Structural Cylinders. *Journal of Soil Mechanics and Foundation Division*, ASCE 94 SM4, pp. 833-858.

Huo, H., Bobet, A., Fernández, G. and Ramírez, J., (2005). Load Transfer Mechanisms between Underground Structure and Surrounding Ground: Evaluation of the Failure of the Daikai Station, *Journal of Geotechnical and Geoenvironmental Engineering*, ASCE, Vol. 131, No. 12, pp. 1522-1533.

http://www.koeri.boun.edu.tr , Website of Department of Earthquake Engineering. Boğaziçi University, Last Update: April 8, 2010.KOERI. Last visited on: August, 15th, 2010.

http://nisee.berkeley.edu/. Website of National Information Service for Earthquake Engineering. PEER, NGA Strong Motion Database. Last Update: March 30, 2010. PEER, 1999. Last visited on: August, 15th, 2010.

Geoconsult, (2002). Anatolian Motorway Gümüşova Gerede Section - Strecth 2 – Bolu Tunnel By-pass Rock Support Class Distribution, *Report No: 45.110/TN/TUG/R/EX/001*.

Kuesel, T.R. (1969). Earthquake Design Criteria for Subways, J. Struct. Div., ASCE ST6, 1213-1231.

Linda Al Atik, (2009). Calculation of weighted average 2008 NGA models, *PEER*.

Matsubara, K., Hirasawa, K., and Urano, K. (1995). On the Wavelength for Seismic Design of Underground Pipeline Structures. *Proceedings of the First International Conference on Earthquake Geotechnical Engineering*, pp. 587-590.

Meissner, H. (1996). Tunnelbau unter Tage - Empfehlungen des Arbeitskreises 1.6 *Numerik in der Geotechnik*. Geotechnik , 99-108.

Merritt, J.L., Monsees, J.E., Hendron, A.J., Jr., (1985). Seismic design of underground structures, *Proceedings of the 1985 Rapid Excavation Tunneling Conference*, vol. 1, pp. 104-131.

Mononobe, N., Matsuo, H. (1929). On The Determination of Earth Pressures During Earthquakes, Proceedings, *World Engineering Congress*.

Newmark, N.M. (1968). Problems in wave propagation in soil and rock, *Proceedings of the International Symposium on Wave Propagation and Dynamic Properties of Earth Materials*.

Okabe, S. (1926). General theory on earth pressure and seismic stability of retaining wall and dam, *Journal of Japan Society of Civil Engineers*, Vol. 12, No. 1, pp 123-134.

Owen, G.N., Scholl, R.E., (1981). Earthquake engineering of large underground structures, Report no. *FHWA RD-80 195*. Federal Highway Administration and National Science Foundation.

Peck, R.B., Hendron, A.J., Jr., and Mohraz, B. (1972). State of the Art of Soft-Ground Tunneling. *Proceedings of the RETC 1972*; Vol. 1: pp. 259-285.

Penzien, J., Wu, C.L. (1998). Stresses in Linings of Bored Tunnels. *Earthquake*

Penzien, J. (2000). Seismically Induced Raking of Tunnel Linings. *Earthquake Engineering and Structure Dynamics 29*, pp. 683-691.

PLAXIS 2D Scientific Manual, version 8.2 (2002). Delft University of Technology & PLAXIS B.V.

PLAXIS 2D Dynamics Manual, version 8.2 (2002). Delft University of Technology & PLAXIS B.V.

Power, M.S., Rosidi, D., and Kaneshiro, J. (1996). Vol. III Strawman: Screening, Evaluation, and Retrofit Design of Tunnels. Report Draft. *National Center for Earthquake Engineering Research*, Buffalo, New York.

Schnabel, P. B., (1973). Effects of Local Geology and Distance from Source on Earthquake Ground Motions, *PhD Thesis, University of California*, Berkeley, California.

St. John, C.M., Zahrah, T.F. (1987). Aseismic design of underground structures, *Tunneling Underground Space Technology*. 2 (2)., 165 197. *Engineering and Structure Dynamics 27*, pp. 283-300.

Şimşek O. (2001). Bolu Tunnel Re-Alignment At Stretch 2F Tunnel Section Geological and Geotechnical Report Volume-1; *IC Consulenten Ziviltechnicer GmbH Report no: 45.110/2F/T/R/GE-GT/001.*

TÜBİTAK, (2006). Compilation of National Strong Ground Motion Database in Accordance with International Standards, *Research Project, No. 105G016.*

Unterberger, W. and Brandl, J., (2000). The effect of recent earthquake in Turkey on the Bolu Tunnels, Felsbau.

Üçer, S. (2006). Comparison of 2D and 3D Finite Element Models of Tunnel Advance in Soft Ground: A Case Study on Bolu Tunnels, *M.Sc. Thesis, Department of Civil Engineering, METU.*

Vucetic, M., Dobry, R., (1991). Effect of Soil Plasticity on Cyclic Response, *Journal of Geotechnical Engineering*, ASCE, Vol. 117, No. 1.

Wang, J.N. (1993). Seismic Design of Tunnels, Monograph 7, Parsons Brinckerhoff Quade & Douglas, Inc..

APPENDIX A

EERA ANALYSES MODELING PARAMETERS FOR BOLU STATION

SITE MOTION

In this appendix, modeling parameters utilized at Bolu Station in EERA analyses for the ground motion including the variation of shear wave velocities and unit weight, relevant modulus degradation and damping curves are presented

Table A.1 Bolu Station site soil profile.

	Layer Number	Soil Material Type	Number of sublayers in layer	Thickness of layer (m)	Maximum shear modulus G_{max} (MPa)	Initial critical damping ratio (%)	Total unit weight (kN/m³)	Shear wave velocity (m/sec)	Location and type of earthquake input motion	Location of water table
Surface	1	5		2.0	125.94		19.00	255	Outcrop	
	2	5		6.5	132.57		20.00	255		W
	3	1		4.5	132.57		20.00	255		
	4	2		5.2	394.70		20.00	440		
	5	3		5.3	394.70		20.00	440		
	6	3		3.0	394.70		20.00	440		
	7	4		4.0	513.77		20.00	502		
	8	6		33.0	513.77		20.00	502		
Bedrock	9	7			2242.61		22.00	1000		
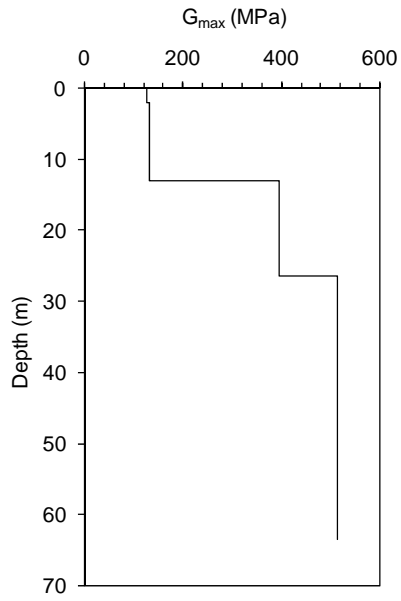
Figure A.1 G_{max} versus depth plot for the Bolu Station site.
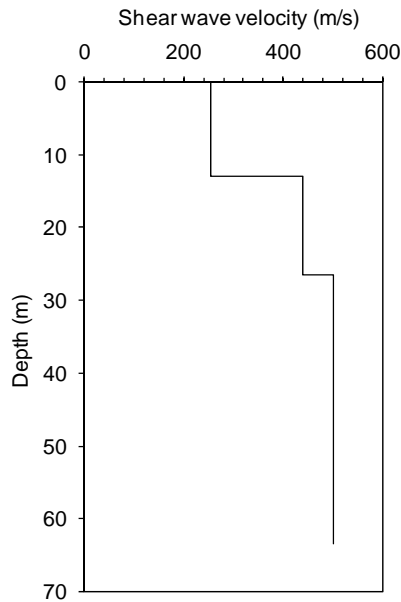
Figure A.2 Shear wave velocity versus depth plot for the Bolu Station site.

Unit weight (kN/m³)
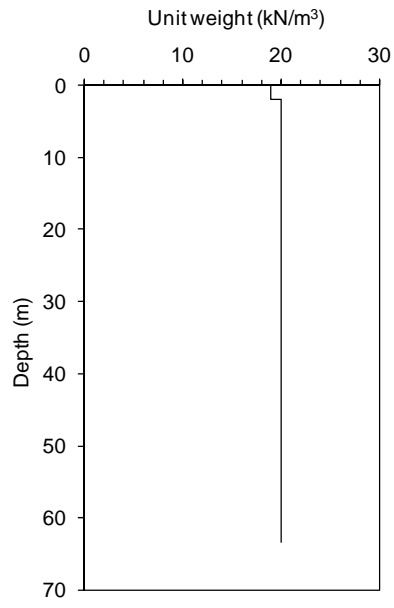
Depth (m)

Figure A.3 Unit weight versus depth plot for the Bolu station site.
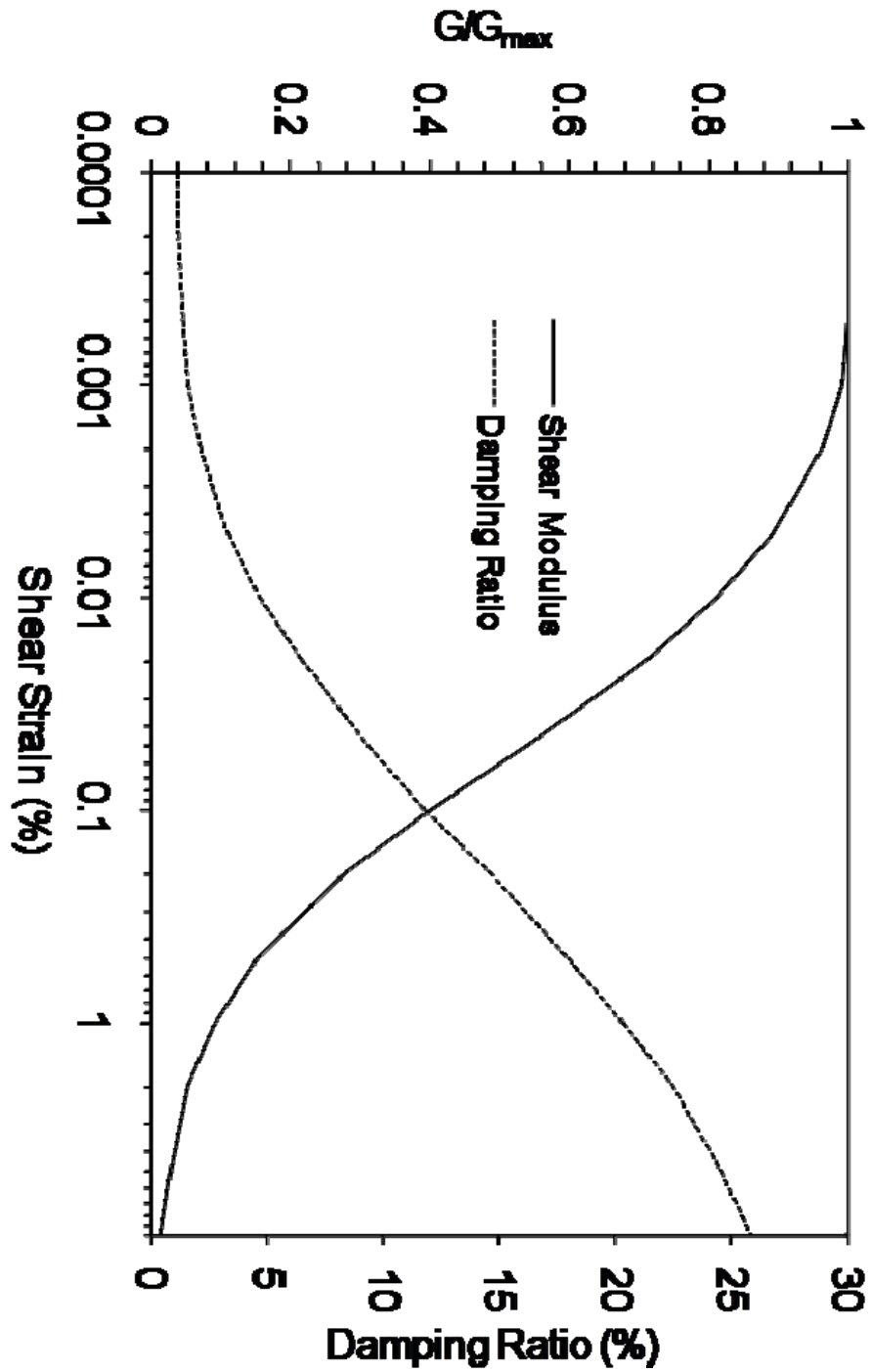
Figure A.4 Modulus degradation and damping curves for clay (PI=14) (after Vucetic and Dobry, 1991) *(soil material type 1)*.
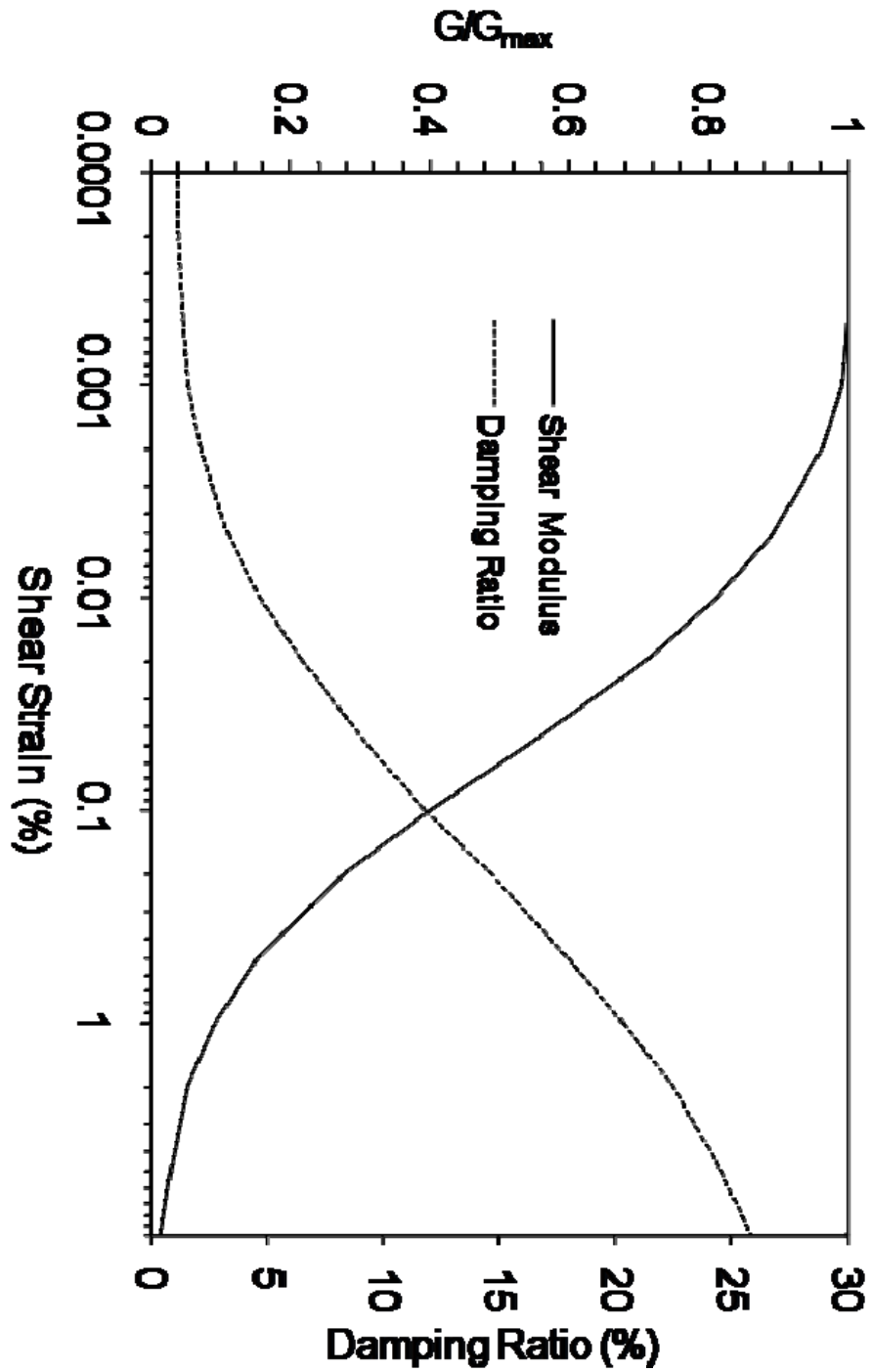
Figure A.5 Modulus degradation and damping curves for clay (PI=16) (after Vucetic
and Dobry, 1991) *(soil material type 2)*.
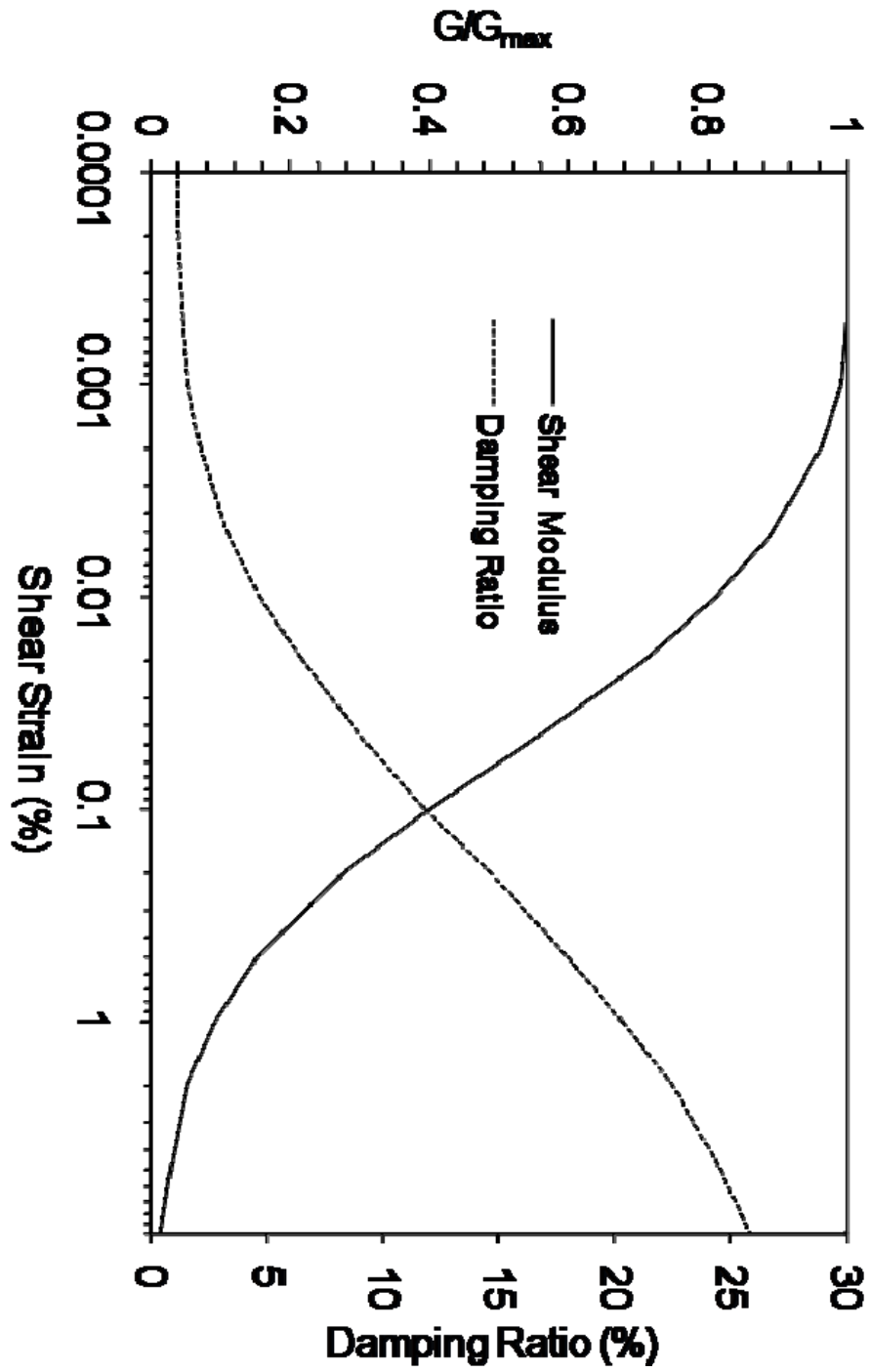
Figure A.6 Modulus degradation and damping curves for clay (PI=28) (after Vucetic and Dobry, 1991) *(soil material type 3)*.
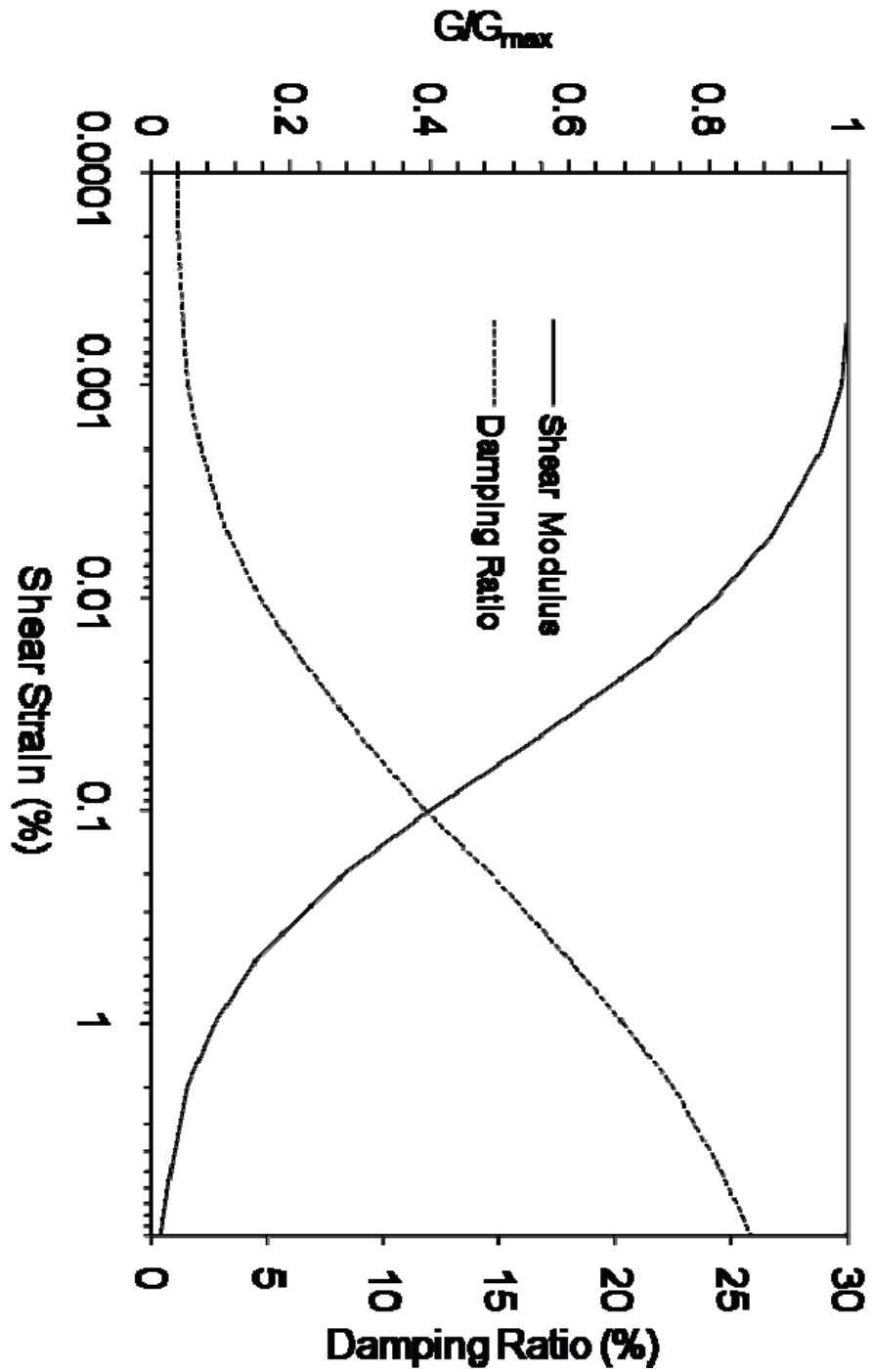
Figure A.7 Modulus degradation and damping curves for clay (PI=32) (after Vucetic and Dobry, 1991) *(soil material type 4)*.
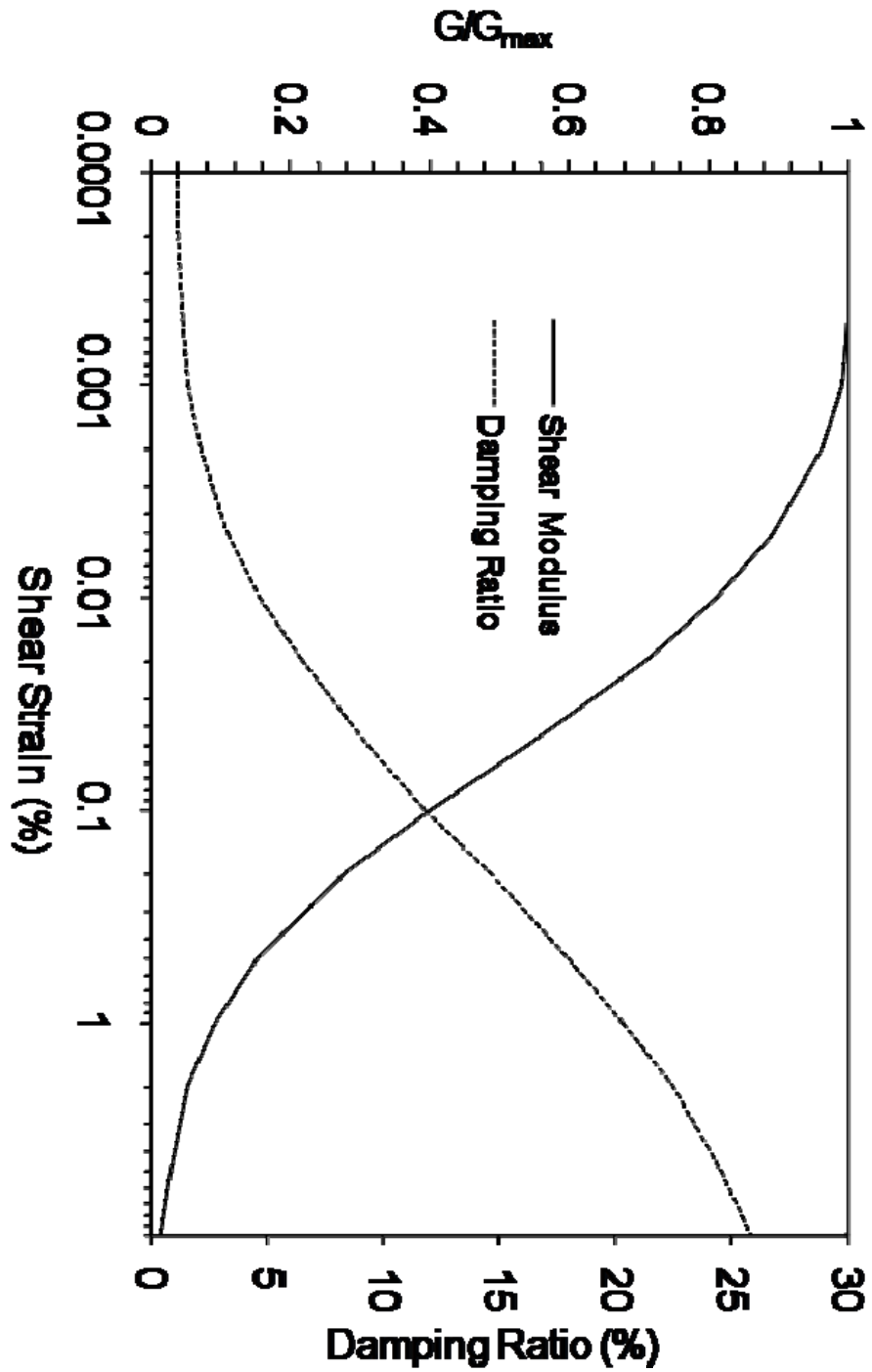
Figure A.8 Modulus degradation and damping curves for clay (PI=38) (after Vucetic and Dobry, 1991) *(soil material type 5)*.
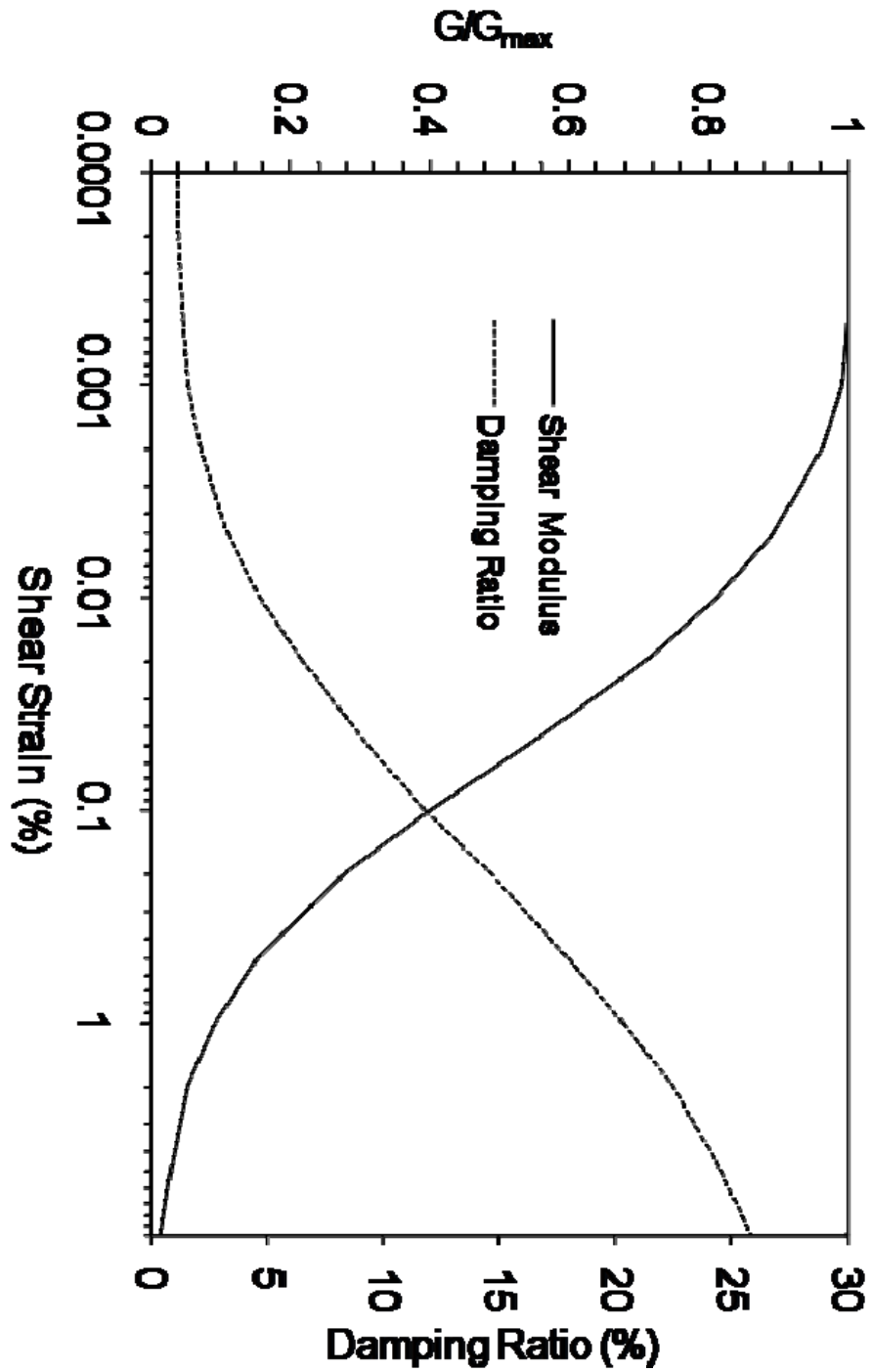
Figure A.9 Modulus degradation and damping curves for clay (PI=40) (after Vucetic and Dobry, 1991) *(soil material type 6)*.
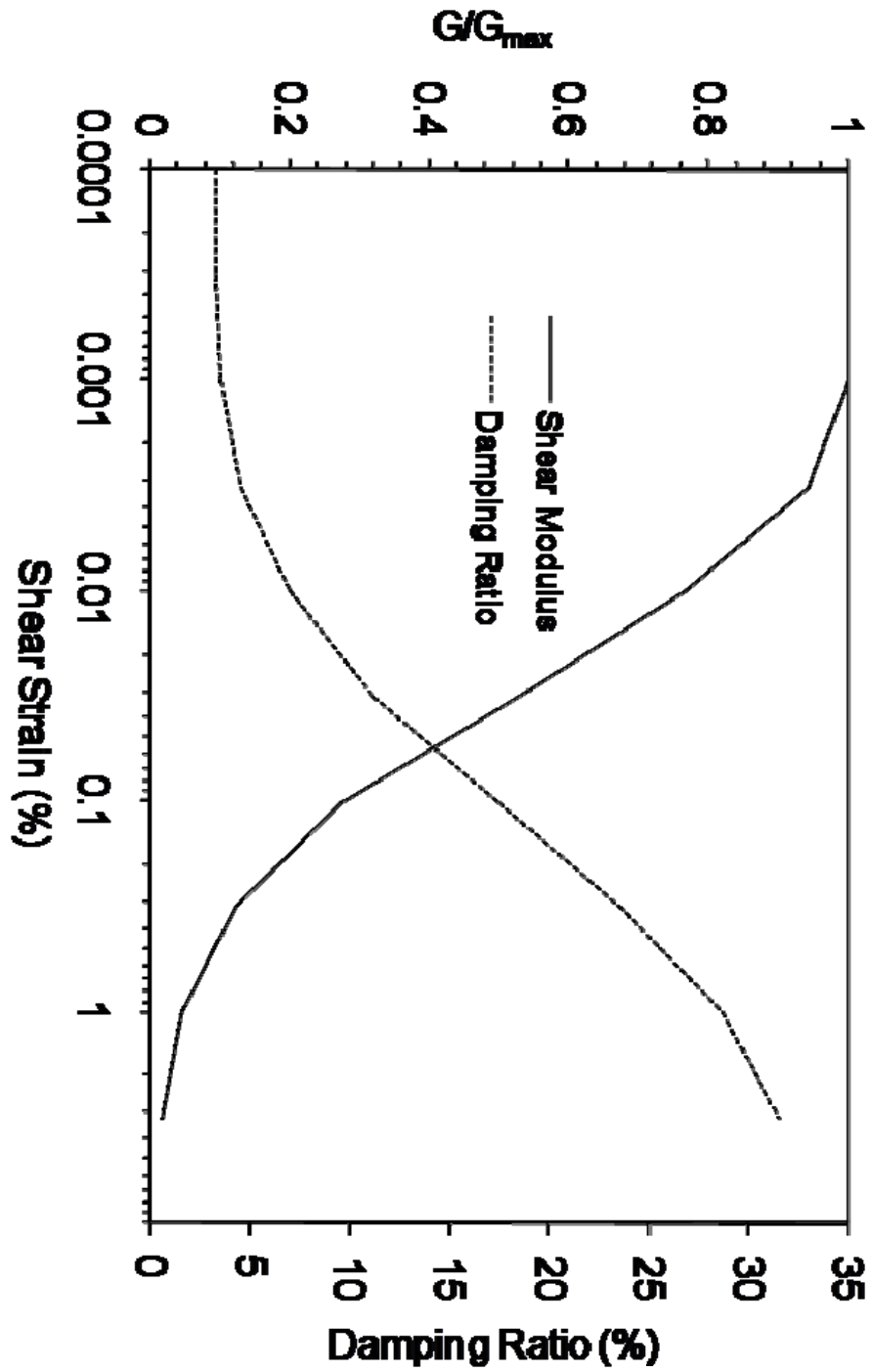
Figure A.10 Modulus degradation and damping curves for rock (average) (after Schnabel, 1973) *(soil material type 7)*.

APPENDIX B

MODELING PARAMETERS OF EERA ANALYSES FOR BOLU TUNNEL

SITE MOTION

In this appendix, modeling parameters utilized at Bolu Tunnels site in EERA analyses for the ground motion including the variation of shear wave velocities and unit weight, relevant modulus degradation and damping curves are presented

Table B.1 Bolu Tunnel site soil profile.

	Layer Number	Soil Material Type	Number of sublayers in layer	Thickness of layer (m)	Maximum shear modulus G_{max} (MPa)	Initial critical damping ratio (%)	Total unit weight (kN/m³)	Shear wave velocity (m/sec)	Location and type of earthquake input motion	Location of water table
Surface	1	7	3	15.0	137.615		20.00	259.808		
	2	6	3	21.0	467.890		20.00	479.062		
	3	2	3	39.0	1018.349		20.00	706.753		
	4	4	15	75.0	1682.110		20.00	908.336		W
	5	5	13	65.0	2337.156		20.00	1070.689		
	6	5	1	4.0	2660.000		20.00	1142.248		
	7	5	1	5.0	2702.110		20.00	1151.254		
	8	5	1	5.0	2748.899		20.00	1161.178		
	9	5	1	4.0	3070.110		22.00	1170.038		
	10	5	1	3.0	3525.206		22.00	1253.763		
	11	5	1	2.0	3555.519		22.00	1259.142		
	12	5	1	2.0	3579.771		22.00	1263.429		
	13	5	1	2.0	3604.021		22.00	1267.701		
	14	5	1	3.0	3634.335		22.00	1273.021		
	15	5	1	3.0	3670.711		22.00	1279.376		
	16	5	1	3.0	3707.087		22.00	1285.700		
	17	5	1	3.0	3743.463		22.00	1291.992		
	18	5	1	3.0	3779.839		22.00	1298.255		
	19	5	1	3.0	3816.215		22.00	1304.487		
Bedrock	20	3			4198.165		22.00	1368.211	Outcrop	
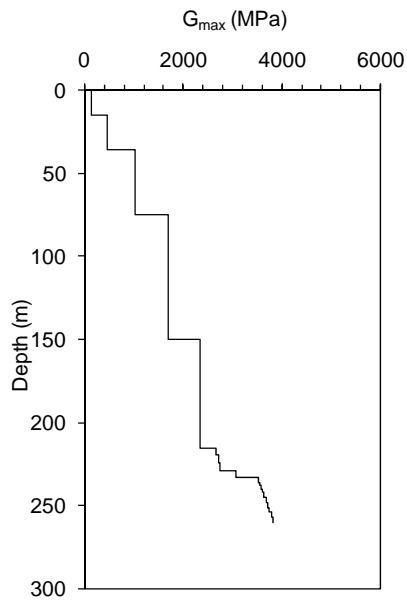
Figure B.1 G_{max} versus depth plot for the Bolu Tunnels site.
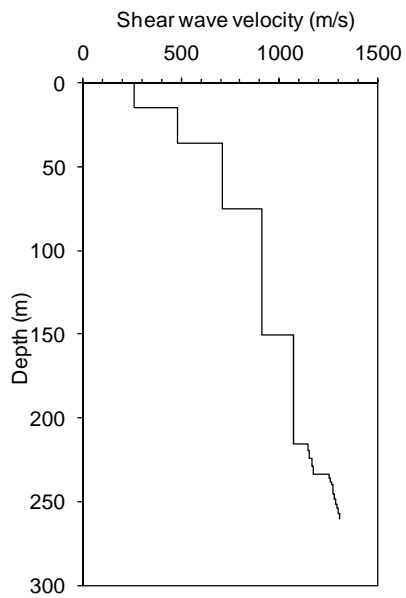
Figure B.2 Shear wave velocity versus depth plot for the Bolu Tunnels site.
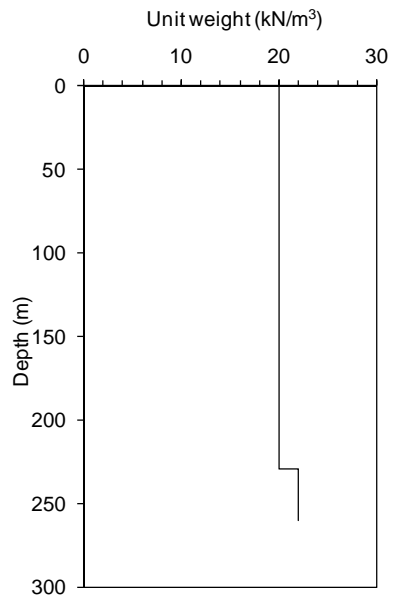
Figure B.3 Unit weight versus depth plot for the Bolu Tunnels site.
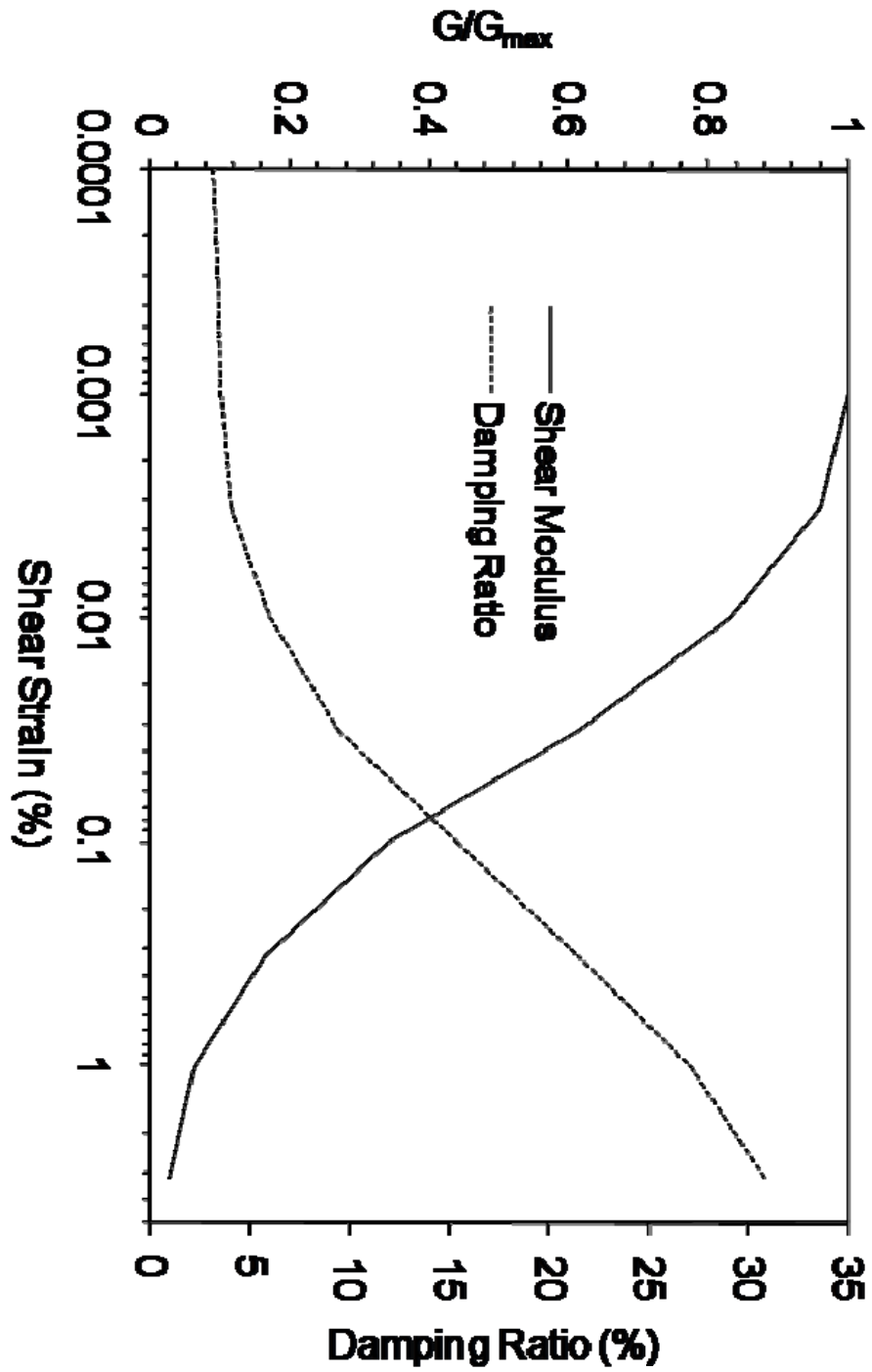
Figure B.4 Modulus degradation and damping curves for rock 0-15 m (EPRI, 1993). *(soil material type 7).*
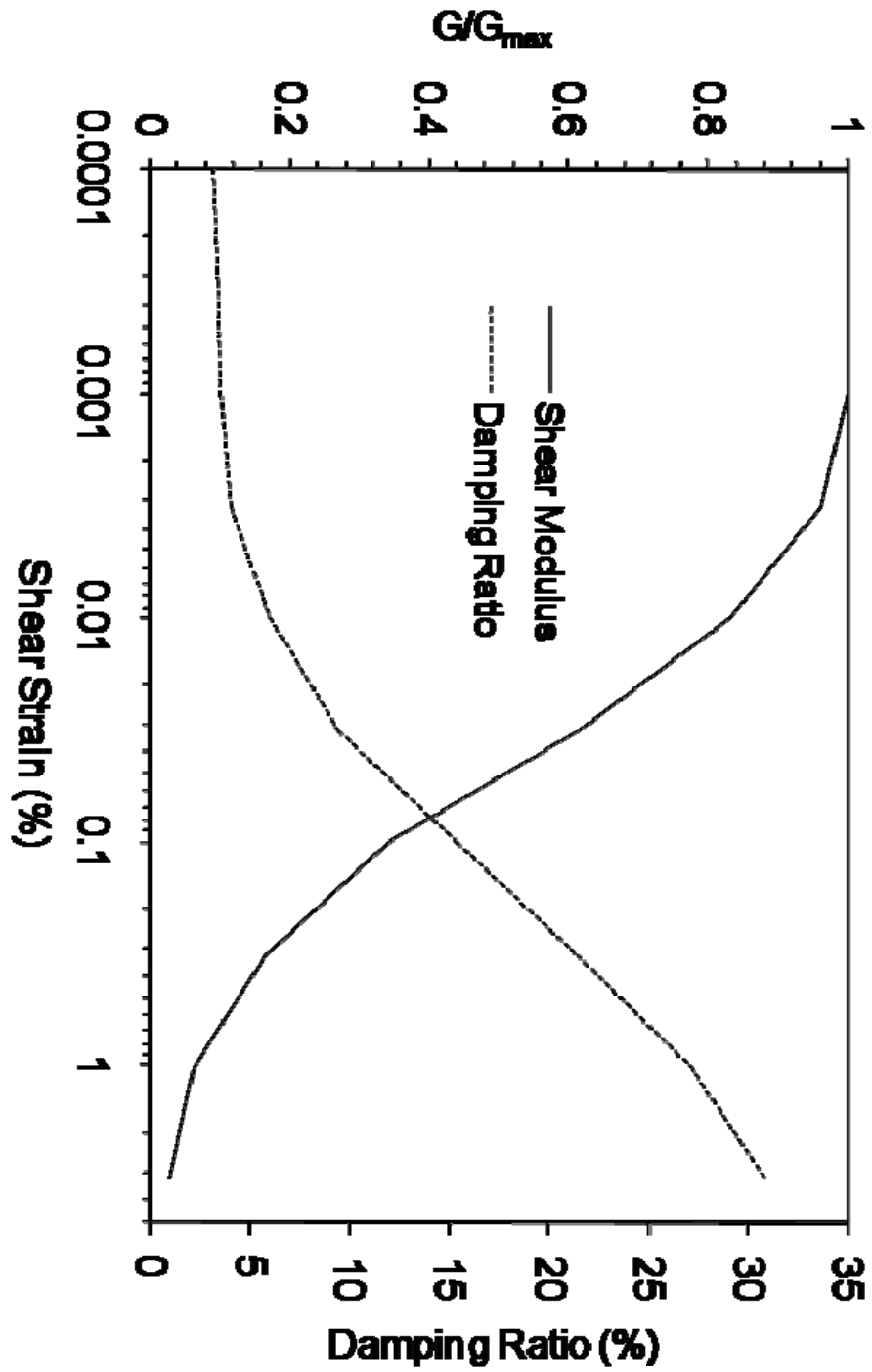
Figure B.5 Modulus degradation and damping curves for rock 15-36 m (EPRI, 1993).
(soil material type 6)
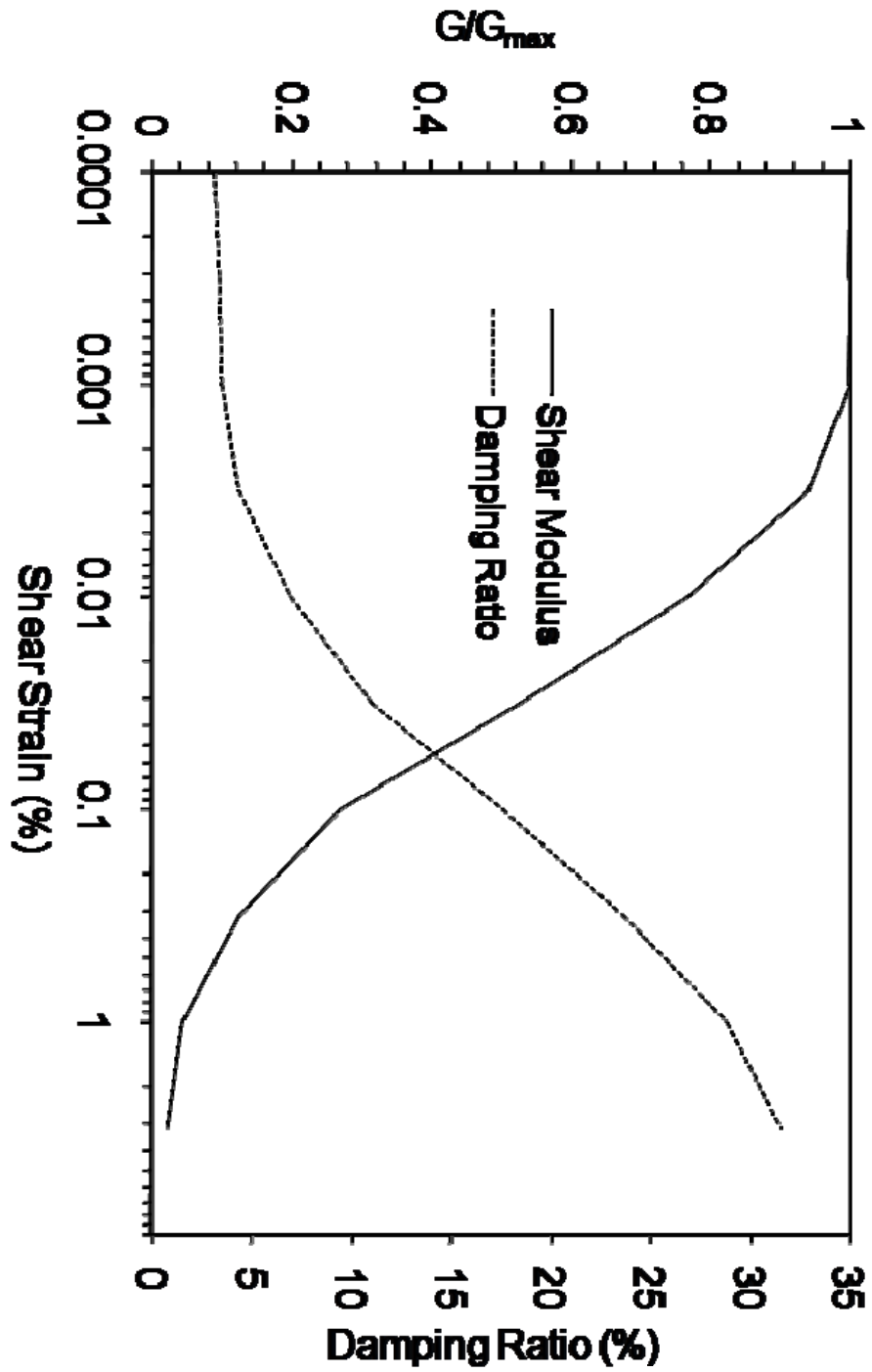
Figure B.6 Modulus degradation and damping curves for rock 36-75 m (EPRI, 1993).
(soil material type 2)
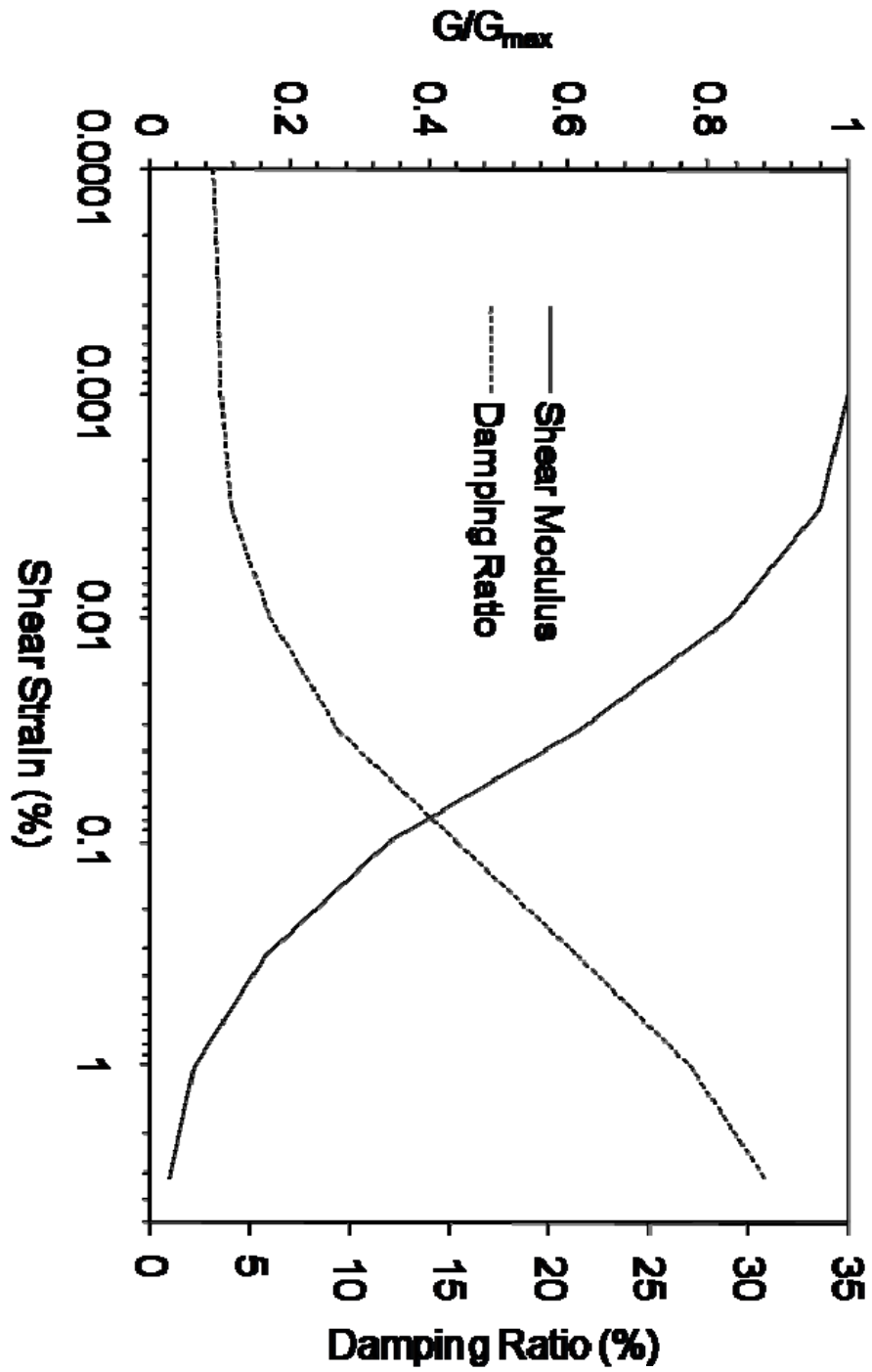
Figure B.7 Modulus degradation and damping curves for rock 75-150 m (EPRI, 1993). *(soil material type 4)*
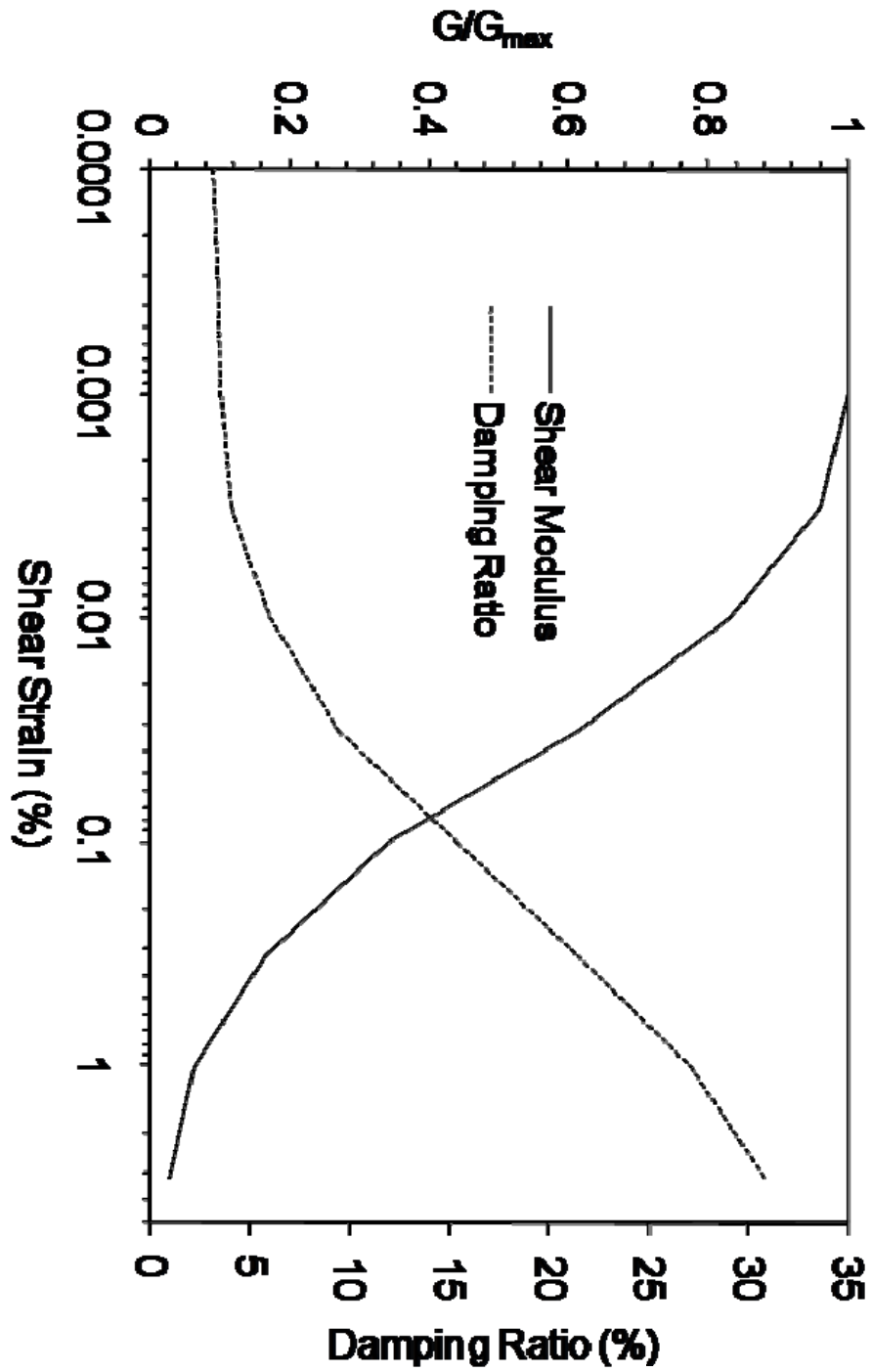
Figure B.8 Modulus degradation and damping curves for rock 150-200 m (EPRI, 1993). *(soil material type 5)*
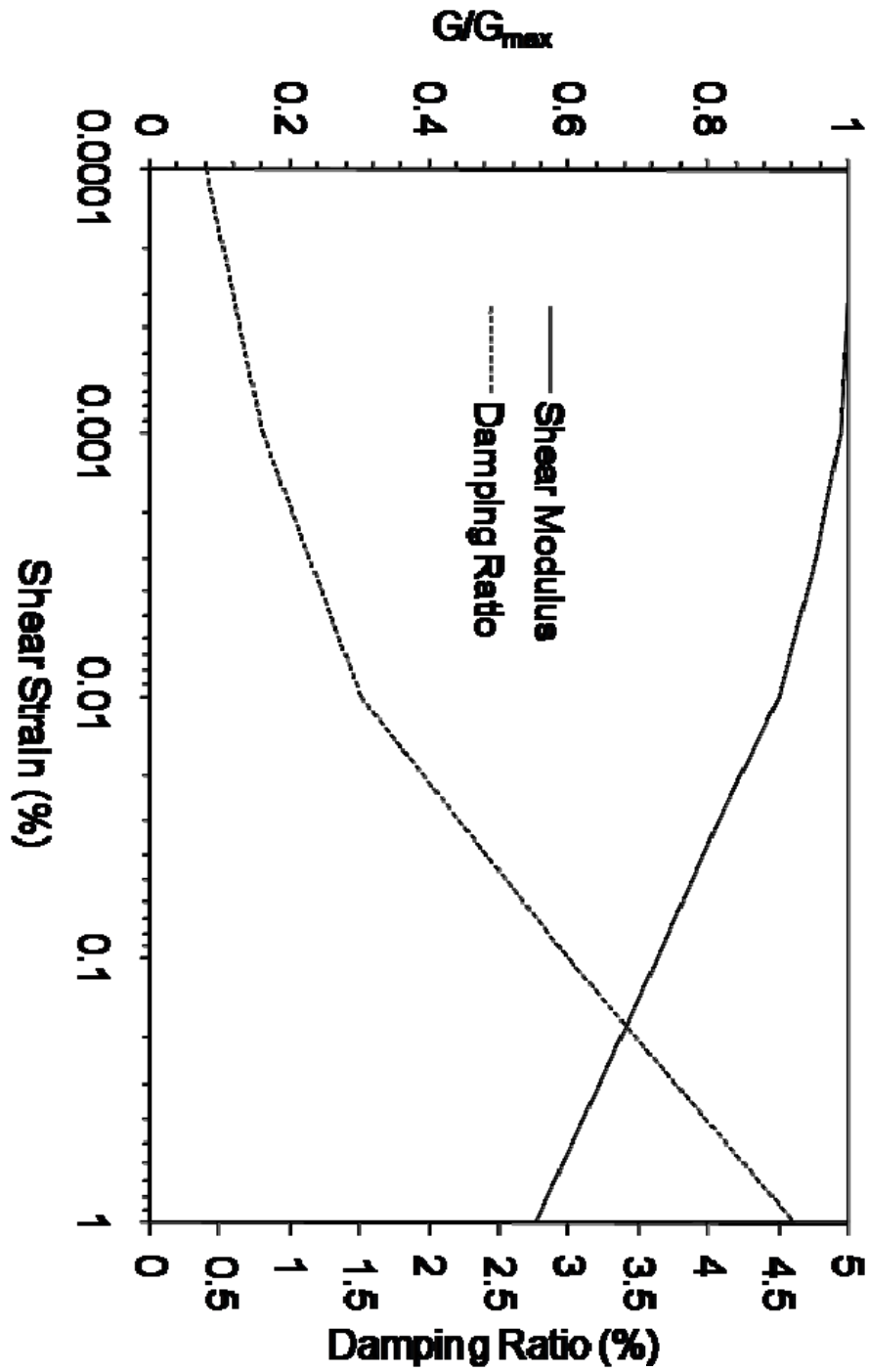
Figure B.9 Modulus degradation and damping curves for rock (average) (after Schnabel, 1973) *(soil material type 3)*